

rate on the Ash Meadows section of the fault is no more than 0.1 mm per year and that it is likely to be an "order of magnitude less." The values included in the analysis and their associated probability weights are 0.01 mm per year (0.2), 0.04 mm per year (0.6), and 0.1 (0.2).

Bare Mountain Fault. The Bare Mountain fault is the major down-to-the-east normal fault that forms the west side of Crater Flat basin. Along the west side of Crater Flat basin, the fault is well expressed geomorphically for approximately 16 km, which is taken as the minimum total fault length. Near the southern end of the basin, the fault may bend to the southeast and continue for another 6 km. Based on the gravity data, we believe that the fault does not continue farther south as a single structure. The southernmost limit of the fault is mapped at its projected intersection with geophysical anomalies that are coincident with the proposed Highway 95 fault. M_{MAX} depends on the total fault length. A maximum rupture length of 16 km corresponds to Mw 6.5 (± 3). However, Mw 6.5 is assumed to be the minimum upper-bound magnitude for surface faulting earthquakes. Therefore, given a rupture length of 16 km, the values included in the analysis and their associated probability weights are Mw 6.5 (0.8) and Mw 6.8 (0.2) (Table DFS-1). Similarly, a maximum rupture length of 22 km corresponds to Mw 6.6 (± 3) and, in this case, the values included in the analysis and their associated probability weights are Mw 6.5 (0.2), Mw 6.7 (0.6), and Mw 7.0 (0.2).

Various slip rates have been reported for the Bare Mountain fault. Reheis (1988) reports 1.75 m of vertical displacement in deposits estimated to be 9 ka, suggesting a slip rate of 0.19 mm per year (Piety, 1995). However, if this represents displacement from a single event, the slip rate is unconstrained. Based on the results of mapping and of trench investigations at three locations along the Bare Mountain fault, L.W. Anderson and R.E. Klinger (USBR, written communication, 1996b) conclude that the slip rate is "quite low," about 0.01 mm per year or less. Based on uplift rates calculated from apatite fission-track thermochronometry and interpretation of alluvial fan sedimentation, Ferrill *et al.* (1996, p. 2-28 to 2-30) argue that the slip rate increases toward the south and suggest that it could be as high as 0.28 mm per year. Structural cross sections of the faults in the site vicinity (Section 4.3.5) indicate that the local west-dipping faults intersect the Bare Mountain fault at depth and, presumably, are truncated by the Bare Mountain fault because it has a much greater

throw than the local faults. In this model, the slip rate on the Bare Mountain fault should be equal to or greater than the sum of the slip rates on the west-dipping (antithetic) faults (i.e., \geq approximately 0.05 mm per year). Clearly, there is still considerable uncertainty in the slip rate on the Bare Mountain fault. In our judgment, the most likely value is in the range of 0.05 to 0.1 mm per year. The values included in the analysis and their associated probability weights are 0.01 mm per year (0.1), 0.05 mm per year (0.4), 0.1 mm per year (0.4), and 0.28 mm per year (0.1).

4.3 LOCAL FAULT SOURCES

Local faults having recognized Quaternary displacement are included as fault-specific seismic sources in the seismic source model. The Ghost Dance fault also is included because it is the largest fault within the footprint of the proposed repository. The locations of the principal Quaternary faults included in this analysis are based primarily on the mapping of Simonds *et al.* (1995). The principal local faults included in the seismic source model are shown on Figure DFS-8.

Other mapped faults in the site vicinity (e.g., the Exile Hill fault, the Midway Valley fault, the Iron Ridge fault, and the northwest-trending faults such as the Yucca Wash, Sever Wash, and Pagany Wash faults) are not included as seismic sources because there is no evidence of Quaternary displacement along any of these bedrock faults. Structural models (e.g., the vertical axis block-rotation model) suggest that these faults might move in response to movements along the principal block-bounding faults. However, with the possible exception of minor fractures in calcite-silica-cemented regolith at the bedrock/alluvial-colluvial contact, the available information (USGS, written communication, 1996) indicates there have been no displacements on any of these faults younger than middle to late Quaternary. Data from numerous trenches indicate there have been repeated surface faulting events on the block-bounding faults during this same interval. The cumulative displacements on these faults in the Tertiary bedrock are small, not more than a few tens of meters. These small intrablock faults represent secondary accommodation structures that probably are related primarily to late Miocene deformation. If the intrablock faults can produce earthquakes, we assumed they would be small, having magnitudes less than or equal to the maximum random earthquake for the site-vicinity source zone (see Section 4.1).

4.3.1 Activity

There is documented Quaternary displacement on all the local fault sources except for the Ghost Dance fault (USGS, written communication, 1996; Simonds *et al.*, 1995). The Quaternary offsets are assumed to be associated with past seismogenic fault displacements, so the probability of activity is assumed to be 1.0. Non-seismogenic mechanisms might account for some of the "paleoseismic events" identified in the fault trenches. For example, a mudflow layer due to a storm event might be misinterpreted as a scarp-derived colluvial wedge from a faulting event. Alternatively, paleoseismic events may be missing from the record because of erosion or the absence of diagnostic characteristics for recognizing individual events. Regardless of the problems associated with the interpretation of individual events, we believe that the Quaternary slip rates derived from the Yucca Mountain trenches provide a reliable indicator of the seismic potential of the faults (assuming that the uncertainties in the amount, sense, and age of the displacement have been correctly factored into the assessment).

In contrast to the other local fault sources, no direct evidence of Quaternary displacement has been observed on the Ghost Dance fault, and the available evidence suggests that there has been no displacement since at least the middle Pleistocene (E.M. Taylor *et al.*, USGS, written communication, 1996). Analogies to other north-south-trending intrablock faults such as the Midway Valley fault and the Exile Hill fault indicate that Quaternary displacements on the block-bounding faults have created only minor adjustments such as fracturing on the larger intrablock faults (Wesling *et al.*, 1993; F.H. Swan *et al.*, Geomatrix Consultants, written communication, 1995; and E.M. Taylor *et al.*, USGS, written communication, 1996). Therefore, we consider it unlikely that the fault is active and capable of generating significant earthquakes; the assigned probability weights are "active" (0.05), and "not active" (0.95). The potential for fault displacement on the Ghost Dance fault is addressed separately in Section 5.

4.3.2 Distributed Faulting Versus Independent Fault Sources

A Quaternary volcanic ash deposit occurs as infilling in fractures and/or along the fault plane in several fault exploration trenches in the Yucca Mountain vicinity. Based on the occurrence of this ash, it has been suggested that there may have been simultaneous rupture

on subparallel faults, including faults on either side of Yucca Mountain (S.K. Pezzopane *et al.*, USGS, written communication, 1996a). Because of the limitations in geologic dating techniques, it cannot be demonstrated that the displacements associated with the so-called "ash event" occurred during a single earthquake. Nonetheless, the physical evidence is sufficiently compelling to warrant consideration in the hazard model.

Simultaneous rupture on two faults does not require that they be physically connected at depth. Distributed fault behavior could occur with both of the structural (end-member) models that are considered in this assessment (Section 4.3.5). Accordingly, whether the faults exhibit distributive fault behavior or behave independently has no major effect on the overall geometry of the local fault sources. It does, however, affect the assessment of the length of the maximum single-event fault rupture. Given distributed fault behavior, the maximum rupture length is not constrained by the length of an individual fault.

Figure DFS-9 is a logic tree showing the dependence of the local fault model on distributive versus independent fault behavior. Relatively low weight is assigned to the distributive fault behavior model (0.05) because of the lack of convincing historical analogs for the postulated "ash-event."

Figures DSF-10 and DSF-11 are logic trees that outline the approaches used to characterize the local fault sources given independent and distributive fault behavior, respectively. The components of the logic tree are described in the following sections.

4.3.3 Total Length

The Quaternary fault scarps are short, rarely more than a kilometer or two long, and discontinuous (Simonds *et al.*, 1995). This may, in part, be due to the character of the fault displacements, but it is largely due to the effects of erosion and deposition since the scarps were formed. In this assessment, we assumed that the generally north-south-trending faults are linked together along strike. For example, the Paintbrush Canyon and Stage Coach Road faults are modeled as a single 20- to 30-km-long fault. The uncertainty in the overall length is due to uncertainties in how far the Quaternary faulting extends to the north and/or the south. The total length of faulting is considered two ways. First, given that the local faults are independent seismic sources, uncertainties in the total length of the individual faults are

considered. Second, given the possibility of distributive faulting, the uncertainty in the total combined length of the local faults that could be involved in a distributive faulting event is considered.

Total Fault Length (Independent Fault Behavior). Figure DFS-8 and Table DFS-2 present alternatives for the total fault length and the assigned probability weights for each of the local fault sources.

Paintbrush Canyon/Stagecoach Road Fault. Four alternatives are considered, as follows.

1. Quaternary faulting is limited to the reach of the fault having evidence of Quaternary displacement, as shown on Simonds *et al.* (1995), i.e., fault segment B-E on Figure DFS-8. This option is given the greatest weight (0.68).
2. Quaternary faulting extends about 1.5 km farther north along the mapped bedrock fault splay that has the same strike as the fault south of Yucca Wash. This option corresponds to fault segment A-E on Figure DFS-8. This is given a low weight (0.2) because: the observed Quaternary displacements die out at the north end of Alice Ridge; no evidence for Quaternary displacement has been found on the Paintbrush Canyon fault north of Yucca Wash; and the projected intersection between the buried Yucca Wash fault would be a reasonable place for the Quaternary faulting to terminate.
3. Quaternary faulting extends about 7.5 km farther south to the projected intersection between the Stagecoach Road and proposed Highway 95 faults. This alternative, which corresponds to fault segment B-F on Figure DFS-8, is also given low weight (0.1) because there is no evidence for Quaternary displacement.
4. Quaternary faulting extends both north and south (fault segment A-F on Figure DFS-8). The probability of this is equal to the combined probability of options 2 and 3 above (0.02).

Bow Ridge Fault. The southern end of the Bow Ridge fault is taken at its projected intersection with the Paintbrush Canyon fault (location K on Figure DSF-8). Two alternatives are considered for the northern extent of Quaternary faulting; either the north end of Exile Hill (location H on Figure DFS-8), or its projected intersection with the Yucca Wash fault (location G). It is unlikely that Quaternary faulting extends much beyond the northern end of Exile Hill. Alluvial surfaces have been mapped across the northward projection of the

fault that are equivalent to and older than the youngest faulted colluvial deposits on the west side of Exile Hill (J.R. Wesling *et al.*, Geomatrix Consultants, written communication, 1992; Swan *et al.*, Geomatrix Consultants, written communication, 1995). Therefore, the greatest weight (0.8) is assigned to segment KH (Table DSF-2).

Solitario Canyon Fault. The northern end of the Solitario Canyon fault is well constrained by bedrock mapping. It is unlikely that the fault extends any farther north than its projected intersection with the Yucca Wash fault (Scott and Bonk, 1984; Day *et al.*, 1996c). The southern end of the fault is less certain, and two alternatives are considered (Table DFS-2). It is likely that the limit of Quaternary faulting coincides with the southernmost extent of the mapped Quaternary traces, as shown on the fault activity map by Simonds *et al.* (1995). This alternative (segment L-M on Figure DFS-8) is assigned a weight of 0.7. It is unlikely that the Solitario Canyon fault extends farther south than its projected intersection with the Stagecoach Road fault. This alternative (segment L-N on Figure DFS-8) is assigned a weight of 0.3 (Table DSF-2).

Windy Wash/Fatigue Wash Faults. The Northern Windy Wash, Fatigue Wash, and Southern Windy Wash faults are assumed to be linked along strike and are treated as a single fault zone. The Quaternary faulting is discontinuous, and the total length of the fault system is uncertain. Four alternatives are considered in the model (Table DFS-2).

1. Quaternary faulting is limited to the reach of the fault having evidence of Quaternary displacement, as shown on Simonds *et al.* (1995), i.e., fault segment P-R on Figure DFS-8. This option is given the greatest weight (0.57).
2. Quaternary faulting extends about 1.5 km farther north, ending at the projected intersection of the Northern Windy Wash fault with the Yucca Wash fault. This option corresponds to fault segment O-R on Figure DFS-8. This is given a relatively low weight (0.3) because no evidence for Quaternary displacement has been found along section O-P.
3. Quaternary faulting extends about 3.5 km farther south to the projected intersection between the Southern Windy Wash fault and the proposed Highway 95 fault. This alternative, which corresponds to fault segment P-S on Figure DFS-8, is also given low weight (0.1) because there is no evidence for Quaternary displacement.

4. Quaternary faulting extends both north and south (fault segment O-S on Figure DFS-8). The probability of this is equal to the combined probability of options 2 and 3 above (0.03).

Northern and Southern Crater Flat Faults. Based on the geologic cross sections and structure contour maps described in Section 4.3.5, the Northern and Southern Crater Flat faults intersect the Bare Mountain fault at a relatively shallow depth, and it is unlikely that they are linked along strike. The narrow down-dip width of the fault is consistent with the short mapped surface traces. Therefore, the total fault lengths are taken as the mapped fault lengths shown on the fault activity map by Simonds *et al.* (1995).

Ghost Dance Fault. Based on the detailed mapping within the controlled area (Simonds *et al.*, 1995; Day *et al.*, 1996c), the Ghost Dance fault is well defined for a distance of about 3 km (segment Y-Z, Figure DSF-8). Bedrock mapping indicates that the fault dies out at its northern end and that it does not extend north of location YY on Figure DSF-8. The southern termination of the fault is less distinct. The maximum length of the Ghost Dance fault is about 9 km if one assumes that the fault extends from location YY southward and includes the Abandoned Wash fault (i.e., segment YY-ZZ on Figure DSF-8). The geologic evidence for a continuous 9-km-long fault is not strong. Nonetheless, we assign a relatively high weight to a total fault length of 9 km because this assessment is conditional on the fault being an active seismogenic feature. A 3-km-long fault extending to seismogenic depths and acting as an independent seismic source is not very likely. A total fault length of 3 km (segment X-Y on Figure DSF-8) is assigned a weight of 0.3; a total length of 9 km (segment XX-ZZ) is given a weight of 0.7 (Table DSF-2).

Total Fault Length (Distributive Fault Behavior). Given the uncertainty in the total lengths of the individual faults described above, the sum of their lengths (total combined length) could be as long as 101.2 km, or as short as 84.5 km.¹ If the Northern and Southern Crater Flat faults are only minor features, the minimum combined total length is 69.9 km.

¹ NOTE: These totals were calculated based on the distributed fault model, so that fault segment M-N of the Solitario Canyon fault was assumed to exist. The Ghost Dance fault was not included because, unlike the other local fault sources, there is a very low probability that it is an active fault.

Three scenarios are defined to account for the uncertainty in the total length of faulting given the distributed fault model (Figure DSF-10). These are:

Scenario A - the minimum value for the total length, minus the Northern and Southern Crater Flat faults, which in this scenario are inferred to represent minor secondary features;

Scenario B - the maximum value for the total fault length minus the Northern and Southern Crater Flat faults; and

Scenario C - the maximum value for the total fault length including the Northern and Southern Crater Flat faults.

The fault segments as shown on Figure DFS-8, total length, and assigned probability weight for each of these scenarios are presented in Table DFS-3.

4.3.4 Maximum Fault Rupture Length

Estimates of the rupture length associated with the maximum earthquake depend on whether the local faults behave independently or whether multiple traces rupture simultaneously (distributive faulting) (Figure DSF-9). The maximum rupture length per event on the local faults is discussed below for each type of fault behavior.

Maximum Rupture Length for Independent Fault Behavior. If the local faults behave independently, the maximum rupture length depends on the total fault length and on the length of the longest part of the fault that is expected to rupture during a single event. Given the range of total fault lengths presented in Table DFS-2, the following alternatives were considered:

- Rupture of 100 percent of the total fault length. For long faults, such as the Paintbrush Canyon/Stagecoach Road fault, this was given a low weight. For short faults such as the Northern Crater Flat and Southern Crater Flat faults, 100 percent rupture of the total fault length is assigned a probability of 1.

- Rupture of the longest geometrically defined fault segment. Depending on the strength of the evidence for defining fault segments, this approach was generally given the most weight.
- Rupture of two or more geometrically defined fault segments.

The basis for the alternative maximum rupture lengths considered for each of the local fault sources (assuming independent fault behavior) and the assigned probability weights are given in Table DSF-4.

Maximum Rupture Length for Distributive Fault Behavior. Based primarily on paleoseismic data from trenches, S.K. Pezzopane *et al.* (USGS, written communication, 1996a) propose nine rupture scenarios, Z through R, that are consistent with our distributed fault model. That is, the inferred rupture scenarios suggest the possibility of simultaneous rupture on multiple fault traces in the vicinity of Yucca Mountain. These rupture scenarios are used to evaluate the range of values for single-event fault ruptures associated with the distributed fault model. We used a somewhat different approach to define the rupture lengths associated with each scenario. S.K. Pezzopane *et al.* (USGS, written communication, 1996a) constrain the minimum and maximum rupture length for each scenario based on the spatial distribution of the trenches. We used the trench data and geometrically defined fault segments to assess the length of surface fault rupture associated with each scenario. If the trench data suggest that two fault segments could have ruptured at the same time, we assumed that 100 percent of each segment ruptured unless trench data suggest otherwise. Our approach also incorporates the uncertainty in the total mapped length of the site-vicinity faults. Therefore, in some cases, we derive rupture lengths longer than the maximum values interpreted by S.K. Pezzopane *et al.* (USGS, written communication, 1996a). Given below are the rupture length estimates—both ours and those of S.K. Pezzopane *et al.*—associated with each rupture scenario.

RUPTURE SCENARIO	RUPTURE LENGTH IN KM (PEZZOPANE, <i>et al.</i> , 1996B, TABLE 5-3)	RUPTURE LENGTH IN KM (THIS STUDY)
Z	8.5 to 22	23.4 to 36.4
Y	18.5 to 25.5	25
X	15 to 24	18.9 to 24.9
W	10 to 22	30.6
V	9 to 15.5	14.8
U	10.5 to 23	55.5 to 59
T	14 to 20	< 15
S	9.5 19.5	< 15
R	8.5 to 22	< 15

The ranges indicated above are permitted by the data. The timing of paleoseismic events is imprecise, and the data do not necessarily indicate that single-event ruptures that are this long have occurred. Given a distributed faulting event, there is a great deal of uncertainty in the rupture length that would be associated with the maximum earthquake. The scenario earthquakes summarized above suggest values from less than 15 km up to about 60 km. Fifteen km is judged to be the minimum value that should be considered for the maximum rupture length given the distributed fault model. Using our approach to define the rupture lengths associated with the scenario earthquakes, and considering only those events having values greater than about 15 km, the average rupture is about 30 km. Using values proposed by S.K. Pezzopane *et al.* (USGS, written communication, 1996a, Table 5-3), the average is closer to 20 km.

The range of values for the surface fault rupture length associated with the maximum earthquake (given the distributed fault model) and the assigned probability weights are:

Maximum Rupture Length (Distributed Fault Model)	
15 km	(0.2)
20 km	(0.35)
30 km	(0.35)
60 km	(0.1)

Pattern of Fault Rupture for Distributive Fault Behavior. The following procedures were used to model the pattern of fault rupture based on the distributive fault behavior model.

- Earthquakes associated with ruptures ≤ 10 km long are assumed to occur as a single rupture randomly distributed on the mapped Quaternary faults (i.e., the local fault sources).
- Earthquakes associated with ruptures > 10 km and ≤ 25 km long are assumed to occur as two parallel ruptures of equal length that occur randomly on local fault sources. Earthquakes associated with ruptures > 25 km and ≤ 45 km long are assumed to occur as three parallel ruptures of equal length that occur randomly on local fault sources.
- Earthquakes associated with ruptures > 45 km long are assumed to occur as four parallel ruptures of equal length that occur randomly on local fault sources.

The selection of the cutoff points (10 km, 25 km, and 45 km) between single, double, triple, and quadruple parallel ruptures was somewhat arbitrary. They were chosen to minimize unreasonably short ruptures while permitting simultaneous rupture on all four principal local faults during the largest events. Alternative values could be used to test the sensitivity of the results to these postulated values. We did not propose alternative values because we believe they will have no significant impact on the overall hazard results.

4.3.5 Downdip Fault Geometry (Dip and Width)

Structural models were used to estimate the down-dip geometry of the local faults. Our understanding of the tectonics of the Yucca Mountain region is influenced by the tectonic interpretations of this region developed during the past 30 years of detailed studies. The first generation of these studies led to the proposal that Crater Flat basin formed as a caldera complex (Carr *et al.*, 1986). Carr's work was followed by more detailed mapping of the east side of Crater Flat basin (Yucca Mountain) by Scott (1990), who proposed that the faults exposed on the surface in Crater Flat basin sole into a shallow detachment fault at the Paleozoic-Tertiary contact. At about the same time, Schweickert (1989) proposed that a regional, northwest-striking, right-slip fault extends under Crater Flat basin and is concealed under a detachment fault. In the latest generation of work, the detailed mapping started by Scott has been extended across the western half of the basin and beyond (Faulds *et al.*, 1994; Fridrich, 1997), and the surface geology and trench exposures of the Quaternary faults in the basin have been mapped (Simonds *et al.*, 1995; J.W. Whitney *et al.*, USGS, written communication, 1996a). This latest work has led to a proposal that Crater Flat is a pull-apart

basin that formed in response to the combined extensional and strike-slip strain regime of the Walker Lane belt (Fridrich, 1997), as originally advocated by Wright (1989).

The latest generation of tectonic studies at Yucca Mountain (e.g., J.W. Whitney *et al.*, USGS, written communication, 1996a) largely have rejected the detachment fault hypothesis proposed by Scott (1990). Southwest Research Institute scientists (Young *et al.*, 1993) suggested that the Paleozoic-Tertiary contact is too shallow for a detachment fault under Yucca Mountain, based on computer modeling of the proposed structure in balanced cross sections. Gravity and reflection surveys (Snyder and Carr, 1984; Brocher *et al.*, 1996) across Crater Flat basin provide evidence that the Paleozoic-Tertiary contact is offset by several large, high-angle features, which is difficult to reconcile with this contact being a detachment fault of the sort invoked by Scott. Scott's model predicts that the Tertiary rocks were transported westward relative to the underlying Paleozoic rocks before the uplift of Bare Mountain. However, recent mapping has shown that the uplift of Bare Mountain was roughly coeval with formation of the extensional faults in Crater Flat basin and that a linear swarm of 14 Ma dikes is not offset significantly (if at all), as predicted at the Tertiary/Paleozoic contacts at the northeast and southeast corners of Bare Mountain (Fridrich, 1997). Scott invoked the widely accepted model in which the detachment fault allows lateral translation of extensional strain between the zone of brittle extensional faulting in the upper plate and the zone of ductile extension in the lower plate. Because any detachment fault under the Crater Flat basin would be truncated by the Bare Mountain range-front fault, it would be a rootless structure that would lack any kinematic impetus to move in Scott's model. For these reasons, our analysis gives Scott's detachment model a very low weight (Figures DSF-10 and DSF-11).

Carr *et al.*'s (1986) hypothesis, that the Crater Flat basin formed as a caldera complex, has been rejected by nearly all ensuing workers for the following reasons. (1) The structures of the Crater Flat basin are products of northwest-directed extension and right-slip strain (Scott, 1990; Minor *et al.*, 1996; Fridrich, 1997). They thus are consistent with patterns of late Cenozoic tectonism in the Great Basin as a whole. In contrast, the structures formed by calderas accommodate principally vertical strain (tumescence, collapse, and resurgence) over the subcaldera magma body and radial and concentric strain peripheral to the magma

chamber (Smith and Bailey, 1968). (2) If a caldera complex is buried under Crater Flat basin, it must be older than 13.1 Ma because the sources for all of the younger major ash-flow sheets of the southwest Nevada volcanic field have been identified (Sawyer *et al.*, 1994). In that the Crater Flat basin formed at about 12.7 Ma, any buried caldera under the basin was a fossil structure when the basin formed and, therefore, is irrelevant to the formation of this basin. We give the caldera model zero weight in our analysis for the reasons stated above and because this model provides no explanation for the Quaternary faulting in this basin.

The rapid succession of different tectonic interpretations of the Crater Flat basin during the past 30 years is an indication of the level of scientific uncertainty involved. Because of the large uncertainty, we consider a range of hypotheses. The strongest weight is assigned to the simplest, most conventional approach. The alternative models, which are assigned relatively low weights, are included primarily to facilitate assessment of the effect these models have on the overall seismic hazard at Yucca Mountain.

Domino Model. Our preferred model assumes that the faults exposed at the surface in Crater Flat basin extend as high-angle, planar faults to seismogenic basement (12 to 16 km), except where the geometry dictates that they run into another, larger-throw fault before they reach that depth, as discussed below. We call this the Domino model. The theoretical basis and supporting evidence for the Domino model consists of the following points.

- (1) The 1992 Little Skull Mountain earthquake (Mw 5.7), which had its epicenter about 10 km east of Yucca Mountain, provides the only ground-truth evidence on the subsurface geometry of faults and on the relationship between faulting and earthquakes in the Yucca Mountain region.
- (2) The foci of the main Little Skull Mountain shock and aftershocks defined a planar, high-angle fault that extends from the upper crust down to at least 12 km (Harmsen, 1994; Smith *et al.*, 1996).
- (3) The nature of this earthquake is consistent with the majority of data on historical earthquakes in the Great Basin in that most significant (greater or equal to magnitude 5) earthquakes in this province are due to movement on normal faults that are high-angle, planar, and extend to depths of 10 to 15 km (the brittle-ductile transition).

- (4) Moreover, the lack of evident ground breakage associated with the Little Skull Mountain quake is consistent with the fact that most quakes in this province having a magnitude of less than 6 have no associated ground breakage.
- (5) If we can use the Little Skull Mountain quake as an analogue for what to expect at Yucca Mountain, then the Quaternary ground breakage along distances of several kilometers and more on Yucca Mountain faults having slips in individual events of as much as 1 m suggests that the Quaternary faulting events on Yucca Mountain were associated with large earthquakes (greater than magnitude 6). By inference, we believe it is valid to take the relationship of earthquake magnitude to fault rupture length (and other parameters) developed using the historical data from the Great Basin as a whole and use them to predict the potential magnitude of earthquakes at Yucca Mountain, based on the Quaternary record of surface fault rupture there.

The Domino model represents the simplest, most conventional approach because it assumes that Yucca Mountain is not seismically anomalous relative to the rest of the Great Basin. This is our preferred model because, although it is possible that Yucca Mountain may be seismically anomalous relative to the rest of the Great Basin, we believe that arguments suggesting that it is are scientifically weak. Therefore, the Domino model is assigned a very high weight (0.8) relative to the Detachment model (0.2) in the hazard analysis (Figures DSF-10 and DSF-11).

An optional feature we placed within our Domino model is the Highway 95 fault (discussed below), based on an interpretation of Slemmons (personal communication, 1997). Slemmons invoked this fault, based on airphoto lineament patterns, to explain a structural geometry problem. The Quaternary faults in Crater Flat basin show a pattern of southward increase in slip rates, with maximum rates documented near the southern terminations of recent activity. This geometric pattern is highly anomalous and suggests that the faults may be abruptly terminating against another structure, such as a northwest-striking right-slip fault along the southern boundary of the basin.

Detachment Model. A detachment layer at depths of 5 to 8 km below the surface may be used to satisfy the geometry arguments advanced by Southwest Research Institute (Young *et al.*, 1993) and to be consistent with gravity and reflection data. We used this basic fault geometry to characterize the proposed detachment models, which include:

- Scott's model in which the detachment acts as the master fault in the basin that all of the intrabasin faults sole into;
- Wernicke's (1995) model in which a master detachment fault is considered a separate seismic source; and
- Schweickert's model in which a regional-scale strike-slip fault that is a potential seismic source extends under Crater Flat basin under a shallow detachment fault.

Also considered were the ideas advanced principally by O'Leary (personal communication, November 20, 1996 Workshop), who proposed that the large difference in the mechanical behavior of the Tertiary volcanic and Paleozoic sedimentary rocks under Yucca Mountain may result in an abrupt, downward change in the style of faulting across the Paleozoic-Tertiary contact. This contact would be a passive zone of detachment that accommodates an upward change in structural behavior in the rocks. The predominantly northeast-striking, left-oblique normal faults that cut the volcanic rocks have allowed a large component of distributed right-slip strain across the basin (Fridrich *et al.*, 1997). The major point of this passive detachment model is that the distributed strike-slip strain in the volcanic surface rocks could reflect motion along a discrete strike-slip fault at seismogenic depths under Crater Flat basin. Unlike the model proposed by Schweickert, the concealed strike-slip fault would be confined to Crater Flat basin. Such a fault has been postulated beneath the Crater Flat basin, and was informally referred to as the cross-basin fault (I. Stamatakos, SSC Workshop 2). The potential for a hidden strike-slip fault beneath Crater Flat basin is addressed in Section 4.4.2.

Estimated Downdip Geometry of Local Faults. To develop defensible interpretations of subsurface fault geometry under Crater Flat basin, we constructed a suite of cross sections and structural contour maps of the exposed Quaternary faults using two geometric styles, which we view as end-member geometries: (1) a planar fault geometry, and (2) a strongly listric geometry that merges with a detachment layer. We then used these maps and sections to develop the downdip widths of the faults, listed below. For this exercise, we used the measurements of fault attitudes of Simonds *et al.* (1995) as a starting constraint and assumed that the fault planes exposed on the surface represented the steepest parts of the faults. In theory, normal faults form at an angle of 50 to 70 degrees in most rocks because this is the

angle of maximum shear stress, assuming that the principal compressive stress is vertical. As these faults approach the surface, however, they tend to steepen to attitudes approaching vertical because there is no shear stress at the surface of the Earth. Another assumption we made is that fault dip decreases smoothly with depth. In our planar sections and maps, the decrease in fault dip with depth is very small; in the listric model, the faults sole into a subhorizontal detachment fault at about 6 km below the surface.

We used a trial-and-error approach in constructing our maps and sections to arrive at subsurface geometries that we consider most credible. For example, we joined the two segments of the Paintbrush fault and the Stagecoach Road fault as a single fault at shallow depths because: (1) these three mapped fault segments are roughly coplanar; (2) if not joined, these three fault segments had length-to-width ratios in the planar model that are inconsistent with established aspect ratios of faults in the Great Basin based on historical seismic and paleoseismic data; and (3) the documented single-event slip on the Stagecoach Road fault segment is too large for a fault as short as this, based on historical fault data, suggesting that this segment is part of a longer fault. We joined the northern and southern segments of the Windy Wash fault with the Fatigue Wash fault at shallow depth for the same reasons. The two other major faults in our maps and sections are the Solitario Canyon and Bare Mountain faults, both of which were mapped as single segments.

Having made the above assumptions, we found that the Paintbrush Canyon/Stagecoach Road fault, the Solitario Canyon fault, and the Windy Wash/Fatigue Wash fault cannot come together at shallow depth; the most credible geometry appears to be that they are independent faults. The projections of the other faults in the basin (i.e., the Bow Ridge and Northern and Southern Crater Flat faults) all intersect one of the four major faults at depths much shallower than the brittle-ductile transition. These faults thus either may be splays of the Paintbrush Canyon/Stagecoach Road or Solitario Canyon faults, or, in the case of the Northern and Southern Crater Flat faults, may be minor faults that are antithetic to the Bare Mountain fault. In the Domino (planar) model, the three major intrabasin faults (the Paintbrush Canyon/Stagecoach Road fault, the Solitario Canyon fault and the Windy Wash/Fatigue Wash fault) are antithetic faults to the Bare Mountain fault because they project into the Bare Mountain fault at depths that are near or above the brittle-ductile transition. In the Detachment (listric) model, the Paintbrush Canyon/Stagecoach Road fault is the master

Crater Flat faults, which run into the Bare Mountain fault first. In the hazard analysis, given the Detachment model, the Paintbrush Canyon/Stagecoach Road fault is modeled as a shallow-dipping, seismogenic source that extends beneath the Crater Flat Basin (Table DSF-5).

In the Domino (planar) fault model, the faults probably are not truly planar. They probably are slightly curved, which would explain the observed regions of roll-over in stratal dips in the hanging walls of these faults. Minimal curvature was used in constructing the cross sections. However, in the hazard analysis, the faults are modeled as planar features, and the average dip was used. To account for uncertainties in the actual dip and downdip width of the faults, the analysis includes a range of values represented by the alternative geometries (Alternatives A and B) shown on Table DSF-5 for the Domino model.

4.3.6 Quaternary Slip Rates (Seismic Moment Rates)

Quaternary slip rates are used in conjunction with fault areas (including the uncertainties in total fault lengths and downdip fault widths) to compute a range of values for the average seismic moment rate for each local fault source. Except for the Ghost Dance fault, the Quaternary slip rates for the local faults are based on the reported results of detailed paleoseismic investigations. In general, these reported slip rates are reasonably well constrained by the available data; nonetheless, there are uncertainties in the amount of cumulative displacement, the age of the displaced units and, in some cases, the relation between the apparent vertical displacements measured in the trenches to the net slip on the fault (i.e., where there may be a significant component of lateral slip). To account for these uncertainties, a range of values is considered for each local fault. In most cases, the range is represented by three values: the maximum and minimum slip rates indicated by the data, and a preferred value, which were assigned subjective probability weights of 0.2, 0.2, and 0.6, respectively. Where preferred values were not reported, maximum and minimum slip rates are given, and a subjective probability weight of 0.5 is assigned to both values.

The range of values assigned to the Ghost Dance fault is based on the amount of post-Tiva Canyon displacement, using the procedures described in Section 5.0 (Fault Displacement Hazard). The preferred value, which we assigned a subjective probability of 0.6, is the weighted average from the three approaches used in the fault displacement assessment. The

minimum and maximum values calculated using these techniques are each assigned a subjective probability of 0.2.

Table DFS-6 presents the range in values, assigned weights, and sources of data for the reported slip rates. In several cases the slip rates presented in Table DFS-6 indicate a greater range of uncertainty than the reported slip rates either because data from several closely spaced trenches have been generalized and/or we believe that there is greater uncertainty than represented by the reported values (e.g., in some case we made allowances for a greater amount of lateral slip).

There appears to be a systematic increase from north to south in both the amount of cumulative bedrock displacement and in the Quaternary slip rates on the local faults. To preserve this spatial variability in the rate of seismic moment release, the longer faults are divided into segments characterized by different slip rates. These fault segments do not necessarily represent rupture boundaries. We assumed that single-event ruptures may extend across these boundaries.

4.3.7 Maximum Magnitude

Given the range of fault geometries, we used two methods to calculate earthquake magnitude. We used empirical relations that relate maximum rupture length to magnitude and similar relations that relate maximum rupture area to magnitude (Wells and Coppersmith, 1994, relations for all fault types). In addition to the uncertainty in the fault rupture parameters (length and downdip width), which is addressed by the range of values included in the logic trees, there also is uncertainty associated with the data sets used in formulating the empirical relations themselves. This uncertainty was included in the analysis by calculating $M_{MAX} \pm 1\sigma$.

Several other approaches and empirical relations are available for estimating earthquake magnitudes (e.g., Slemmons, 1982; Bonilla *et al.*, 1984; Wyss, 1979; dePolo and Slemmons, 1990). We concluded that by incorporating the uncertainty ($\pm 1\sigma$) in the Wells and Coppersmith (1994) relations, we would adequately capture the uncertainty associated with estimation techniques in general.

The rupture-area-versus-magnitude approach is given more weight than the rupture-length-versus-magnitude approach because it incorporates more of the parameters that affect the size of an earthquake and because the rupture-length-versus-magnitude relation is insensitive to significant variations in possible downdip geometries. The rupture area approach is assigned a weight of (0.6), the rupture length approach is assigned a weight of (0.4).

4.3.8 Recurrence Models

The same earthquake recurrence models used to characterize the regional fault sources also were used to characterize the local fault sources (i.e., an exponential recurrence model, a characteristic earthquake recurrence model, and a maximum moment model; see Section 4.2). However, we believe that there is greater potential for variability in the size of earthquakes based on distributed fault behavior than there would be if the faults behave independently. Therefore, the probability weights assigned to each earthquake recurrence model depend on the fault behavior model for the local fault sources (Figure DFS-12). Regardless of the fault behavior model, the greatest weight (0.6) was assigned to the characteristic earthquake model because the results of detailed paleoseismic studies along active faults have shown that the characteristic model is more representative of the seismicity of an individual fault than are exponential models that represent the seismicity of regions, which contain faults of various sizes. Given distributive fault behavior, more emphasis is given to the exponential model (Figure DFS-12).

4.4 HYPOTHETICAL FAULT SOURCES

In addition to the known regional and local fault sources, we included two hypothetical fault sources in the seismic hazard model. These are: the Highway 95 fault that has been proposed by Slemmons (1977), and a buried strike slip-fault that has been postulated based on proposed tectonic models (Schweikert, 1989). The existence of these faults and rate of Quaternary activity, if they exist, are uncertain. The locations of these features (as modeled in this analysis) are shown on Figure DFS-13. The seismic source parameters used to characterize the hypothetical fault sources are presented in Table DFS-7.

4.4.1 Proposed Highway 95 Fault

Slemmons (1977) proposes a fault zone, which he refers to as the "Carrara feature," along U.S. Highway 95 between the fluvial Beatty scarp near the Amargosa River to the south end of Yucca Mountain. Based on its strike (subparallel to the Furnace Creek fault), the predominant sense of slip would likely be left-lateral strike-slip.

The approach used to model the proposed Highway 95 fault is the same as the approach used to model the regional fault sources except that a low weight (0.1) is assigned to the probability that this feature is an active structure. We assigned a low probability of activity because no evidence has been found for faulting along this trend. The suspected fault-related features that have been investigated (e.g., the Beatty scarp) were found to be erosional/depositional in origin and not due to Quaternary faulting.

Because of the lack of evidence for faulting, the total length of the feature is uncertain. Two lengths are considered in the analysis: 11 km, which corresponds to the section of the lineament adjacent to the southwest flank of Bare Mountain; and 27 km, which assumes that faulting could extend southeastward to its projected intersection with the north-south-trending Amargosa/Gravity (Ash Meadows) fault. Based on the gravity data, we believe it unlikely that strike-slip faulting extends any farther southeast. The two values for the total fault length are given equal weight (maximum uncertainty). M_{MAX} depends on total fault length. A maximum rupture length of 11 km corresponds to M_w 6.3 ($\pm 1/4$). However, M_w 6.5 is considered the minimum upper-bound magnitude for surface faulting earthquakes. Therefore, given a rupture length of 11 km, the values included in the analysis and their associated probability weights are M_w 6.5 (0.7) and M_w 6.8 (0.3) (Table DFS-7). Similarly, a maximum rupture length of 27 km corresponds to M_w 6.7 ($\pm 1/4$). In this case, the values included in the analysis and their associated probability weights are M_w 6.5 (0.2), M_w 6.7 (0.6), and M_w 7.0 (0.2).

There are no reported slip rates for the proposed Highway 95 fault. Slip rates are estimated here based on the inferred rate of extension in the southern part of the Crater Flat basin. The sum of the vertical slip rates on the Quaternary faults in the southern part of the basin is approximately 0.05 to 0.1 mm per year (C.J. Fridrich *et al.*, USGS, written communication, 1996, Figure 2-9). Depending on the average dip of the north-south faults, the rate of

extension could be equivalent to, or about half of, the vertical rate (i.e., 45 degrees versus about 65 degrees). By assuming that all the extension is being taken up on the proposed Highway 95 fault, we estimated the slip rate to be in the range of 0.01 to 0.05 mm per year, with a preferred value of about 0.027 mm per year (based on preferred dips of 55 to 60 degrees). The values and associated probability weights included in the analysis are: 0.01 mm per year (0.3), 0.03 mm per year (0.4), and 0.05 mm per year (0.3). Nearly equal weights were given to all three values to reflect the high degree of uncertainty in the slip rate.

4.4.2 Postulated Hidden Strike-Slip Fault Beneath Crater Flat Basin

Given a detachment zone model, there could be hidden strike-slip faults below the detachment layer (e.g., Schweickert, 1989). The hidden strike-slip faulting could be local (restricted to Crater Flat basin) or regional. There is little physical evidence to support the existence of a hidden strike-slip fault (Section 1.0). The probability that there is an active hidden strike-slip source is given even less weight than the activity assessment for the Highway 95 fault (0.05 versus 0.1). The primary reason for including a postulated strike-slip fault in the analysis (given the detachment model) is to enable us to test the sensitivity of the results to this hypothesis.

The location of such a fault is unknown. For this analysis, we assumed that the fault strikes parallel to, and lies 40 to 50 km east of, the Death Valley/Furnace Creek fault system. To model uncertainty in location, equal weight was given to a strike-slip fault having a 90 degree dip that is either along the northeastern margin, southwestern margin, or down the center of the zone shown on Figure DFS-13. To model uncertainty in the length of the zone, two alternatives were considered. If the fault is restricted to Crater Flat basin, it has a total length of about 30 km (segment A-B on Figure DFS-13). If the fault is regional, it was assumed to extend about 100 km in either direction from Crater Flat basin and to have a total length of about 200 km (segment C-D). These alternatives were given equal weight (i.e., maximum uncertainty).

We used different approaches to estimate the maximum earthquake magnitude depending on the structural model (local strike-slip faulting restricted to Crater Flat basin versus regional strike-slip faulting). Given the local strike-slip model, the maximum rupture dimensions are constrained by the length of the basin, the depth of the detachment zone, and the maximum

depth of the seismogenic crust. The same methods used to calculate earthquake magnitudes for the local fault sources (Section 4.3.7) were used for the hypothetical buried strike-slip faults, except that more weight was given the area-versus-magnitude relation, because the structural model significantly restricts the fault width and the length-versus-magnitude relation is insensitive to this parameter. Given the local strike-slip model, the area-versus-magnitude technique is assigned a weight of 0.8, and the length-versus-magnitude technique is assigned a weight of 0.2 (Table DFS-7).

Given the regional strike-slip model, the maximum fault rupture length is unconstrained. In this case, the maximum earthquake magnitude is based on our judgment regarding the largest events that would be consistent with the lack of surface evidence for a throughgoing strike-slip fault. The threshold for surface fault rupture is generally in the range of magnitude 6 to 6.2, but larger historical events have occurred without producing surface fault rupture. It is unlikely that repeated events larger than about magnitude 7 could occur without producing surface evidence. Given the regional strike-slip model, the values included in the analysis and their associated probability weights are Mw 6.0 (0.3), Mw 6.5 (0.5), and Mw 7.0 (0.2).

There are no reported slip rates for a postulated hidden strike-slip fault beneath Crater Flat basin. For this analysis, we assumed that all the horizontal extension on the Quaternary faults at the surface occurs as strike slip on a northwest-trending fault at depth. Accordingly, the range of slip rates estimated for the Highway 95 fault also was used for the postulated hidden strike-slip fault (Table DFS-7).

5.0

FAULT DISPLACEMENT

The objective of the fault displacement characterization is to develop general procedures and perform evaluations for input to assess the probability of fault displacement (hazard curves that relate annual probability to amount of displacement) for any location within the controlled area at Yucca Mountain, given the structural characteristics at the specified location. Nine test calculations sites were identified during Seismic Source Characterization (SSC) Workshop 4 to represent the range of expected fault conditions within the Controlled

Area. At two locations, four alternative fault conditions are considered. The locations of the nine test calculation sites are shown on Figure DFS-14. They include:

- (1) the Bow Ridge fault where it crosses the Exploratory Studies Facility (ESF);
- (2) the Solitario Canyon fault where it trends toward the repository block;
- (3) the Drill Hole Wash fault where it crosses the ESF;
- (4) a point along the Ghost Dance fault near the center of the controlled area;
- (5) a point along the Sundance fault west of the ESF;
- (6) a minor unnamed fault west of Dune Wash;
- (7) a point 100 m east of the Solitario Canyon fault that has:
 - (a) a small fault having 0.5 to 2 m cumulative displacement,
 - (b) a shear having about 10 cm cumulative displacement,
 - (c) a fracture having no measurable displacement, or
 - (d) intact rock;
- 8) a point midway between the Solitario Canyon and Ghost Dance faults that has:
 - (a) a small fault having 0.5 to 2 m cumulative displacement,
 - (b) a shear having about 10 cm cumulative displacement,
 - (c) a fracture having no measurable displacement, or
 - (d) intact rock;
- 9) a point along the Exile Hill fault in Midway Valley where fractures having no measurable offset have been observed in Quaternary alluvium.

5.1 GENERAL APPROACH FOR CHARACTERIZING FAULT DISPLACEMENTS

The underlying basis for assessments of fault displacement hazard is that future fault slip will recur at the same locations and in the same manner as geologically recent displacements (ASCE, 1997). Future fault displacements are most likely to occur on pre-existing faults, and the likelihood of future displacements is related to the frequency of most recent displacements. Accordingly, the most reliable assessments of the potential for fault

displacement are based on direct geologic evidence regarding the recent history (Quaternary) of past displacements.

Quaternary deposits that would enable direct assessment of recent faulting are not present over most of the Controlled Area. Also, many of the features encountered at the level of the proposed repository cannot be related directly to observed surface faults. Therefore, the analysis must rely on indirect methods that relate the character of the displacements observed in the repository host rock (late Miocene Tiva Canyon Tuff) to the probable Quaternary displacement history on these features based on our knowledge of the geologic evolution of Yucca Mountain. The methods used are calibrated using data from selected locations for which we have data on fault displacement in both the Tiva Canyon Tuff and the overlying Quaternary deposits.

Fault slip rate is the basic parameter used in this analysis to characterize the potential for the fault displacement. It is a useful parameter for: (1) assessing the fault displacement history (e.g., for comparing late Miocene faulting to Quaternary faulting on a given structure); (2) for comparing the relative hazard posed by different faults; and (3) for constraining the recurrence and/or the slip per event on a given fault. The following relation between slip rate (SR), average recurrence interval (RI), and average displacement per event (D) is important because the slip rate effectively constrains the hazard (amount of displacement and likelihood of occurrence):

$$SR = \frac{D}{RI}$$

Given the low slip rates on faults at Yucca Mountain, the average displacements must be small, or the average recurrence intervals must be long. Based on estimates of slip rate, one can use information on the average recurrence interval to calculate the average displacement per event. Alternatively, one can use information on displacement per event to calculate recurrence interval. Both approaches are used in this analysis to assess the fault displacement hazard on features for which we have slip rates (i.e., features having a measurable cumulative displacement). If the features have no detectable cumulative offset (no slip and, therefore, no slip rate), a different approach is required. The displacement characterization based on fault-

slip rate are presented in Section 5.2. The potential for displacement along fractures and in unbroken rock is discussed in Section 5.3.

5.2 POTENTIAL FOR DISPLACEMENT ON IDENTIFIED FAULTS

The logic tree used to characterize the fault displacement on the identified faults in the controlled area is shown on Figure DFS-15. The parameters used to characterize the fault displacement include:

- fault activity,
- the cumulative displacement on post-Tiva Canyon Tuff,
- the average Quaternary slip rate,
- the average displacement per event,
- the average recurrence interval, and
- the event-to-event variability in the displacement per event at a point along a fault.

Each of these factors is discussed below.

5.2.1 Fault Activity

In the context of assessing fault displacement hazard, the activity of a fault is the likelihood that the feature has undergone movement (slip) in response to tectonic forces during the present tectonic regime (the Quaternary). It includes all types of fault slip (primary and secondary faulting), except displacements due to near-surface gravitational effects such as landslides, effects of liquefaction, and effects of differential compaction.

If the fault at a test calculation site has had Quaternary displacement, we assigned it a probability of activity of 1.0 (unless there is evidence that suggests the displacements were not tectonic). Only the north-south block-bounding faults at Yucca Mountain have demonstrated evidence of Quaternary displacement. These include the Bow Ridge fault (Test Calculation Site #1) and the Solitario Canyon fault (Test Calculation Site #2). These faults are assigned a probability of activity of 1.0 (Table DFS-8).

Two zones of fractures having no detectable slip have appeared at least twice in the Quaternary alluvial and colluvial deposits that overlie north-northeast-trending bedrock faults

along the east side of Exile Hill in Midway Valley (Test Calculation Site #9; F.H. Swan *et al.*, Geomatrix Consultants, written communication, 1995; W. R. Keefer and J. W. Whitney, USGS, written communication, 1996). The fracturing occurred repeatedly (at least twice) during stratigraphically distinct episodes. Non-tectonic mechanisms for the formation of these fractures cannot be ruled out, but it seems unlikely given the consistent orientation of the fractures, the continuity of the zones along strike, the coincidence of the western zone of Quaternary fractures with the Exile Hill fault, and the fact that individual fractures in the Quaternary deposits can be traced into faults in the underlying Tertiary bedrock. The Exile Hill fault is assigned a probability of activity of 0.8.

In Section 4.3.1, we assigned a very low probability (0.05) that the Ghost Dance fault (Test Calculation Site #4) is active and capable of generating significant earthquakes. In addition to the lack of evidence for Quaternary displacement, the low weight reflects our interpretation that the small-displacement intrablock faults probably represent secondary accommodation structures rather than primary, earthquake-generating structures. Because the fault displacement hazard assessment includes the effects of both primary and secondary faulting, the probability that a fault can move is not necessarily the same as the probability that it can generate significant earthquakes. The evidence suggests there has been no displacement on the Ghost Dance fault since at least the middle Pleistocene (E.M. Taylor *et al.*, USGS, written communication, 1996a). However, very small movements similar to the fractures observed along the Exile Hill fault cannot be precluded. Based on analogy to the Exile Hill fault and consideration of structural models that suggest that the Ghost Dance fault could move in response to displacements on the block-bounding faults, we give a low but significant probability that the Ghost Dance fault has experienced a small amount of Quaternary displacement. That the fault is active and capable of displacement is assigned a probability of 0.4.

There is no evidence that any of the northwest-trending faults in the vicinity of Yucca Mountain have experienced Quaternary displacement. These include the Drill Hole Wash fault (Test Calculation Site #3) and the Sundance fault (Test Calculation Site #5). Middle Pleistocene and older deposits overlie northwest-trending faults exposed in trenches on the east side of Exile Hill, providing direct evidence of no displacement during the period of repeated displacements along the north-south block-bounding faults (F.H. Swan *et al.*,

Geomatrix Consultants, written communication, 1996). This strongly suggests that the faults are not kinematically linked under the present tectonic regime. However, Quaternary displacement cannot be precluded at Test Calculation Sites #3 and #5. Right-slip movement on northwest-striking faults is compatible with some structural models for Yucca Mountain (e.g., vertical axis rotation of the structural blocks). Day *et al.* (1996c, p. 2-6) present evidence that the north-striking and northwest-striking faults have been kinematically linked sometime during their displacement history. Movement on the northwest-striking faults is compatible with the inferred orientation of the present stress field. Considering these factors, we assign a very low probability that there has been Quaternary displacement on Drill Hole Wash and Sundance faults. The probability of activity assigned to these structures is 0.01.

The activity of the unnamed fault west of Dune Wash is more uncertain. Its north-south trend and position relative to the block-bounding faults suggest a potential for slip similar to that of the Ghost Dance fault. We assigned it the same probability of activity (0.4).

Test Calculation Sites #7 and #8 contain very small faults, fractures, or unbroken rock at two locations within the proposed repository area: one 100 m east of the Solitario Canyon fault, the other midway between the Solitario Canyon and Ghost Dance faults. The activity of fractures and unbroken rock is addressed in Section 5.3.1. Small-displacement faults (less than about 3 m) are common throughout the Controlled Area. The following factors should be considered when assessing the activity of these features.

- **Orientation.** Paleoseismic evidence of Quaternary displacement has been found only along the north-south-trending faults. Faults having other trends presumably have a much lower probability of being active (perhaps an order of magnitude or more).
- **Faults that die out during the Miocene.** Many of the small-displacement faults die out upward within the Tertiary section and are pre-latest Miocene in age, precluding any Quaternary displacement. Where this can be demonstrated, the probability of future displacement should be assessed using the approach outlined in Section 5.3.

- **Position relative to active block-bounding faults.** Secondary deformation is more likely to occur on the hanging wall than on the footwall; the zone of deformation typically is much narrower on the footwall of normal faults.
- **Distance from the active block-bounding faults.** Secondary deformation typically is most concentrated immediately adjacent to and within a few meters of a fault. It can, however, occur tens, hundreds, and even thousands of meters from the primary fault trace. There is no relation that reliably predicts the amount or likelihood of secondary faulting related to distance from a primary fault trace. Nonetheless, based on historical earthquakes, it is reasonable to infer that the probability of secondary faulting decreases significantly (by an order of magnitude or greater) at distances more than a few meters to a few tens of meters from a primary fault.

The only information given about Test Calculation Sites #7 and #8 is their location (distance from the active block-bounding faults) and the cumulative displacement of the Tertiary bedrock. Both locations are thousands of meters from the Bow Ridge fault. Secondary (hanging wall) deformation at these locations caused by slip on the Bow Ridge fault is unlikely. Test Calculation Site #7 is 100 m east of the main trace of the Solitario Canyon fault (i.e., in the footwall), but it is about the same distance west of a northeast-trending splay of the Solitario Canyon fault. Test Calculation Site #8 is more than 800 m east of the Solitario Canyon fault. The probability that there has been Quaternary displacement at either of these locations is judged to be extremely low. Based on its closer proximity to one of the active block-bounding faults, Test Calculation Site #7 is assigned a higher probability of activity than site #8. The probability of activity assigned to small faults (either 10 cm or 2 m cumulative slip) at sites #7 and #8 are 0.05 and 0.01, respectively.

5.2.2 Cumulative Displacement and Age of the Tiva Canyon Tuff

At most of the test calculation sites, the only basis for estimating fault slip rate is the cumulative net slip of the faulted bedrock. At the proposed repository level, this is the 12.7 ± 1.3 Ma Tiva Canyon Tuff. Table DFS-8 gives the cumulative net slip of the Tiva Canyon Tuff at the nine test calculation sites. The reported values are specific to the individual sites and do not represent average values along the length of the fault. The cumulative displacements are based on: geologic maps and geologic cross sections of Yucca Mountain (Scott and Bonk, 1984; W.C. Day *et al.*, USGS, written communication, 1996c,d), and geologic reports (J.D. Gibson *et al.*, SNL, written communication, 1992, Tables 4-1 and 4-2;

F.H. Swan *et al.*, Geomatrix Consultants, written communication, 1995, Table 9). Values shown may differ somewhat from previously published values because, in some cases, adjustments were made for a lateral component to net slip, and/or allowances were made for more uncertainty in the range of values.

Except for test calculation sites 7b, 7c, 8b, and 8c, where the displacements are inferred to be known based on direct observation, the displacements are reported as a range of values to include uncertainties related to:

- measurement errors (associated with measurement of dip slip from geologic cross sections and measurement of stratigraphic throw across the fault from geologic maps having 10- to 20-foot contour intervals);
- extrapolations of the dip slip along the strike of the fault in cases where the measured bedrock displacements are not coincident with the test calculation site; and/or
- uncertainties in the lateral slip component of the net slip.

The range of values and assigned probability weights for the cumulative displacement of the Tiva Canyon Tuff are presented in Table DFS-8.

The age of the Tiva Canyon Tuff used in this analysis, 12.7 ± 1.3 Ma, is based on the range of values presented in tables compiled by J.D. Gibson *et al.* (1990, and SNL, written communication, 1992, Table 4-1).

5.2.3 Average Quaternary Slip Rate

Four approaches were used to estimate the average Quaternary slip rate. Where paleoseismic data are available on the amount and timing of Quaternary displacements, these data were used to calculate the slip rate directly. In most cases, however, there is little or no geologic information to directly assess the Quaternary slip rate. Therefore, estimates also are made based on site-specific assessments of cumulative net slip of the Tiva Canyon Tuff and three different structural/historical interpretations of the late Cenozoic evolution of faulting at Yucca Mountain. Locations for which there are data on both the post-late Miocene and Quaternary displacements (e.g., Test Calculation Sites #1, #2, and #9) provide a means for

calibrating the reliability of the methods based on the post-Tiva Canyon Tuff cumulative net slip. The basis for each approach is described below.

Quaternary Slip Rates Based on Paleoseismic Data. Where possible, the rate of deformation is based on the amount of displacement and ages of Quaternary deposits, soils, and/or geomorphic features overlying the faults. The Quaternary slip rates (and the associated uncertainty) for the Bow Ridge and Solitario Canyon faults are based on the results of detailed paleoseismic investigations at or near Test Calculation Sites #1 and #2. The Quaternary slip rate on the Ghost Dance fault is based on the absence of evidence for Quaternary displacement, inferences about the threshold of detection and analogy to the Exile Hill fault (F.H. Swan *et al.*, Geomatrix Consultants, written communication, 1995). The range of values and the corresponding probability weights used in the fault displacement hazard analysis are presented in Table DFS-9.

Uniform Slip Rate, Post-Tiva Canyon Tuff. In this interpretation, the average post-Tiva Canyon slip rate is assumed to be approximately equal to the average late Quaternary slip rate. Slip rates are calculated by dividing the post-Tiva Canyon Tuff cumulative net slip by 12.7 ± 1.3 Ma.

Uniform Slip Rate, Post-Rainier Mesa. J.D. Gibson *et al.* (SNL, written communication, 1992, p. 72) suggest that an abrupt decrease in the slip rate on the block-bounding faults at Yucca Mountain may have occurred prior to 7 Ma (dashed line on Figure DFS-16). This abrupt decrease in slip rate may correlate to the marked decrease in silicic volcanic activity. Structural data (Scott and Bonk, 1984) indicate that most (70 to 80 percent) of the displacement on the Bow Ridge and Paintbrush Canyon faults predates the deposition of the Rainier Mesa member of the Timber Mountain Tuff (11.6 ± 1 Ma). In this interpretation, 80 percent of the post-Tiva Canyon displacement is interpreted to have occurred prior to deposition of the Rainier Mesa, and the average post-Rainier Mesa slip rate is inferred to be approximately equal to the average late Quaternary slip rate. Slip rates are calculated by dividing 20 percent of the post-Tiva Canyon Tuff cumulative displacement by 11.6 ± 1 Ma.

Decreasing Slip Rate Model. J.D. Gibson *et al.* (1990 and SNL, written communication, 1992) suggest an alternative interpretation of the slip rates on the Bow Ridge

and Paintbrush Canyon faults in which the slip rates have decreased continuously since the late Cenozoic (solid line on Figure DFS-16). W.C. Day *et al.* (USGS, written communication, 1996b) present data that indicate that the rate of crustal extension in the Crater Flat basin has been decreasing since the middle Miocene, when the rate of extension is estimated to have been between 18 and 40 percent, to the Quaternary (Figure DFS-17). Their estimates of the Quaternary rate of extension range from 0.1 percent to 0.7 percent. This suggests that Quaternary slip rates could be between 0.3 percent and 3.9 percent of the late Miocene rate.

In this interpretation, the Quaternary slip rate is estimated by multiplying the late Miocene slip rate by a reduction factor. The late Miocene (i.e., post-Tiva Canyon, pre-Rainier Mesa) slip rate is calculated by dividing 80 percent of the post-Tiva Canyon displacement by the interval between the deposition of these units. The duration of this interval is uncertain. The difference between the preferred ages for the two units (i.e., 12.7 Ma and 11.6 Ma) suggests an interval of 1.1 Ma. Considering the reported uncertainties in the ages of the two units yields a maximum age of 4.4 Ma, which is unreasonably long, and a minimum age difference of - 0.5 Ma, which is geologically impossible because the Rainier Mesa is not older than the Tiva Canyon Tuff. The interval between the deposition of the Tiva Canyon Tuff and the deposition of the Rainier Mesa member of the Timber Mountain Tuff is probably within the range of 1.1 ± 0.6 Ma.

Accordingly, the average Quaternary slip rate (SR) is:

$$SR = \frac{0.8 D_{tc}}{1.1 \pm 0.6 \text{ Ma}} RF$$

where D_{tc} is the cumulative net slip on the Tiva Canyon Tuff and RF is the reduction factor, which is in the range of 0.3% to 3.9%.

Slip rates calculated using this approach are compared to rates based on paleoseismic information in Table DFS-10 to assess the reliability of the interpretation. Reduction factors of 2.1 % (the midpoint of the range) to 3.9% (the minimum reduction based on Fridrich *et al.* data; Figure DFS-17) yield rates that are in general accord with the estimates based on

paleoseismic information. A reduction factor of 0.3 % (the maximum reduction suggested by Fridrich *et al.* data) yielded values that are considered too low (Table DFS-10). Based on this comparison, the probability weights assigned to the values for the reduction factor are: 0.3 % (0.04), 2.1 % (0.48), and 3.9 % (0.48) (Figure DFS-18).

Relative Weights Assigned to Techniques for Estimating Slip Rate. Quaternary slip rates based on paleoseismic data are not available for all the test calculation sites. Therefore, the relative weights assigned to the four techniques described above are dependent on the availability of paleoseismic data (Figure DFS-18). Slip rates based on the amount of displacement and ages of faulted Quaternary units provide the most reliable indication of the current slip rate and are given the greatest weight (0.7) if these data are available. There is not a strong consensus among geologists as to which of the three models for the late Cenozoic evolution of faulting at Yucca Mountain is most likely. Therefore, the three slip rate models based on the cumulative net slip of the Tiva Canyon Tuff are assigned equal weights.

5.2.4 Potential for Fault Rupture

The approaches described above are used to calculate the probability distribution for the Quaternary slip rate at each of the nine test calculation sites. Given the slip rate, the average interval between displacement events can be calculated by dividing the average displacement per event by the slip rate. Alternatively, the average displacement per event can be calculated by multiplying the slip rate times the average recurrence interval. Both methods are given equal weight in the fault displacement hazard analysis (Figure DFS-15).

Site-specific assessments of the average displacement per event and the average recurrence interval are made for each of the faults at the nine test calculation sites based on the available information (Table DFS-11). To the extent possible, these assessments are based on fault specific data on the size and timing of Quaternary faulting events. Where there are no data on the size and/or timing of Quaternary displacements (e.g., due to the absence of evidence of displacement, or due to the lack of suitable Quaternary strata), the displacement per event and recurrence interval are characterized based on analogy to similar faults.

#1 Bow Ridge Fault

Average Displacement Per Event. C.M. Menges and J.W. Whitney (USGS, written communication, 1996b, Table 4.4.3) report a maximum range of from 1 to 80 cm for the net slip associated with past surface faulting events on the Bow Ridge fault at Trench 14D, which is at the same latitude as the ESF-Bow Ridge fault crossing. If 80 cm is taken as the upperbound displacement, this suggests an average slip per event of about 46 cm (i.e., 80 cm/1.73; see Table DFS-13).¹ Menges and Whitney's preferred values for individual events identified in this trench are: 13 cm, 14 cm, and 44 cm. If 44 cm represents the maximum displacement at this location, one would expect the average displacement to be about 25 cm (44 cm/1.73), which is close to the numerical average of their preferred values (i.e., 24 cm). Based on these observations, the range of values for the average slip per event where the Bow Ridge fault crosses the ESF is considered to be 10 cm (0.15); 20 cm (0.7); and 40 cm (0.15).

Average Recurrence Interval. C.M. Menges and J.W. Whitney (USGS, written communication, 1996b, Table 4.4.5) report a range of 70 ka to 215 ka for the average recurrence interval on the Bow Ridge fault at this location (Trench 14D). Their preferred range is between 100 ka and 140 ka. Based on these data, we considered the following range of values for the average slip rate: 70 ka (0.1); 100 ka (0.4); 140 ka (0.4); and 215 ka (0.1).

#2 Solitario Canyon Fault

Average Displacement Per Event. Site #2 is located on the Solitario Canyon fault approximately midway between trenches SCF-T4 and T8. The Quaternary fault displacement data reported by A.R. Ramelli *et al.* (Nevada Bureau of Mines and Geology, written communication, 1996, Table 4.7.3) indicate that the cumulative displacement and the average displacement per event increase to the south. Accordingly, one would expect the average displacement at site #2 to be greater than the values obtained at trench SCF-T4 and less than those at T8.

The values reported from trench SCF-T4 (A.R. Ramelli *et al.*, Nevada Bureau of Mines and Geology, written communication, 1996, Table 4.7.3) range from fractures having no movement up to 40 cm. If 40 cm is the maximum at this location, it suggests an average

¹ The relation between maximum and average displacement used here is based on analysis of the variability in the single event displacements observed in the Yucca Mountain trenches. (See Section 5.2.5 for details.)

displacement per event of about 23 cm (40 cm/1.73). The average displacement for the three most recent events is about 20 cm.

The maximum values reported from trench T-8 range from 10 cm to 130 cm. If 130 cm is the upperbound displacement for a single event at this location, it suggests an average displacement per event of ≤ 75 cm (i.e., 130 cm/1.73). Averaging the reported values from the four most recent events yields an average displacement per event of about 50 cm.

Extrapolating these data suggests the average displacement per event at site #2 probably is in the range of 35 to 45 cm. Because of the uncertainty inherent in such an extrapolation, a wider range of values is considered. The range of values considered in the fault displacement hazard analysis for the average displacement per event at site #2 on the Solitario Canyon fault is: 20 cm (0.2); 40 cm (0.6); and 60 cm (0.2).

Average Recurrence Interval. Based on the results of paleoseismic investigations, A.R. Ramelli *et al.* (Nevada Bureau of Mines and Geology, written communication, 1996, p. 4.7-48) suggest that the minimum recurrence interval on the Solitario Canyon fault is about 35 ka and the maximum is about 100 ka. Based on the occurrence of three or four events during about the past 200 ka, they estimate that the average recurrence interval ranges from 50 to 70 ka. The values included in the fault displacement hazard analysis and the assigned probability weights are: 35 ka (0.2); 50 ka (0.3); 70 ka (0.3); and 100 ka (0.2).

#4 Ghost Dance Fault

Average Displacement Per Event. With the possible exception of fractures, there is no evidence of Quaternary movement on the Ghost Dance fault (E.M. Taylor *et al.*, USGS, written communication, 1996a). However, we assign a low probability that movement can occur in the future. Three approaches were used to characterize the possible average displacement per event.

- (1) If the Ghost Dance fault is considered to be an independent seismogenic source, which is judged to be very unlikely (see Section 4.3.1), the Wells and Coppersmith (1984) relation between average displacement and fault rupture length can be used to calculate the average displacement along strike associated with rupture of the entire length of the fault. The data set of historical earthquakes

on which this relation is based is only marginally applicable to faults as short as the Ghost Dance fault, which has a mapped length of about 3 km (Day *et al.*, 1996b, p. 2-6). If the Ghost Dance fault is combined with the Abandoned Wash fault, the total fault length is about 9 km. Using this approach, rupture lengths of 3 to 9 km suggest a maximum value for the average displacement in the range of 8 to 22 cm.

- (2) If displacement on the Ghost Dance fault occurs as secondary deformation in the hanging wall of either the Bow Ridge or Paintbrush Canyon faults, the maximum displacement on the Ghost Dance fault would be significantly less than the slip per event on either of these faults. Based on displacement per event data summarized by S.K. Pezzopane *et al.* (USGS, written communication, 1996a, Table 5-1), the average displacement per event on the Bow Ridge and Paintbrush Canyon faults (i.e., at about the same latitude as Test Calculation Site #4 on the Ghost Dance fault) is about 24 cm and 55 cm, respectively. If the secondary displacements scale in proportion to the cumulative bedrock displacement on these faults, the average slip per event on the Ghost Dance fault is about 5 cm (25m/130m x 24 cm per event for the Bow Ridge fault; or 25m/300m x 55 cm per event for the Paintbrush Canyon fault).
- (3) Considering the Quaternary displacement history on the Ghost Dance fault to be similar to the small north-south intrablock faults in Midway Valley, suggests that Quaternary movements have been limited to fractures having slip amounts that are less than the threshold of detection. The threshold of detection on the fracturing events in Midway Valley ranges from a few millimeters or less (essentially zero displacement) to not more than 5 cm (F.H. Swan *et al.*, Geomatrix Consultants, written communication, 1995).
- (4) Considering all three approaches, the range of values included in the hazard characterization for the average displacement per event at site #4 on the Ghost Dance fault is: 0.05 cm (almost zero displacement) (0.3); 1 cm (0.25); 3 cm (0.2); 5 cm (0.15); 10 cm (0.07); and 15 cm (0.03).

Average Recurrence Interval. The available data indicate there has been no displacement on the Ghost Dance fault for approximately the past 100 ka (no displacements since the late Pleistocene). If the Ghost Dance fault can move in the present tectonic regime, the recurrence interval is presumably longer than about 100 ka. In the context of neotectonic studies, average recurrence intervals longer than half a million years probably are not meaningful. Given the lack of any evidence suggesting a particular recurrence interval, we assumed that, if the fault can move, the average recurrence interval is essentially equally

likely to be anywhere in the range of 100 to 500 ka with a slight chance that the recurrence interval could be as short as 50 ka. The range of values included in the fault displacement hazard analysis and the assigned probability weights are: 50 (0.005); 100 ka (0.1); 200 ka (0.25); 300 ka (0.25); 400 ka (0.25); and 500 ka (0.145).

#3 Drill Hole Wash Fault and #5 Sundance Fault

No evidence of Quaternary displacement has been discovered along any of the northwest-striking faults in the Yucca Mountain area. If the faults are capable of movement in the present tectonic regime, the movement probably occurs in response to movement on the more active north-striking Quaternary faults. The average displacement per event is certainly less than that along the north-south block-bounding faults and probably is less than the Ghost Dance fault. For the purpose of the fault displacement hazard analysis, the same displacement and recurrence parameters used to characterize the average displacement per event and average recurrence interval on the Ghost Dance fault also were used to characterize the Drill Hole Wash and Sundance faults.

#6 Unnamed Fault West of Dune Wash

There are no data on the Quaternary displacement history of this fault. Its orientation and location within the Yucca Mountain block are similar to the Ghost Dance fault, but it has a shorter total fault length and smaller cumulative displacement. Except for the difference in slip rate, site #6 is considered to have a potential for displacement that is similar to that of site #4 on the Ghost Dance fault (Table DFS-8). The same parameters used to characterize the average displacement per event and average recurrence interval on the Ghost Dance fault also were used to characterize the unnamed fault at Test Calculation Site #6.

Test Calculation Sites #7a, #7b, #8a, and #8b

The fault displacement hazard at these sites was treated the same except that sites #7b and #8b have lower slip rates due to their smaller cumulative displacement (10 cm versus 2 m), and site #7 is assigned a higher potential for activity (Table DFS-8) than site #8 because it is closer to an active block-bounding fault (Section 5.2.1).

Average Displacement Per Event. If movement can occur on these small intrablock faults, the average displacement per event would be less than or similar to that of Exile Hill fault

(see below). The same range of values included in the analysis for the Exile Hill fault is used to characterize the 2-m faults. In characterizing the 10-cm faults, the range is extended to include a minimum value of 0.05 cm and more weight is assigned to the low end of the range (Table DFS-11).

Average Recurrence Interval. There are no data that suggest how these short, small-displacement faults and shears behave during repeated faulting events. Therefore, a wide range of behavior is considered. If these features are capable of movement, the minimum recurrence is a single event during the present tectonic regime. For the purpose of this analysis, the period of the present tectonic regime is considered to be the Quaternary, or approximately the past 1.6 ma. The maximum recurrence rate would occur if minute displacements occurred every time there is a large-magnitude local earthquake in the immediate vicinity (e.g., on the block-bounding faults). The results of paleoseismic investigations (USGS, written communication, 1996) suggest that surface faulting events on the block-bounding faults might occur as frequently as about once every 50,000 years. This is judged to be an upper bound for the average recurrence interval for events large enough to produce secondary displacement within the Yucca Mountain block. Given the lack of evidence for a particular recurrence interval, we judge that the average recurrence interval is more or less equally likely to be anywhere in the range of 100 to 500 ka (the same as for the Ghost Dance fault) and that there is a small chance that the recurrence interval could be as long as 1.6 ma or as short as 50 ka. The range of values included in the fault displacement hazard analysis and the assigned probability weights are: 50 ka (0.05); 100 ka (0.18); 200 ka (0.18); 300 ka (0.18); 400 ka (0.18); 500 ka (0.18); and 1600 ka (0.05).

#9 Exile Hill Fault in Midway Valley

Average Displacement Per Event. Except for two zones of fractures identified in trenches, the evidence indicates that there has been no Quaternary displacement (within the limits of detection) on the Exile Hill fault in Midway Valley (F.H. Swan *et al.*, Geomatrix Consultants, written communication, 1995; W.R. Keefer and J.W. Whitney, USGS, written communication, 1996). Considering the resolution for detecting displacements, some small displacement can not be ruled out. Three approaches were used to characterize the average displacement per event.

1. The total length of the Exile Hill fault is between < 2 km and 4.4 km. Using these values and the Wells and Coppersmith (1984) relation between average displacement and fault rupture length, we obtained displacements of < 5 cm to 11 cm.
2. If the Exile Hill fault represents secondary deformation in the footwall of the Bow Ridge fault or in the hanging wall of the Paintbrush Canyon fault, the maximum displacement on the Exile Hill fault would be significantly less than the slip per event on either of these faults. Based on displacement per event data summarized by S.K. Pezzopane *et al.* (USGS, written communication, 1996a, Table 5-1), the average displacement per event on the Bow Ridge and Paintbrush Canyon faults is about 24 cm and 55 cm, respectively. Scaling the secondary displacements in proportion to the cumulative bedrock displacement on these faults, suggests the average slip per event on the Exile Hill fault is about 2 cm (10m/130m x 24 cm per event for the Bow Ridge fault, or 10m/300m x 55 cm per event for the Paintbrush Canyon fault).
3. The results of the fault exploration trenches on the east side of Exile Hill indicate that the Quaternary displacements have been less than the threshold of detection. The threshold of detection on the fracturing events in Midway Valley ranges from a few millimeters or less (essentially zero displacement) to not more than 5 cm (F.H. Swan *et al.*, Geomatrix Consultants, written communication, 1995).

Considering these approaches, the range of values included in the hazard analysis for the average displacement per event at site #9 on the Exile Hill fault is: 0.05 cm (almost zero displacement) (0.35); 1 cm (0.3); 3 cm (0.2); 5 cm (0.1); and 10 cm (0.05).

Average Recurrence Interval. The data indicate there has been no detectable displacement on the Exile Hill fault since the Middle Pleistocene or longer. Given the lack of evidence suggesting a particular recurrence interval, we consider that, if the fault can move, the average recurrence interval is more or less equally likely (i.e., maximum uncertainty) to be anywhere in the range of 100 to 500 ka. The range of values included in the fault displacement hazard analysis and the assigned probability weights are: 100 ka (0.1); 200 ka (0.25); 300 ka (0.25); 400 ka (0.25); and 500 ka (0.15).

5.2.5 Event-to-Event Variability

The procedures described above provide a means for assessing the probability of average displacements at a specified fault crossing. It is also important to know how much

displacements are likely to vary from the average displacement. The event displacement data from Yucca Mountain paleoseismic investigations were compiled to assess: (1) the relationship between average displacement and the maximum displacement during successive events at a point along the fault; and (2) the variability in the amount of displacement during successive events at a point along the fault (not to be confused with the variability in displacement along strike during a single event).

S.K. Pezzopane *et al.* (USGS, written communication, 1996a, Table 5-1) compiled the event displacement data from the Yucca Mountain paleoseismic investigations. Table DFS-12 is a summary of the event displacement data for all localities where displacements for three or more events were reported. The average of the reported events is calculated for each locality. The ratio between the size of each event and the average displacement at that locality is also calculated. The maximum reported displacement at each locality ranges from 1.03 to 2.63 times the average displacement; on average (based on 19 localities), the maximum displacement is 1.73 times the average displacement (Table DFS-13).

Figure DFS-19 is a frequency plot showing event-to-event variability in displacement based on the displacement data (ratio of the reported displacement for an event, D , to the average displacement at the same location, AD) presented on Table DFS-12. A generalization of this frequency distribution (i.e., the dashed line on Figure DFS-19) was used to define a triangular distribution for the ratio D/AD . The Facilities Team analyzed the data in Table DFS-12 and found that a better fit is obtained with a gamma distribution (see Appendix H, Section H.2.1). We adopt the distribution given in Appendix H for characterizing the distribution of displacement at a point.

5.3 POTENTIAL FOR DISPLACEMENT ON FRACTURES AND UNBROKEN ROCK

Fractures and unbroken rock have no cumulative displacement and, therefore, no slip rate. Consequently, the slip-rate approach used above to assess the potential for displacement on faults must be modified to assess the potential for displacement on fractures or in unbroken rock. The approach adopted for this analysis is based on the premise that, given the non-

occurrence of an event and a long observation period, the annual probability of the event occurring must be less than 1 divided by the duration of the observation period.

The logic tree for characterizing the displacement hazard on fractures and unbroken rock is presented in Figure DFS-20. The elements considered in assessing displacement hazard at Test Calculation Sites #7c, #7d, #8c, and #8d include:

- the potential for activity,
- relative probabilities associated with the different deformation history models,
- age of the host rock, and
- constraints on the size of an event based on the threshold of detection for fault displacement.

Uncertainties in the age of the host rock were discussed in Section 5.2.2. The other elements are discussed below.

5.3.1 Potential for Activity

If one applies the definition of activity as used to characterize faults (Section 5.2.1), fractures and unbroken rock would be classified as not active (i.e., they have had no displacement during the present tectonic regime), which implies that they have no potential for displacement during future periods of concern for repository performance. From a practical standpoint, this is true. Experience based on observations of historical surface faulting events and on detailed paleoseismic investigations of Quaternary fault movements shows that future fault movements can best be defined by recent past history and that the likelihood of new faulting is negligible (ASCE, 1997, p. 99). However, new faults must form some time. In the context of assessing fault displacement at locations where there has been no detectable displacement, the concept of activity, or potential for activity, is used to mean the relative likelihood that there could be displacement in the future. It is a relative approach whereby faults having known recent displacements would be assigned the highest weight (probability of 1), and intact rock far from active faults would have the lowest potential for activity (at least two or three orders of magnitude less likely). The factors for evaluating fault activity described in Section 5.2.1 were considered in our assessment of the potential for activity on fractures and in unbroken rock. In addition, information on the morphology of the fracture itself, such as degassing tracks that indicate formation during lithification of the tuff, may

provide clues to the origin and potential activity of a fracture. Table DFS-14 gives the subjective probability weights for potential for activity assigned to fractures and unbroken rock at Test Calculation Sites #7 and #8 and describes the basis for the assigned weights.

5.3.2 Probability of an Event Associated with Different Deformation History Models

In Section 5.2.3, three models were presented for characterizing the deformation history at Yucca Mountain. In one model, the rate of deformation has been uniform since deposition of the Tiva Canyon Tuff. In this interpretation, the annual probability of a displacement event, given no prior displacement, is less than 1 over the age of the host rock, which at the repository level is the Tiva Canyon Tuff. This corresponds to an annual probability of $<1 \times 10^{-7}$ (Table DFS-15).

In the other two models, the present rate of deformation is significantly less than the average long-term (post-Tiva Canyon Tuff) rate. If other factors such as the stress field have remained the same, the potential for deformation (movement on existing faults and/or formation of new faults) should be less now than they were during the late Miocene, when the rate is interpreted to have been much higher.

Considering the potential for displacement to be directly proportional to the rate of deformation, the probability of an event relative to the uniform deformation model can be expressed as the ratio between the inferred present rate and the average long-term post-Tiva Canyon rate times the probability of an event for the uniform deformation model. The range of probability values for the different deformation history models is given in Table DFS-15.

As discussed in Section 5.2.3, the three deformation history models are assigned equal weight (Figure DFS-20).

5.3.3 Threshold of Detection

Where there is no apparent displacement, it could be assumed that there has been a displacement too small to be detected. The size of the displacement is constrained by (less than) the threshold of detection. What is, the largest displacement that could have occurred at the location under consideration that could have gone undetected?

The threshold of detection depends on location-specific conditions. Are there sharp, well-defined marker horizons that record/preclude offsets? Is the rock massive or extensively fractured and/or sheared? What is the quality of the exposure? How extensive and detailed were the investigations to detect offsets? For the purpose of this analysis, we infer that the conditions would be typical of those parts of the ESF where the Tiva Canyon Tuff is well exposed and has been mapped in detail. Conditions may vary locally.

Investigations can more confidently preclude small displacements in unbroken rock than along a fracture. Therefore, the threshold of displacement detection is conditional on whether the rock is fractured or unbroken (Figure DFS-20).

Given the characteristics of the Tiva Canyon Tuff, we consider offsets larger than about 10 cm to be recognizable as observable stratigraphic offsets. Displacements smaller than a millimeter would be difficult to preclude, but smaller displacements obviously can occur; nominally we selected half a millimeter as the lower bound displacement. 10 cm and 0.05 cm were taken as the end members for the displacements on fractures. More commonly displacements in the range of 1 to 5 cm can be precluded. The range of values and assigned weights included in the fault displacement hazard analysis for the threshold of detection on well exposed fractures in the Tiva Canyon Tuff are: 0.05 cm (0.145); 0.1 cm, (0.2); 0.5 cm, (0.3); 1.0 cm, (0.2); 3 cm, (0.1); 5 cm, (0.05); and 10 cm, (0.005). The range of values for unbroken rock are: 0.05 cm (0.195); 0.1 cm, (0.3); 0.5 cm (0.25); 1.0 cm, (0.1); 3 cm, (0.1); 5 cm, (0.05); and 10 cm (0.005).

5.4 ESTIMATION OF FAULT DISPLACEMENT

The approach and hazard parameters described above are used to quantitatively assess the probability of fault displacement (hazard curves that relate annual probability to amount of displacement) for the nine test calculations sites. Because the approach used to characterize the hazard on faults is different from the approach used for fractures and unbroken rock, caution should be used when comparing or combining the results. If the input parameters and their uncertainties have been appropriately characterized, the slip-rate based approach used to assess the potential for displacement on faults should yield a realistic assessment of the actual hazard. However, the approach used to assess the displacement hazard on fractures or in

unbroken rock only constrains the upper bound for the hazard; it does not necessarily define the actual hazard. The actual hazard is likely to be less than the resultant values. The threshold of detection parameter gives maximum displacement values and the age of the host rock gives the minimum period for the non-occurrence of an event. The potential for activity parameter may compensate for the conservatism that is inherent in the other parameters, but we suspect the probability of future displacement may be much lower than indicated. This parameter is largely subjective and we have probably been overly conservative in assigning probability weights to potential for activity on fractures and in unbroken rock. Despite these limitations, we feel the results are useful because they indicate the hazard is extremely low.

The nine Test Calculation Sites that were selected to represent the range of conditions expected within the control area. Application of the evaluations of these sites to other parts of the control area is straightforward. However, one important substitution may need to be made depending on the application. Here we have used the displacement data that are location-specific to characterize the potential for displacement at that location. To characterize the potential for fault displacement along the length of a fault, one should use the average post-Tiva Canyon Tuff displacement (or average Quaternary slip rate) along the plane of the fault that intersects the Control Area instead of the average displacement at a specific location along the fault.

REFERENCES

- American Society of Civil Engineers (ASCE), 1997, Seismic and dynamic analysis and design considerations for high level nuclear waste repositories: A report by the Subcommittee on Dynamic Analysis and Design of High Level Nuclear Waste Repositories of the TA Committee on Dynamic Effects of the Technical Activities Division of the Structural Engineering Institute, J. Carl Stepp, ed., ASCE, New York, 185 pp., plus Appendices A through F.
- Anderson, R.E., Bucknam, R.C., Crone, A.J., Haller, K.M., Machette, M.N., Personius, S.F., Barnhard, T.P., Cecil, M.J., and Dart, R.L., 1995b, Characterization of Quaternary and suspected Quaternary faults, regional studies, Nevada and California: U.S. Geological Survey Open-File Report 95-599.
- Anderson, R.E., Crone, A.J., Machette, M.N., Bradley, L., and Diehl, S.F., 1995a, Characterization of Quaternary and suspected Quaternary faults, Amargosa area, Nevada and California: U.S. Geological Survey Open-File Report 95-613, 41 p.
- Atwater, T., 1989, Plate tectonic history of the northeast Pacific and western North America: Geological Society of America, *The Geology of North America*, v. N, p. 21-72.
- Bellier, O., and Zoback, M.L., 1995, Recent state of stress in the Walker Lane zone, western Basin and Range provinces, United States: *Tectonics*, v. 14, n. 3, p. 564-593.
- Bonilla, M.G., Mark, R.K., and Lienkaemper, J.J., 1984, Statistical relations among earthquake magnitude, surface rupture length, and surface fault displacement: *Bulletin Seismological Society of America*, v. 74, p. 2379-2411.
- Brocher, T. M., Hart, P. E., Hunter, W. C., and Langenheim, V. E., 1996, Hybrid-source seismic reflection profiling across Yucca Mountain, Nevada: regional lines 2 and 3: U. S. Geological Survey Open-File Report 96-28.
- Broxton, D.E., Warren, R.G., Byers, F.M., Jr., and Scott, R.B., 1989, Chemical and mineralogical trends within Timber Mountain-Oasis Valley caldera complex, Nevada: Evidence for multiple cycles of chemical evolution in a long-lived silicic magma system: *Journal of Geophysical Research*, v. 94, n. B5, p. 5961-5986.

- Burchfiel, B.C., Hamill, G.S., IV, and Wilhelms, D.E., 1983, Structural geology of the Montgomery Mountains and the northern half of the Nopah and Resting Springs ranges, Nevada and California: Geological Society of America Bulletin, v. 94, p. 1359-1376.
- Carr, W. J., Byers, F. M., Jr., and Orkild, P.P., 1986, Stratigraphic and volcano-tectonic relations of Crater Flat Tuff and some older volcanic units, Nye County, Nevada: U. S. Geological Survey Open-File Report 82-457, 23 p.
- Cornell, C.A., and Wintestein, S.R., 1986, Seismic hazard assessment: Chapter 5, in Hunter, R.L., and Mann, C.J., eds., Techniques for Determining Probabilities of Events and Processes Affecting the Performance of Geologic Repositories: NUREG/CR-3964, 1, P. 127-172, U.S. Nuclear Regulatory Commission, Washington, D.C.
- Cornwall, H.R., 1972, Geology and mineral deposits of southern Nye County, Nevada: Nevada Bureau of Mines and Geology Bulletin 77, 49 p., 1 plate.
- de Polo, C.M., and Slemmons, B.D., 1990, Estimation of earthquake size for seismic hazards, *in* Krimitzsky, E.L. and Slemmons, B.D. eds., Neotectonics in Earthquake Evaluation: Reviews in Engineering Geology, v. VII, Chapter 1, Boulder, CO, Geological Society of America.
- Dohrenwend, J.C., Menges, C.M., Schell, B.A., and Morning, B.C., 1991, Reconnaissance photogeologic map of young faults in the Las Vegas 10 X 20 quadrangle, Nevada, California, and Arizona: U.S. Geological Survey Miscellaneous Field Studies map MF-2182, scale 1:250,000.
- Ekren, E.B., Orkild, P.P., Sargent, K.A., and Dixon, G.L., 1977, Geologic map of the Tertiary rocks, Lincoln County, Nevada: U.S. Geological Survey Miscellaneous Investigations Series Map I-1041, scale 1:250,000.
- Faulds, J. E., Bell, J. W., Feuerbach, and Ramelli, A. R., 1994, Geologic map of the Crater Flat area, Nye County, Nevada: Nevada Bureau of Mines and Geology Map 101, 1:24,000 scale.
- Ferrill, D.A., Stirewalt, G.L., Henderson, D.B., Stamatakos, J.A., Morris, A.P., Spivey, K.H.C., and Wernicke, B.P.C., 1996, Faulting in the Yucca Mountain region: Critical review and analyses of tectonic data from the central Basin and Range: Center for Nuclear Waste Regulatory Analyses Report CNWRA 96-007 or NUREG/CR-6401, San Antonio, Texas, Rev. 01, variously paginated.

- Frankel, A., Mueller, C., Barnhard, T., Perkins, D., Leyendecker, E.V., Dickman, N., Hanson, S., and Hopper, M., 1996, National seismic-hazard maps; documentation June: U.S. Geological Survey Open-File Report 96-532, 110 p.
- Fredrich, C.J., 1997, Tectonic evolution of the Crater Flat basin, Yucca Mountain region, Nevada, in Wright, L.A. and Troxel B. W. (eds.), *Cenozoic Basins of the Death Valley Region, California and Nevada: Geological Society of America Special Paper* (in press).
- Fridrich, C. J., Whitney, J. W., Hudson, M. R., and Crowe, B. M., 1997, Space-time patterns of late Cenozoic extension, vertical-axis rotation, and volcanism in the Crater Flat basin, Nevada, in Wright, L. A. and Troxel B. W. (eds.) *Cenozoic Basins of the Death Valley Region, California and Nevada: Geological Society of America Special Paper* (in press).
- Frizzel, V.A., Jr., and Schulters, J., 1990, Geologic map of the Nevada Test Site, southern Nevada: U.S. Geological Survey Miscellaneous Investigations Series Map I-2046, scale 1:100,000.
- Gibson, J.D., Shephard, L.E., Swan, F.H., Wesling, J.R., and Kerl, F.A., 1990, Synthesis of studies for potential for fault rupture at the proposed surface facilities, Yucca Mountain, Nevada: *Proceedings of International Topical Meeting, High Level Radioactive Waste Management, April 8-12, v. 1, p. 109-116.*
- Gutenberg, B., and Richter, C.F., 1954, *Seismicity of the Earth: Princeton University Press, 2nd edition.*
- Harmsen, S. C., 1994, The Little Skull Mountain earthquake of 29 June, 1992: Aftershock focal mechanisms and tectonic stress field implications: *Bulletin of Seismological Society of America, v. 84, n. 5, p. 1484-1505.*
- Jenkins, O.P., 1962, *Geologic map of California, Trona Sheet: California Division of Mines and Geology, scale 1:250,000.*
- Keefer, W.R., and Pezzopane, S.K., 1996, Quaternary faults in the Yucca Mountain region: Chapter 3, in U.S. Geological Survey (Whitney, J.W., Coordinator), *Seismotectonic Framework and Characterization of Faulting at Yucca Mountain, Nevada: U.S. Geological Survey report to the Department of Energy that fulfills Level 3 Milestone 3GSH100M WBS Number 1.2.3.2.8.3.6, variously paginated.*
- Longwell, C.R., Pampeyan, E.H., Bowyer, B., and Roberts, R.J., 1965, *Geology and mineral deposits of Clark County, Nevada: Nevada Bureau of Mines and Geology Bulletin 62, 218 p., 16 plates.*

- Minor, S. A., Hudson, M. R., and Fridrich, C. J., 1996, Fault-slip data bearing on the tectonic development of northern Crater Flat basin, southern Nevada [abs.]: Geological Society of America Abstracts with Programs, v. 28, no. 7., p. A192.
- Oldow, J.S., Bally, A.W., Av'e Lallmont, H.G., and Leeman, W.P., 1989, Phanuajoic evolution of the North American Cordillera—United States and Canada: Chapter 8 in the geology of North America: Geological Society of America, v. A., p. 139-232.
- Piety, L.A., 1993, Compilation of known and suspected Quaternary faults within 100 km of Yucca Mountain: U.S. Geological Survey Open-File Report 94-112, 404 p., 2 plates.
- Piety, L.A., 1995, Compilation of known and suspected Quaternary faults within 100 km of Yucca Mountain: Technical Report prepared by U.S. Bureau of Reclamation in cooperation with the Nevada Operations Office, U.S. Department of Energy under Interagency Agreement DE-A108-92NV10874; U.S. Geological Survey Open-File Report 94-112.
- Reheis, M.C., 1988, Preliminary study of Quaternary faulting on the east side of Bare Mountain, Nye County, Nevada, in Carr, M.D., and Yount, J.C., eds., Geologic and hydrologic investigations of a potential nuclear waste disposal site at Yucca Mountain, southern Nevada: U.S. Geological Survey Bulletin 1790, p. 103-111.
- Saltus, R. W., and Thompson, G. A., 1996, Why is it downhill from Tonopah to Las Vegas: A case for mantle plume support of the high northern Basin and Range: Tectonics, v. 14, n. 6, p. 1235-1244.
- Sawyer, D.A., Fleck, R.J., Lanphere, M.A., Warren, R.G., Broxton, D.E., and Hudson, M.R., 1994, Episodic caldera volcanism in the Miocene southwest Nevada volcanic field: Revised stratigraphic framework, $^{40}\text{Ar}/^{39}\text{Ar}$ geochronologic framework, and implications for magmatism and extension: Geologic Society of America Bulletin, v. 106, n. 10, p. 1304-1318.
- Scholz, C.H., Barazangi, M., and Sbar, M.L., 1971, Late Cenozoic evolution of the Great Basin, western United States, as an ensialic interarc basin: Geological Society of America Bulletin, v. 82, p. 2979-2990.
- Schweickert, R. A., 1989, Evidence for a concealed strike-slip fault beneath Crater Flat, Nevada: Geological Society of America Abstracts with Programs, v. 21, n. 9, p. A90.

- Scott, R. B., 1990, Tectonic setting of Yucca Mountain, southwest Nevada, in Wernicke, B. P., ed., Basin and Range tectonics at the latitude of Las Vegas, Nevada: Geological Society of America Memoir 176, p. 251-282.
- Scott, R.B., and Bonk, J., 1984, Preliminary geologic map of Yucca Mountain, with geologic sections: U.S. Geological Survey Open-File Report 84-494, scale 1:12,000.
- Simonds, F.W., Whitney, J.W., Fox, K.F., Ramelli, A.R., Yount, J.C., Carr, M.D., Menges, C.M., Dickerson, R.P., and Scott, R.B., 1995, Map showing fault activity in the Yucca Mountain area, Nye County, Nevada: U.S. Geological Survey Miscellaneous Investigations Series, Map I-2520, scale 1:24,000.
- Slemmons, D.B., 1997, Faults and earthquake magnitude, *in* State of the art for assessing earthquake hazards in the United States, Report 6: U.S. Army Engineers Waterways Experiment Station Miscellaneous Paper S-73-1, 129 p.
- Slemmons, 1982, Determination of design earthquake magnitudes for microzonation, in Proceedings, Third International Earthquake Microzonation Conference, Seattle, Washington: Earthquake Engineering Research Institute, v. 1, p. 110-130.
- Smith, K.D., Brune, J.N., Savage, M.K., Anooshehpour, R., dePolo, D, and Sheehan, A.F., 1996, The 1992 Little Skull Mountain earthquake sequence, Southern Nevada Test Site: Bulletin of the Seismological Society of America (in press).
- Smith, R. L., and Bailey, R. A., 1968, Resurgent cauldrons: Geological Society of America Memoir 116, p. 613-662.
- Snyder, D. B., and Carr, W J., 1984, Interpretation of gravity in a complex volcano-tectonic setting, southwestern Nevada: U. S. Geological Survey Open-File Report 81-1349, 50 p.
- Stepp, C., Whitney, J., Wong, I.G., Savy, J., Coppersmith, K., Abrahamson, N., Quittmeyer, R., and Sullivan, T., 1995, A probabilistic analysis of fault displacement and vibratory ground motion and the development of seismic design criteria for Yucca Mountain, Nevada, in Topical Meeting on Methods of Seismic Hazards Evaluation Focus '95: Las Vegas, Nevada, American Nuclear Society, p. 35-42.
- Stewart, J.H., 1988, Tectonics of the Walker Lane belt, western Great Basin-Mesozoic and Tertiary deformation in a zone of shear, in Ernst, W.G., ed., Metamorphism and crustal evolution of the western United States, Rubey Volume VII: Englewood Cliffs, New Jersey, Prentice Hall, p. 683-713.

- Streitz, R., and Stinson, M.C., 1974, Geologic map of California, Death Valley Sheet: California Division of Mines and Geology, scale 1:250,000.
- Swadley, W.C., and Huckins, H.E., 1990, Geologic map of the surficial deposits of the Skull Mountain quadrangle, Nye County, Nevada: U.S. Geological Survey Miscellaneous Investigations Series Map I [1972], scale 1:24,000.
- Veneziano, D., and Van Dyck, J., 1985, Statistical discrimination of "aftershocks" and their contribution to seismic hazard, in *Seismic Hazard Methodology for Nuclear Facilities in the Eastern United States*: EPRI Res. Project No. P101-29, EPRI/SOG 85-1, v. 2, Appendix A-4.
- Wells, D.L., and Coppersmith, K.J., 1994, New empirical relationships among magnitude, rupture length, rupture width, rupture area, and surface displacement: *Bulletin of the Seismological Society of America*, v. 84, p. 974-1002.
- Wernicke, B., 1995, Low-angle normal faults and seismicity—A review: *Journal of Geophysical Research*, v. 10, p. 201,159-20,174.
- Wesling, J.R., Swan, F.H., Thomas, A.P., and Angell, M.M., 1993, Preliminary results of trench mapping at the site of prospective surface facilities for the potential Yucca Mountain repository, Nevada [abs.]: *Geological Society of America, Abstracts with Programs*, v. 25, n. 5, p. 162.
- Wesnousky, S.G., 1986, Earthquakes, Quaternary faults, and seismic hazard in California: *Journal Geophysical Research*, v. 91, p. 12,587-12,631.
- Wright, L. A., 1989, Overview of the role of strike-slip and normal faulting in the Neogene history of the region northeast of Death Valley, California-Nevada, in, Ellis, M. A., ed., *Late Tertiary evolution of the southern Great Basin, Nevada*: Nevada Bureau of Mines and Geology Open-File Report 89-1, p. 1-11.
- Wyss, M., 1979, Estimating maximum expectable magnitude of earthquakes from fault dimensions: *Geology*, v. 7, p. 336-340.
- Young, S.R., Morris, A.P., and Stirewalt, G., 1993, Geometric analysis of alternative models of faulting at Yucca Mountain, Nevada, in *High level radioactive waste management: Proceedings of the Fourth Annual International Conference, Las Vegas, Nevada*, American Nuclear Society, La Grange Park, Illinois, v. 2, p. 1,818-1,825.
- Youngs, R.R., and Coppersmith, K.J., 1985, Implications of fault slip rates and earthquake recurrence models to probabilistic seismic hazard estimates: *Seismological Society of America Bulletin*, v. 75, p. 939-964.

Youngs, R.R., Swan, F.H., III, Power, M.S., Schwartz, D.P., and Green, R.K., 1987, Probabilistic analysis of earthquake and ground shaking hazard along the Wasatch Front, Utah, in Gori, P.O., and Hays, W.W., eds., Assessment of Regional Earthquake Hazards and Risk Along the Wasatch Front, Utah: U.S. Geological Survey Open File Report 87-585, p. M-1 to M-100.

TABLE DSF-1
SEISMIC SOURCE PARAMETERS FOR REGIONAL FAULT SOURCES
 (Page 1 of 2)

Fault (Designation on Fig. DSF-6)	Activity	Length (km)	Dip	Slip Rate (mm/yr)			Maximum Magnitude		
				Preferred	Maximum	Minimum			
1 Hunter Mt./Panamint (HM-PAN)	1	146 [1]	90	2.5 [.6]	3.2 [.2]	1.1 [.2]	7.0 [.2]	7.4 [.6]	7.6 [.2]
2 Furnace Creek/Fish Lake Valley (FC-FLV)	1	149 [1]	90	2.3 [.6]	4.6 [.2]	1.3 [.2]	7.0 [.2]	7.3 [.6]	7.6 [.2]
3 Death Valley (DV)	1	71 [1]	60W	2.5 [.6]	11.5 [.2]	0.08 [.2]	7.0 [.2]	7.2 [.6]	7.5 [.2]
4 Pahrump/Stewart Valley (PRP)	1	41 [1]	90		0.05 [.5]	0.005 [.5]	6.6 [.5]		7.0 [.5]
5 West Springs Mt. (WSM)	1	AB-29 km [5]	60W	0.06 [.6]	0.2 [.2]	0.02 [.2]	6.6 [.2]	6.8 [.6]	7.0 [.2]
		AC-51 km [5]		"	"	"	6.7 [.2]	7.0 [.6]	7.3 [.2]
6 West Pintwater Range (WPR)	1	55 [1]	60W		0.2 [.5]	0.02 [.5]	6.7 [.2]	7.0 [.6]	7.3 [.2]
7 Yucca (YC)	1	25 [1]	60E		0.2 [.5]	0.02 [.5]	6.5 [.2]	6.7 [.6]	7.0 [.2]
8 Emigrant Valley North (?) (EVN)	1	27 [1]	60W		0.2 [.5]	0.02 [.5]	6.5 [.2]	6.7 [.6]	7.0 [.2]
9 Oaks Spring Butte (OAK)	1	22 [1]	60E		0.2 [.5]	0.01 [.5]	6.5 [.2]	6.7 [.6]	7.0 [.2]
10 Belted Range (BLR)	1	50 [1]	60E		0.1 [.5]	0.01 [.5]	6.5 [.2]	6.8 [.6]	7.1 [.2]
11 Kawitch Range (KR)	1	AB-24 km [0.68]	60W		0.01 [.5]	0.001 [.5]	6.5 [.2]	6.7 [.6]	7.0 [.2]
		BC-33 km [0.1]		"	"	6.5 [.2]	6.8 [.6]	7.1 [.2]	
		AD-65 km [0.2]		"	"	6.9 [.2]	7.2 [.6]	7.5 [.2]	
		CD-74 km [0.02]		"	"	6.9 [.2]	7.2 [.6]	7.5 [.2]	
12 Rock Valley (RV)	1	AB-33 km [.6]	90		0.16 [.5]	0.02 [.5]	6.5 [.2]	6.8 [.6]	7.1 [.2]
		AC-47 km [.3]		"	"	6.7 [.2]	7.0 [.6]	7.3 [.2]	
		AD-64 km [.1]		"	"	6.9 [.2]	7.2 [.6]	7.5 [.2]	
13 Wahmonie (WAH)	1	15 [1]	60NW		0.01 [.5]	0.001 [.5]	6.5 [.8]		6.8 [.2]

TABLE DSF-1
SEISMIC SOURCE PARAMETERS FOR REGIONAL FAULT SOURCES
 (Page 2 of 2)

Fault (Designation on Fig. DSF-6)	Activity	Length (km)	Dip	Slip Rate (mm/yr)			Maximum Magnitude		
				Preferred	Maximum	Minimum			
14 Yucca Lake (YCL)	1	13 [1]	60NE		0.2 [.5]	0.02 [.5]	6.5 [.8]	6.8 -- [2]	
15 Eleana Range (ER)	1	11 [1]	60NE		0.2 [.5]	0.02 [.5]	6.5 [.8]	6.8 -- [2]	
16 Peace Camp (PC)	1	AB-19 km [7]	90		0.16 [.5]	0.02 [.5]	6.5 [.2]	6.6 [.6]	6.9 [.2]
		AC-31 km [3]		"	"	6.5 [.2]	6.8 [.6]	7.1 [.2]	
17 Amargosa/Gravity (Ash Meadows) (AM)	1	AB-27 km [0.56]	60W	0.04 [.6]	0.1 [.2]	0.01 [.2]	6.5 [.2]	6.7 [.6]	7.0 [.2]
		BC-43 km [0.2]		"	"	"	6.7 [.2]	7.0 [.6]	7.3 [.2]
		AD-34 km [0.2]		"	"	"	6.6 [.2]	6.9 [.6]	7.2 [.2]
		DC-51 km [0.04]		"	"	"	6.8 [.2]	7.1 [.6]	7.4 [.2]
18 Bare Mountain (BM)	1	AB-16 km [3]	60E	0.1 [.4]	0.05 [.4]	0.28 [.1]	0.01 [.1]	6.5 [.8]	6.8 -- [2]
		AC-22 km [7]		"	"	"	6.5 [.2]	6.7 [.6]	7.0 [.2]
19 Highway 95 (H95)	0.1	AB-11 km [5]	90	0.03 [.4]	0.05 [.3]	0.01 [.3]	6.8 [.3]	6.5 -- [7]	
		AC-27 km [5]		"	"	"	7.0 [.2]	6.7 [.6]	6.5 [.2]

MAXIMUM DEPTH OF FAULTING = 12 km, [.6]; 14 km, [.3], 16 km, [.1]

**TABLE DFS-2
TOTAL FAULT LENGTHS FOR LOCAL FAULT SOURCES
ASSUMING INDEPENDENT FAULT BEHAVIOR**

FAULT (Map Designation, Fig. DFS-8)	Alternative Lengths (Figure DFS-8)	Total Fault Length (km)	Probability
Paintbrush Canyon/Stagecoach Road (PBC)	BE	19.4	(0.68)
	AE	20.9	(0.2)
	BF	26.9	(0.1)
	AF	28.4	(0.02)
Bow Ridge (BWR)	KH	7.6	(0.8)
	GK	10.3	(0.2)
Solitario Canyon (SC)	LM	16.5	(0.7)
	LN	20.6	(0.3)
Windy Wash/Fatigue Wash (WWF)	PR	22.3	(0.57)
	OR	23.8	(0.3)
	PS	25.8	(0.1)
	OS	27.3	(0.03)
Northern Crater Flat (NCF)	LU	6.5	(1)
Southern Crater Flat (SCF)	VX	8.1	(1)
Ghost Dance (GD)	YZ	3.0	(0.3)
	YY-ZZ	9.0	(0.7)

**TABLE DFS-3
TOTAL FAULT LENGTHS FOR LOCAL FAULT SOURCES
ASSUMING DISTRIBUTIVE FAULT BEHAVIOR**

RUPTURE SCENARIO ¹	TOTAL LENGTH	PROBABILITY
Scenario A = BE + HK + LN + PR	69.9 km	(0.2)
Scenario B = AF + GK + LN + OS	86.6 km	(0.6)
Scenario C = AF + GK + LN + OS + TU + VX	101.2 km	(0.2)

¹ Fault segments correspond to the line segments shown on Figure DFS-8

TABLE DFS-4
MAXIMUM FAULT RUPTURE LENGTHS FOR LOCAL FAULT SOURCES
ASSUMING INDEPENDENT BEHAVIOR
 (Page 1 of 2)

FAULT TOTAL LENGTH (km/PROBABILITY)	MAXIMUM RUPTURE LENGTH (km)	PROBABILITY
Paintbrush Canyon/Stagecoach Road		
19.4 / 0.7	19.4 (1)	0.1
	11.1 (2)	0.7
	6.7 (3)	0.2
20.9 / 0.2	20.9 (1)	0.1
	11.1 (2)	0.7
	6.7 (3)	0.2
26.9 / 0.05	26.9 (1)	0.05
	19.7 (4)	0.4
	11.1 (2)	0.4
	6.7 (3)	0.1
28.4 / 0.05	28.4 (1)	0.05
	19.7 (4)	0.5
	11.1 (2)	0.3
	6.7 (3)	0.1
Bow Ridge		
7.6 / 0.8	7.6 (1)	0.7
	4.9 (5)	0.3
10.3 / 0.2	10.3 (1)	0.7
	4.9 (5)	0.3
Solitario Canyon		
16.5 / 0.7	16.5 (1)	0.8
	8.2 (6)	0.2
20.6 / 0.3	20.6 (1)	0.2
	15.4 (7)	0.6
	10.3 (6)	0.2

TABLE DFS-4
MAXIMUM FAULT RUPTURE LENGTHS FOR LOCAL FAULT SOURCES
ASSUMING INDEPENDENT BEHAVIOR
 (Page 2 of 2)

FAULT TOTAL LENGTH (km/PROBABILITY)	MAXIMUM RUPTURE LENGTH (km)	PROBABILITY
Windy Wash/Fatigue Wash		
22.3 / 0.7	22.3 (1)	0.2
	10 (6,8)	0.8
23.8 / 0.2	23.8 (1)	0.2
	10. (6,8)	0.8
25.8 / 0.05	25.8 (1)	0.1
	17.8 (9)	0.2
	10 (8)	0.7
27.3 / 0.05	27.3 (1)	0.1
	17.8 (9)	0.2
	10. (8)	0.7
Northern Crater Flat		
6.5 / 1	6.5 (1)	1.0
Southern Crater Flat		
8.1 / 1	8.1 (1)	1.0
Ghost Dance		
3.0 / 0.3	3.0 (1)	1.0
9.0 / 0.7	9.0 (1)	1.0

NOTES: (1) 100% of total fault length; (2) combined length of Alice Ridge and Fran Ridge segments; (3) length of longest segment, the Alice Ridge segment; (4) combined length of Alice Ridge, Fran Ridge, and Busted Butte segments; (5) length of well-defined north-south section of Bow Ridge fault; (6) approximately 50% of total fault length; (7) length of well-defined north-south section of Solitario Canyon fault adjacent to Yucca Crest; (8) approximate length of either the southern Windy Wash segment or the Fatigue Wash segment; (9) length of the north-south-trending section of the Windy Wash/Fatigue Wash fault system.

**TABLE DFS-5
DOWNDIP GEOMETRY OF LOCAL FAULT SOURCES**

FAULT	DOMINO (PLANAR) FAULT MODEL (0.8)		DETACHMENT FAULT MODEL (0.2)
	ALTERNATIVE A DIP / WIDTH (0.5)	ALTERNATIVE B DIP / WIDTH (0.5)	DIP / WIDTH (1.0)
❶ Paintbrush Canyon/Stagecoach Road Fault: Northern Segment, Paintbrush Canyon Fault Central Segment, Paintbrush Canyon Fault Southern Segment, Paintbrush Canyon Fault Stagecoach Road Fault	60° / 15 km	50° / 17 km	20° / 18 km
	60° / 15 km	50° / 17 km	20° / 18 km
	60° / 15 km	50° / 17 km	20° / 18 km
	60° / 15 km	50° / 17 km	20° / 13 km
❷ Bow Ridge Fault	70° / 8 km	60° / 9 km	48° / 7 km
❸ Solitario Canyon Fault	55° / 13 km	50° / 14 km	42° / 9 km
❹ Windy Wash/Fatigue Wash Fault: Northern Windy Wash Fault Fatigue Wash Fault Southern Windy Wash Fault	60° / 12 km	55° / 13 km	° / 8.5 km
	60° / 12 km	55° / 13 km	45° / 8.5 km
	55° / 10 km	55° / 13 km	45° / 8.5 km
❺ Northern Crater Flat Fault	60° / 9 km	55° / 9.5 km	47° / 8.6 km
❻ Southern Crater Flat Fault	71° / 10 km	60° / 11 km	52° / 8 km
❼ Ghost Dance Fault	90° / 10 km	70° / 11 km	45° / 8 km

TABLE DFS-6
QUATERNARY SLIP RATES ON LOCAL FAULT SOURCES
 (Page 1 of 2)

FAULT	FAULT SEGMENT	SLIP RATE—mm/yr (PROBABILITY)			SOURCES OF DATA
		PREFERRED	MINIMUM	MAXIMUM	
Paintbrush Canyon/Stagecoach Road Fault	Northern Segment PCF	0.002 (0.6)	0.001 (0.2)	0.004 (0.2)	Modified from: C. M. Menges and J. W. Whitney, USGS, written communication, 1996b, Tables 4.4.5 and 4.4.6 (Trench A1). F. H. Swan <i>et al.</i> , Geomatrix Consultants, written communication, 1995, Table C-8 (Trench MWV-T4). Modified from: C. M. Menges and J. W. Whitney, USGS, written communication, 1996b, Tables 4.4.5 and 4.4.6 (Busted Butte exposures). Modified from: C. M. Menges and J. W. Whitney, USGS, written communication, 1996b, Tables 4.4.5 and 4.4.6 (Trenches SCR-T1 and SCR-T3).
	Central Segment PCF	0.017 (0.6)	0.013 (0.2)	0.025 (0.2)	
	Southern Segment PCF	0.01 (0.6)	0.004 (0.2)	0.016 (0.2)	
	Stagecoach Road	0.04 (0.6)	0.01 (0.2)	0.07 (0.2)	
Bow Ridge Fault	G-K	0.003 (0.6)	0.002 (0.2)	0.007 (0.2)	C. M. Menges and J. W. Whitney, USGS, written communication, 1996b, Tables 4.4.6.
Solitario Canyon Fault	L-N	0.01 to 0.03 (0.3) (0.3)	0.002 (0.2)	0.04 (0.2)	A. R. Ramelli <i>et al.</i> , Nevada Bureau of Mines and Geology, written communication, 1996, p. 4.7-49.

TABLE DFS-6
QUATERNARY SLIP RATES ON LOCAL FAULT SOURCES
 (Page 2 of 2)

FAULT	FAULT SEGMENT	SLIP RATE—mm/yr (PROBABILITY)			SOURCES OF DATA
		PREFERRED	MINIMUM	MAXIMUM	
Windy Wash/Fatigue Wash Fault					
Northern Windy Wash	O-P1	0.003 (0.45)	0.001 (0.45)	0.03 (0.1)	Assumed to be similar to Southern Windy Wash segment, but with greater uncertainty. J. A. Coe <i>et al.</i> , USGS, written communication, 1996, p. 4.8-24.
Fatigue Wash	P1-Q	0.002 (0.6)	0.001 (0.2)	0.015 (0.2)	
Southern Windy Wash	Q-S	0.011 (0.6)	0.009 (0.2)	0.027 (0.2)	Reported slip rate available for one of two splays; J. W. Whitney <i>et al.</i> , USGS, written communication, 1996b, p. 4.9-31 to 4.9-32.
Northern Crater Flat Fault	T-U		0.001 (0.5)	0.002 (0.5)	Maximum rate reported to be less than 0.002 mm/yr, J.A. Coe <i>et al.</i> , USGS, written communication, 1996, P.4.11-12 (Trench TR CFF T-2).
Southern Crater Flat Fault	V-X		0.001 (0.5)	0.002 (0.5)	Maximum rate reported to be less than 0.002 mm/yr, E. M. Taylor <i>et al.</i> , USGS, written communication, 1996a, P.4.10-12 (trenches TR CFF T-1 and TR CFF T-1a).
Ghost Dance Fault	YY-ZZ	0.001 (0.6)	0.0001 (0.2)	0.0024 (0.2)	Preferred value equals the weighted average from all these displacement history models described in Section 5.2.3.

**TABLE DFS-7
SEISMIC SOURCE PARAMETERS FOR HYPOTHETICAL FAULTS**

Hypothetical Fault Source	ACTIVITY	LENGTH (km)	DIP (deg.)	DEPTH TO DETACHMENT (km)	SLIP RATE (mm/yr)			MAXIMUM MAGNITUDE		
					PREFERRED	MAXIMUM	MINIMUM			
Highway 95 Fault (H-95)	(0.1)	11 (0.5)	90	na	0.03 (0.4)	0.05 (0.3)	0.01 (0.3)	6.5 (0.7)	6.8 (0.3)	
		27 (0.5)	90	na	" "	" "	" "	6.5 (0.2)	6.7 (0.6)	7.0 (0.2)
Postulated Hidden Strike-Slip Fault (T2-HSS)	(0.05)	30 (0.5)	90	5 to 16 (0.2)	" "	" "	" "	L vs. M (0.2)		A vs. M (0.8)
				6.5 to 14 (0.6)						
				8 to 12 (0.2)						
		200 (0.5)		5 to 16 (0.2)	" "	" "	" "	6.0 (0.3)	6.5 (0.5)	7.0 (0.2)
				6.5 to 14 (0.6)				" "	" "	" "
				8 to 12 (0.2)				" "	" "	" "

Maximum depth of faulting same as for regional fault sources [12 km (0.6), 14 km (0.3), 16 km< (0.1)].

**TABLE DFS-8
 FAULT ACTIVITY AND CUMULATIVE DISPLACEMENT, POST-TIVA CANYON
 TUFF, AT TEST CALCULATION SITES FOR FAULT DISPLACEMENT HAZARD
 ASSESSMENT**

TEST CALCULATION SITE	PROBABILITY OF ACTIVITY	CUMULATIVE DISPLACEMENT POST-TIVA CANYON TUFF (NET SLIP IN M)		
1) Bow Ridge Fault	1.0	125 (0.2)	130 (0.6)	135 (0.2)
2) Solitario Canyon Fault	1.0	350 (0.2)	500 (0.6)	580 (0.2)
3) Drill Hole Wash Fault	0.01	5 (0.2)	15 (0.6)	25 (0.2)
4) Ghost Dance Fault	0.4	20 (0.2)	25 (0.6)	30 (0.2)
5) Sundance Fault	0.01	6 (0.2)	8.5 (0.6)	11 (0.2)
6) Unnamed Fault West of Dune Wash	0.4	3 (0.2)	5 (0.6)	7 (0.2)
7) 100 M East of Solitario Canyon Fault				
a) Small fault	0.05	0.5 (0.2)	0.85 (0.6)	2.0 (0.2)
b) Shear	0.05	0.1 (1.0)	--	--
8) Midway Between Solitario Canyon and Ghost Dance Faults				
a) Small fault	0.01	0.5 (0.2)	0.85 (0.6)	2.0 (0.2)
b) Shear	0.01	0.1 (1.0)	--	--
9) Exile Hill Fault (Midway Valley)	0.8	5 (0.2)	10 (0.6)	15 (0.2)

**TABLE DFS-9
QUATERNARY SLIP RATES
BASED ON PALEOSEISMIC DATA**

Test Calculation Site	Slip Rate (mm per yr)			Basis
1) Bow Ridge Fault	0.002 (0.2)	0.003 (0.6)	0.007 (0.2)	C. M. Menges and J. W. Whitney, USGS, written communication, 1996b, Table 4.4.6
2) Solitario Canyon Fault	0.01 (0.2)	0.02 (0.6)	0.04 (0.2)	Data from trenches SCF-T4 and T8, A. R. Ramelli <i>et al.</i> , Nevada Bureau of Mines and Geology, written communication, 1996 Table 4.7.3
3) Drill Hole Wash Fault	not available			
4) Ghost Dance Fault	less than 0.0005			(See text, Section 5.2.3)
5) Sundance Fault	not available			
6) Unnamed Fault West of Dune Wash	not available			
7) 100 M East of Solitario Canyon Fault	not available			
8) Midway Between Solitario Canyon and Ghost Dance Faults	not available			
9) Exile Hill Fault (Midway Valley)	less than 0.0005			F. H. Swan <i>et al.</i> , Geomatrix Consultants, written communication, 1995

**TABLE DFS-10
SLIP RATES CALCULATED USING
DECREASING SLIP RATE MODEL WITH DIFFERENT
REDUCTION FACTORS (RF) COMPARED TO SLIP RATES BASED ON
PALEOSEISMIC DATA**

FAULT	SLIP RATE (mm PER YR) ^{*1}			
	DECREASING SLIP RATE MODEL (REDUCTION FACTORS AS A PERCENT OF THE LATE MIOCENE SLIP RATE)			SLIP RATE BASED ON PALEOSEISMIC DATA
	2.1 %	3.9 %	0.3 %	
Paintbrush Canyon Fault (Trench MWV T4)	0.0057±	0.011±	0.0008±	0.017±
Bow Ridge Fault (Test Calculation Site #1)	0.0025±	0.0046±	0.0004±	0.003±
Solitario Canyon Fault (Test Calculation Site #2)	0.0095±	0.0177±	0.0014	0.02±
Ghost Dance Fault (Test Calculation Site #4)	0.0005±	0.0009±	0.0001	<0.0005
Exile Hill Fault (Test Calculation Site #9)	0.0002±	0.0004±	0.0003±	<0.0005

^{*1} Slip rates shown here are based on preferred values for displacement and age; the uncertainties in these values were incorporated in the fault displacement hazard analysis.

TABLE DSF-11 (Page 1 of 2)
DISPLACEMENT PER EVENT AND RECURRENCE PARAMETERS FOR
FAULT DISPLACEMENT HAZARD ASSESSMENT

Displacement Approach		Recurrence Approach	
Average Displacement Per Event (cm)	Probability	Average Recurrence Interval (X 1000 Years)	Probability
#1 BOW RIDGE FAULT			
40	0.15	215	0.1
20	0.7	140	0.4
10	0.15	100	0.4
		70	0.1
#2 SOLITARIO CANYON FAULT			
60	0.2	100	0.2
40	0.6	70	0.3
20	0.2	50	0.3
		35	0.2
#3 DRILLHOLE WASH FAULT			
15	0.03	500	0.145
10	0.07	400	0.25
5	0.15	300	0.25
3	0.2	200	0.25
1	0.25	100	0.1
0.05	0.3	50	0.005
#4 GHOST DANCE FAULT			
15	0.03	500	0.145
10	0.07	400	0.25
5	0.15	300	0.25
3	0.2	200	0.25
1	0.25	100	0.1
0.05	0.3	50	0.005
#5 SUNDANCE FAULT			
15	0.03	500	0.145
10	0.07	400	0.25
5	0.15	300	0.25
3	0.2	200	0.25
1	0.25	100	0.1
0.05	0.3	50	0.005

TABLE DSF-11 -(Page 2 of 2)
DISPLACEMENT PER EVENT AND RECURRENCE PARAMETERS FOR ASSESSMENT OF
FAULT DISPLACEMENT HAZARD

Displacement Approach		Recurrence Approach	
Average Displacement Per Event (cm)	Probability	Average Recurrence Interval (X 1000 Years)	Probability
#6 UNNAMED FAULT WEST OF DUNE WASH			
15	0.03	500	0.145
10	0.07	400	0.25
5	0.15	300	0.25
3	0.2	200	0.25
1	0.25	100	0.1
0.05	0.3	50	0.005
#7 100 M EAST OF SOLITARIO CANYON FAULT			
(A) 2 m Displacement			
10	0.05	1600	0.05
5	0.1	500	0.18
3	0.2	400	0.18
1	0.3	300	0.18
0.5	0.35	200	0.18
		100	0.18
		50	0.05
(B) 10 cm Displacement			
10	0.005	1600	0.05
5	0.05	500	0.18
3	0.2	400	0.18
1	0.35	300	0.18
0.5	0.3	200	0.18
0.05	0.095	100	0.18
		50	0.05
#8 MIDWAY BETWEEN SOLITARIO CANYON AND GHOST DANCE FAULTS			
(A) 2 m Displacement			
10	0.05	1600	0.05
5	0.1	500	0.18
3	0.2	400	0.18
1	0.3	300	0.18
0.5	0.35	200	0.18
		100	0.18
		50	0.05
(B) 10 cm Displacement			
10	0.005	1600	0.05
5	0.05	500	0.18
3	0.2	400	0.18
1	0.35	300	0.18
0.5	0.3	200	0.18
0.05	0.095	100	0.18
		50	0.05
#9 MIDWAY VALLEY (EXILE HILL FAULT)			
10	0.05	500	0.15
5	0.1	400	0.25
3	0.2	300	0.25
1	0.3	200	0.25
0.5	0.35	100	0.1

TABLE DSF-12
SUMMARY OF DISPLACEMENT PER EVENT DATA FROM
YUCCA MOUNTAIN PALEOSEISMIC INVESTIGATIONS
 (Page 1 of 2)

Locality Site	Average Displacement	EVENT (Reported Displacement in cm -- Pezzopane et al. 1995, Table 5-1) [Ratio: Event Displacement / Average Displacement]							
		Z	Y	X	W	V	U	T	S
Tr 14D	23.67	44 1.86	13 0.55	14 0.59	0.00	0.00			
Tr CFF-T2A	29.60	3 0.10	5 0.17	40 1.35	50 1.69	50 1.69			
Tr CFF-T1A	19.33	18 0.93	20 1.03	20 1.03	0.00	0.00			
Tr CF 1	61.33	0.00	25 0.41	105 1.71	54 0.88	0.00			
Tr SCF-T2	61.25	5 0.08	70 1.14	100 1.63	70 1.14	0.00			
Tr A1	38.00	6 0.16	39 1.03	7 0.18	100 2.63	0.00			
BB4	89.57	44 0.49	28 0.31	47 0.52	167 1.86	142 1.59	105 1.17	94 1.05	
MWV-T4	55.00	20 0.36	62 1.13	98 1.78	40 0.73	0.00	0.00	0.00	
RV3	290.75	267 0.92	362 1.25	204 0.70	330 1.13	0.00	0.00	0.00	

TABLE DSF-12
SUMMARY OF DISPLACEMENT PER EVENT DATA FROM
YUCCA MOUNTAIN PALEOSEISMIC INVESTIGATIONS

(Page 2 of 2)

Locality Site	Average Displacement	EVENT (Reported Displacement in cm – Pezzopane et al. 1995, Table 5-1) [Ratio: Event Displacement / Average Displacement]							
		Z	Y	X	W	V	U	T	S
SCF-T3	41.67	10 0.24	80 1.92	35 0.84	0.00	0.00	0.00	0.00	
SCF-T4	18.33	5 0.27	0.00	30 1.64	20 1.09	0.00	0.00	0.00	
SCF-T8	52.50	10 0.19	120 2.29	30 0.57	50 0.95	0.00	0.00	0.00	
SCR-T1	45.00	40 0.89	42 0.93	47 1.04	51 1.13	0.00	0.00	0.00	
SCR-T3	52.20	43 0.82	59 1.13	57 1.09	67 1.28	35 0.67	0.00	0.00	
Tr CF-2 [north wall]	39.38	4 0.10	20 0.51	23 0.58	20 0.51	73 1.85	45 1.14	50 1.27	80 2.03
Tr CF-2 [south wall]	34.63	4 0.12	12 0.35	50 1.44	42 1.21	28 0.81	16 0.46	60 1.73	65 1.88
Tr CF2.5	20.75	6 0.29	20 0.96	42 2.02	15 0.72	0.00	0.00	0.00	
Tr CF-3 [north wall]	44.80	4 0.09	33 0.74	87 1.94	35 0.78	65 1.45	0.00	0.00	
Tr CF-3 [south wall]	42.00	3 0.07	35 0.83	88 2.10	0.00	0.00	0.00	0.00	

TABLE DSF-13
RELATIONSHIP BETWEEN AVERAGE DISPLACEMENT
AND MAXIMUM DISPLACEMENT AT A POINT ALONG A FAULT
(Event -to-Event Variability)

LOCALITY	$D_{\max}/D_{\text{average}}$ **
Tr 14D	1.86
Tr CFF-T2A	1.69
Tr CFF-T1A	1.03
Tr CF 1	1.71
Tr SCF-T2	1.63
Tr A1	2.63
BB4	1.86
MWV-T4	1.78
RV3	1.13
SCF-T3	1.92
SCF-T4	1.64
SCF-T8	2.29
SCR-T1	1.13
SCR-T3	1.28
Tr CF-2	1.85
[north wall]	
Tr CF-2	1.44
[south wall]	
Tr CF2.5	2.02
Tr CF-3	1.94
[north wall]	
Tr CF-3	2.1
[south wall]	
RANGE	1.03 to 2.63
AVERAGE	1.73

** From Table DSF-12

**TABLE DFS-14
POTENTIAL FOR ACTIVITY
ON FRACTURES AND IN INTACT BEDROCK**

Test Calculation Site	Potential Activity	Basis
<p>#7 100 m East of Solitario Canyon Fault</p> <p>c) Fracture</p> <p>d) Intact Bedrock</p>	<p>< 0.05</p> <p>< 0.005</p>	<p>Likelihood of occurrence judged to be less than the probability of activity on a fault that has displacement at the same location (Table 7.2-1)</p> <p>Likelihood of occurrence judged to be at least an order of magnitude less than the probability of activity on a fault or fracture at the same location.</p>
<p>#8 Midway Between Solitario Canyon and Ghost Dance Faults</p> <p>c) Fracture</p> <p>d) Intact Bedrock</p>	<p>< 0.01</p> <p>< 0.001</p>	<p>Likelihood of occurrence judged to be less than the probability of activity on a fault that has displacement at the same location (Table 7.2-1)</p> <p>Likelihood of occurrence judged to be an order of magnitude less than the probability of activity on a fault or fracture at the same location.</p>

TABLE DFS-15
PROBABILITY OF DISPLACEMENT "EVENTS" (Pe)
ACROSS FRACTURES IN UNBROKEN ROCK
GIVEN DIFFERENT MODELS OF DEFORMATION HISTORY

- (A) Uniform Deformation Post Tiva-Canyon (Ttc).

$$\text{Probability of "Event"} \leq \frac{1}{\text{Age of Host Rock}}$$

$$Pe \leq \frac{1}{(12.7 \pm 1.3) \times 10^6}$$

$$Pe \leq 1 \times 10^{-7}$$

- (B) Uniform Deformation Rate Post-Rainier Mesa.

$$Pe \leq \frac{\text{post - Rainier Mesa deformation rate}}{\text{post - Tiva Canyon deformation rate}} \text{ (Pe Model A)}$$

$$Pe \leq \left(\frac{0.2 / 11.6 \pm 1.0 \text{ Ma}}{1 / 12.7 \pm 1.3 \text{ Ma}} \right) (1 \times 10^{-7})$$

$$Pe \leq 1.8 \times 10^{-8} \text{ to } 2.6 \times 10^{-8}$$

- (C) Decreasing Deformation Rate.

$$Pe \leq \frac{(\text{late Miocene deformation rate})(\text{reduction factor})}{\text{post - Tiva Canyon deformation rate}} \text{ (Pe Model A)}$$

$$Pe \leq \left(\frac{(0.8 / 1.1 \pm 0.6 \text{ ma})(0.021 \pm 0.018)}{1 / 12.7 \pm 1.3 \text{ Ma}} \right) (1 \times 10^{-7})$$

$$Pe \leq 2.1 \times 10^{-9} \text{ to } 5.9 \times 10^{-8}$$

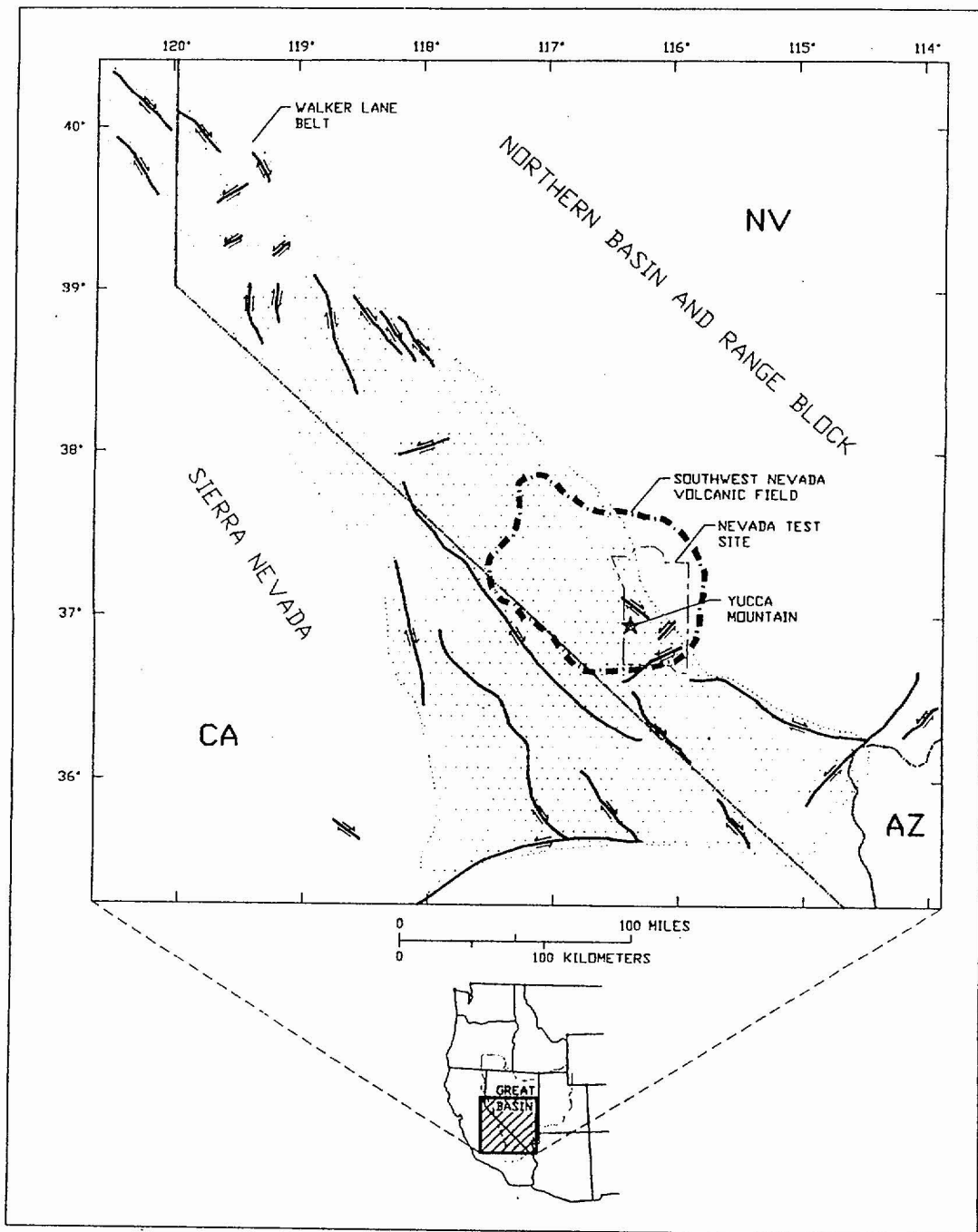


Figure DFS-1 Map showing location of Yucca Mountain (star) in the southwest Nevada volcanic field (Broxton et al., 1989, of the western Great Basin, with schematic representations of faults of the Walker Lane Belt that have strike-slip components of offset (dip-slip offsets not shown). Modified from Stewart (1988)

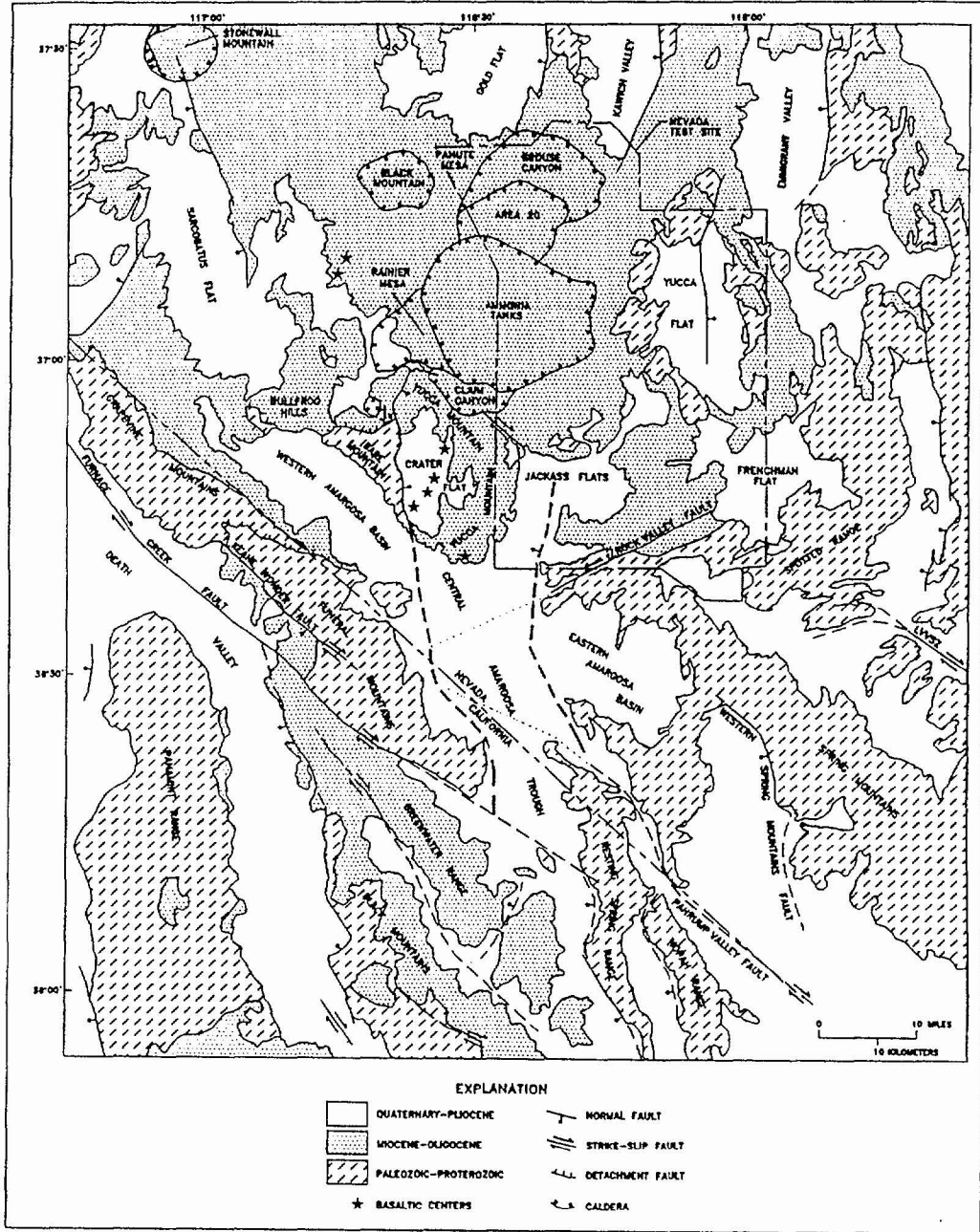


Figure DFS-2 Generalized map of the Yucca Mountain region showing major physiographic features and faults. Compiled from Jenkins, 1962; Longwell et al., 1965; Cornwall, 1972; Streitz and Stinson, 1974; Ekren et al., 1977, Burchfield et al., 1983; Wright, 1989; Frizzell and Schulters, 1990; Piety, 1993; Sawyer et al., 1994

Declustered Catalog	Source Zonation	Spatial Variability	Sources	Maximum Magnitude
---------------------	-----------------	---------------------	---------	-------------------

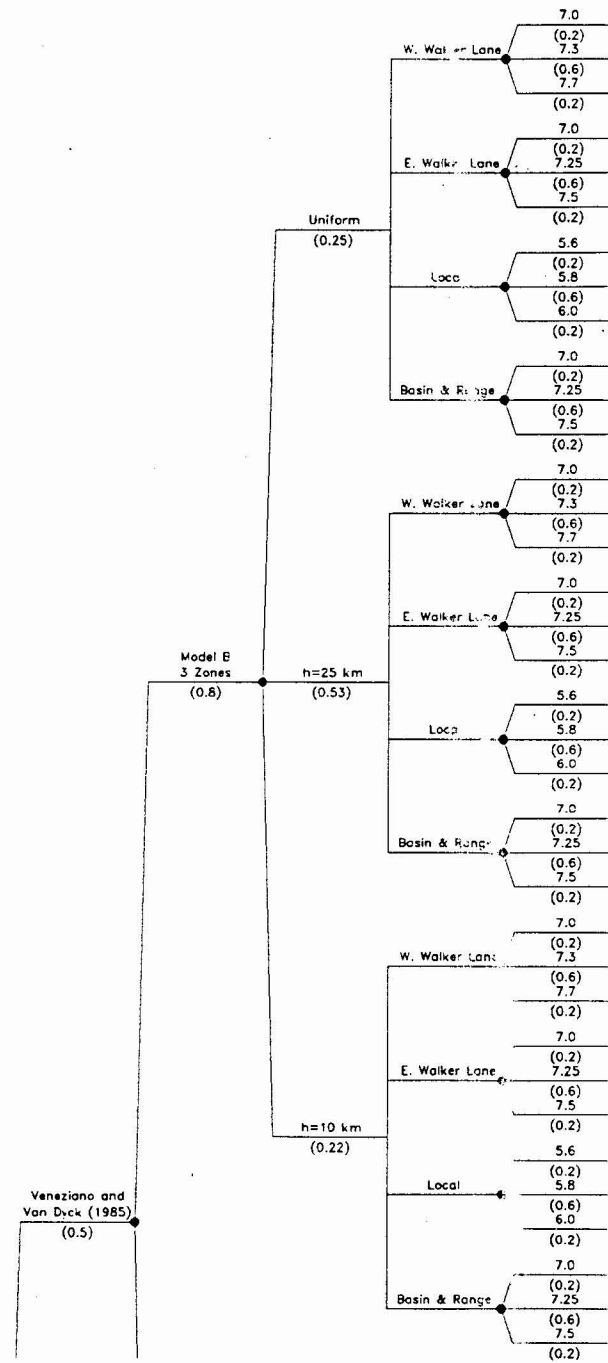


Figure DFS-3 Logic tree defining seismic source zones associated with two alternative models

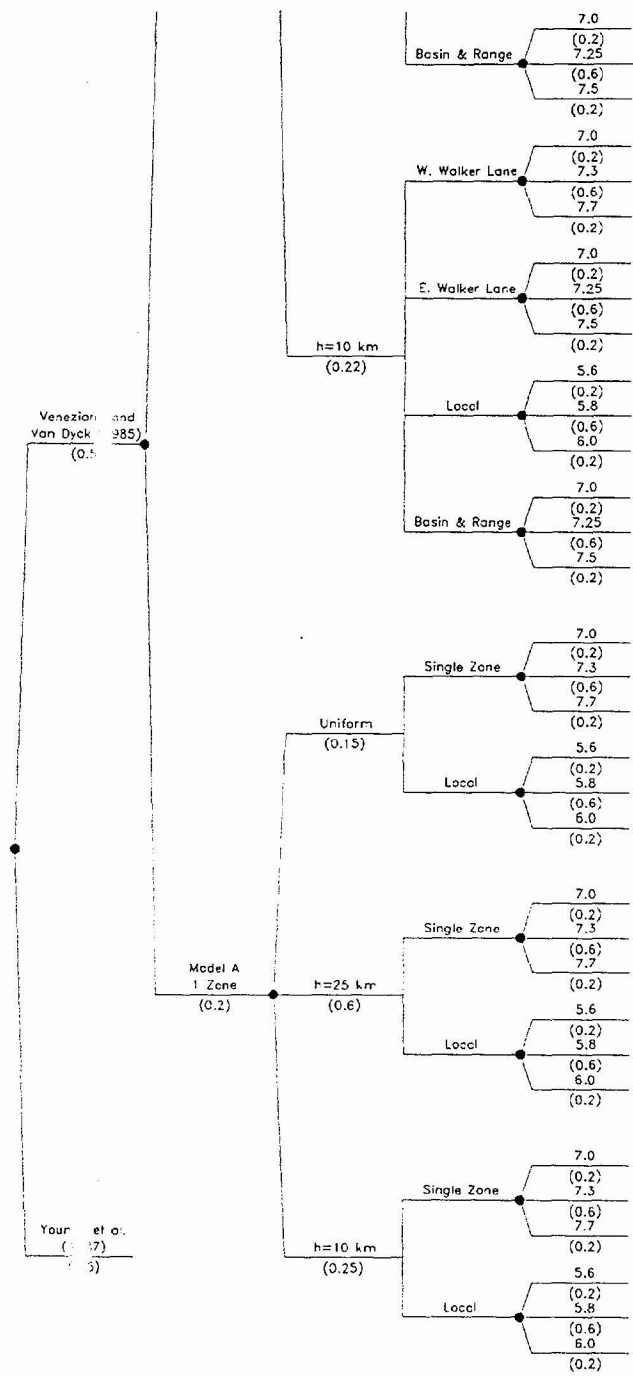


Figure DFS-3 (Cont'd) Logic tree defining seismic source zones associated with two alternative models

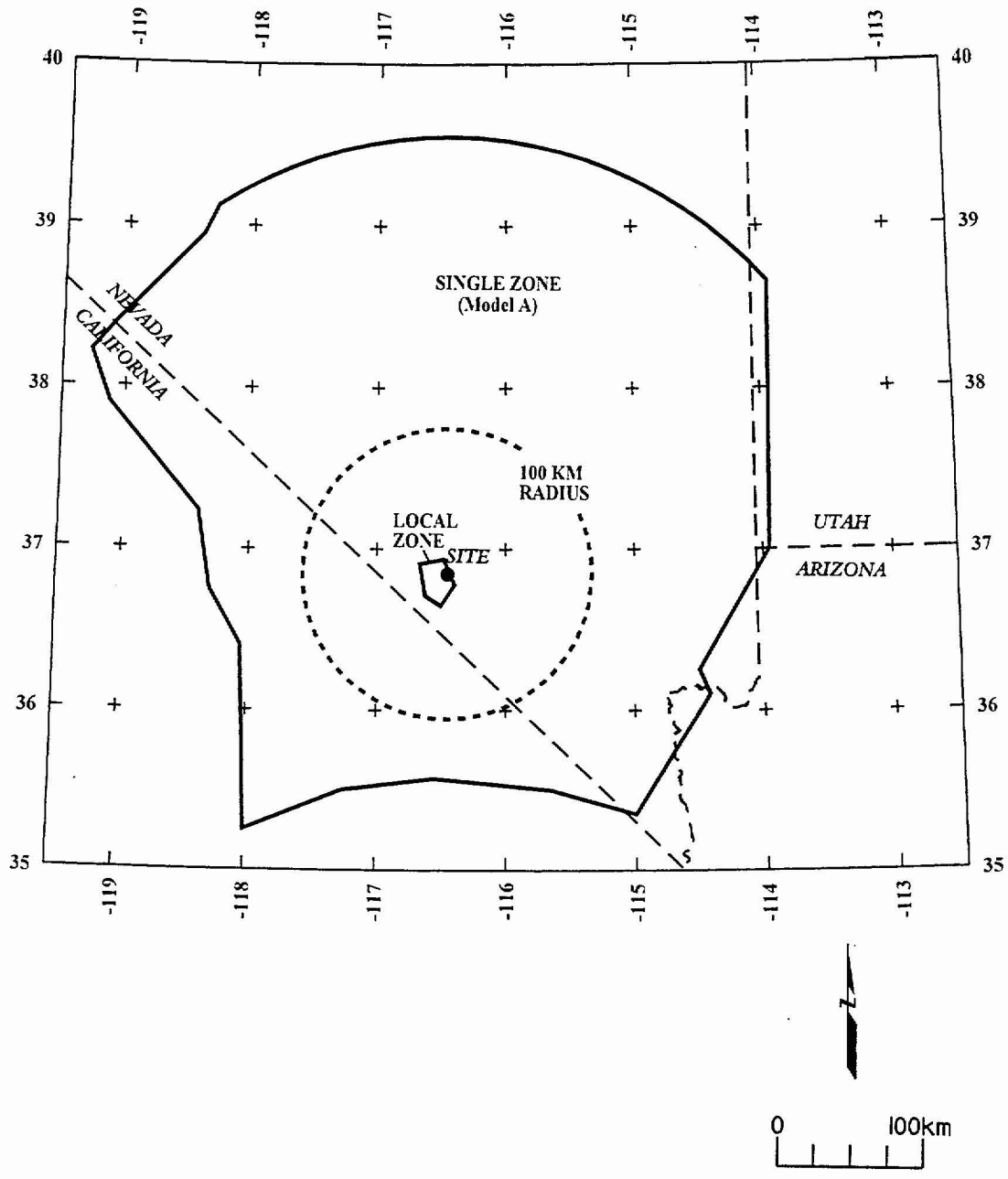


Figure DFS-4 Map showing boundaries of seismic source zones, Model A (one zones plus site vicinity).

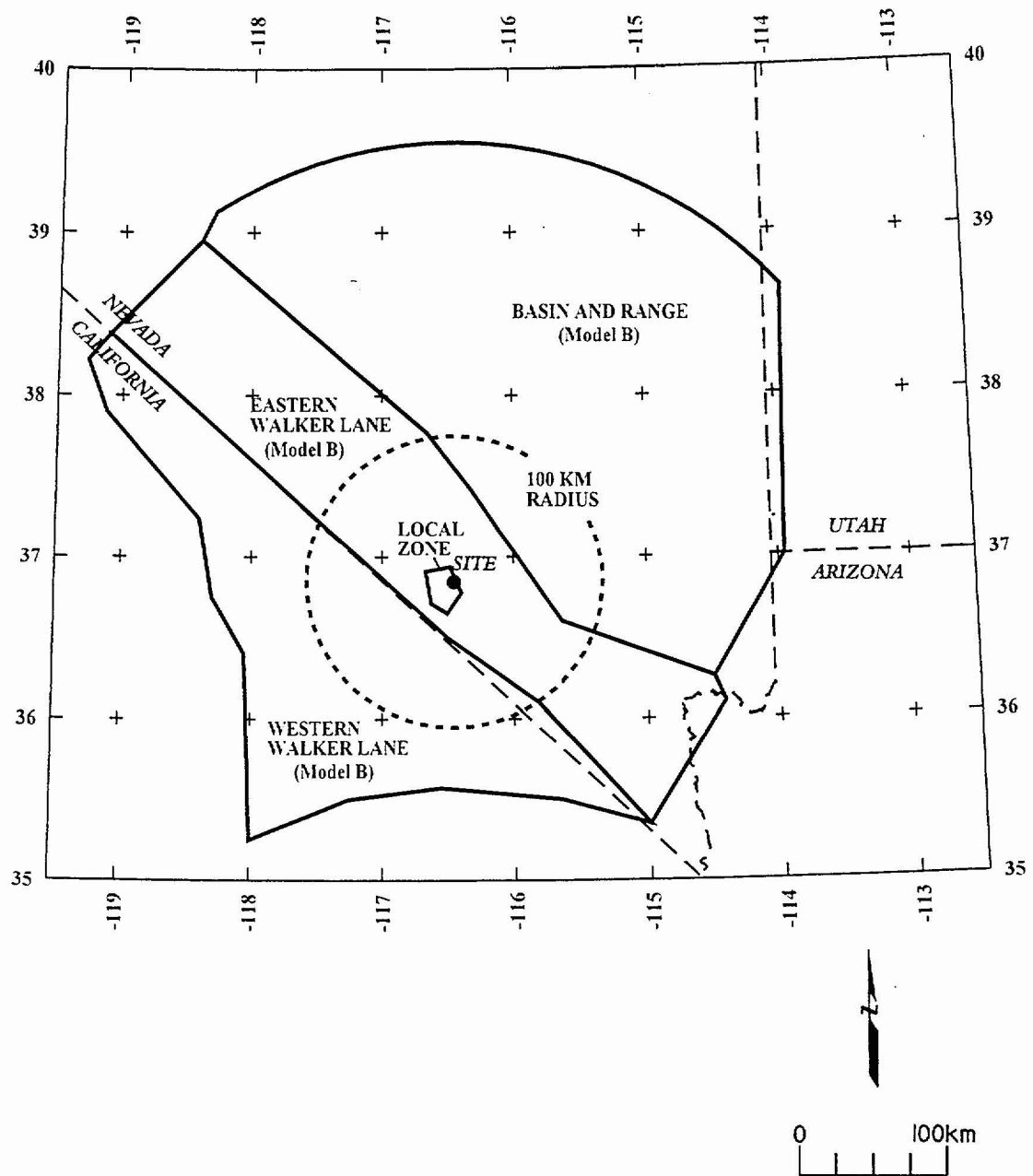
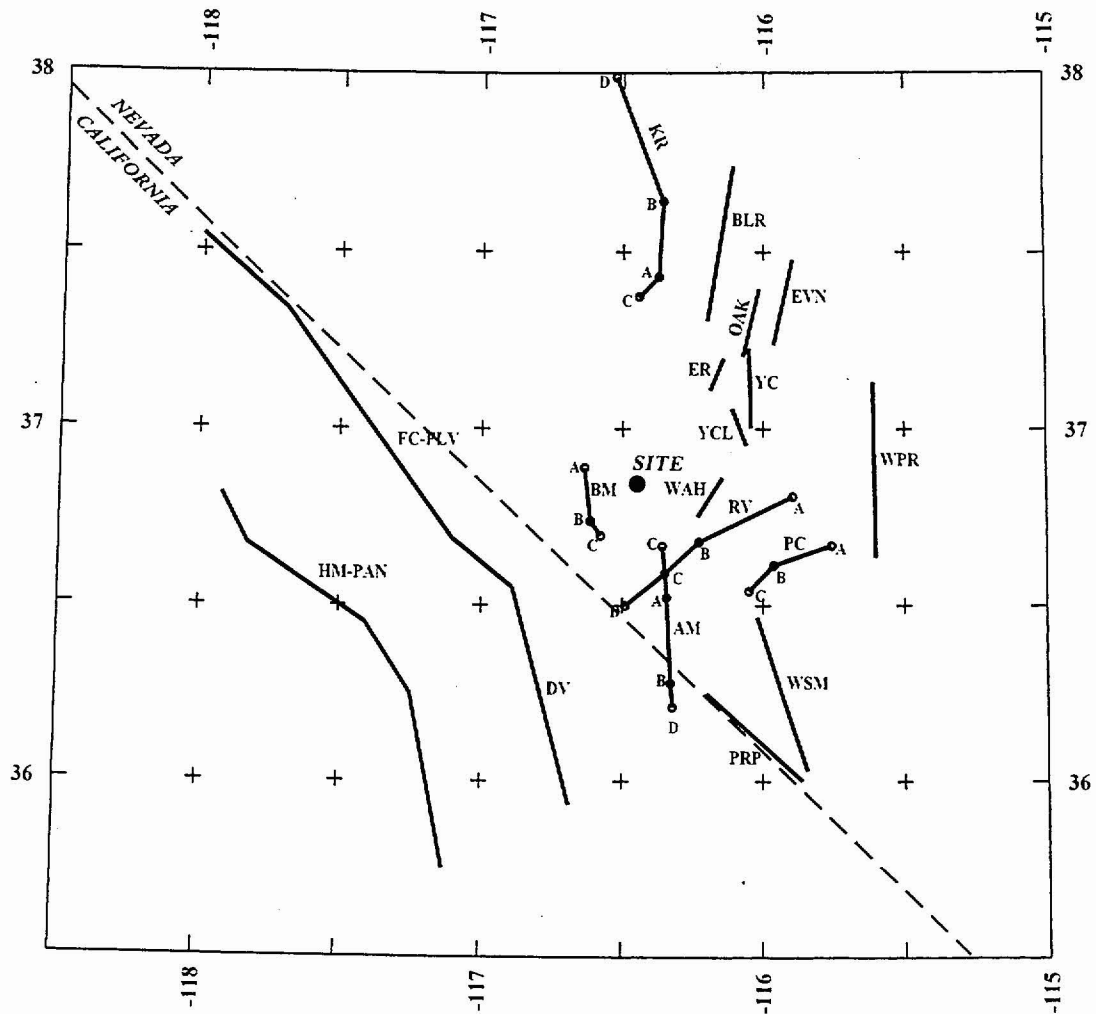


Figure DFS-5 Map showing boundaries of seismic source zones, Model B (three zones plus site vicinity).



EXPLANATION

Fault Lengths:



NOTES: Fault names are listed in Table DFS-1
Fault segments described in text

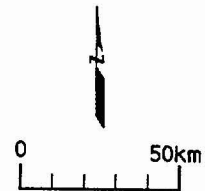


Figure DFS-6 Map showing identified late Quaternary faults included as regional fault sources in the seismic source model

<i>Regional Fault Source</i>	<i>Fault Dip</i>	<i>Maximum Depth Of Faulting</i>	<i>Total Fault Length</i>	<i>Maximum Magnitude (Mw)</i>	<i>Slip Rate (mm/yr)</i>	<i>Earthquake Recurrence Model</i>
------------------------------	------------------	----------------------------------	---------------------------	-------------------------------	--------------------------	------------------------------------

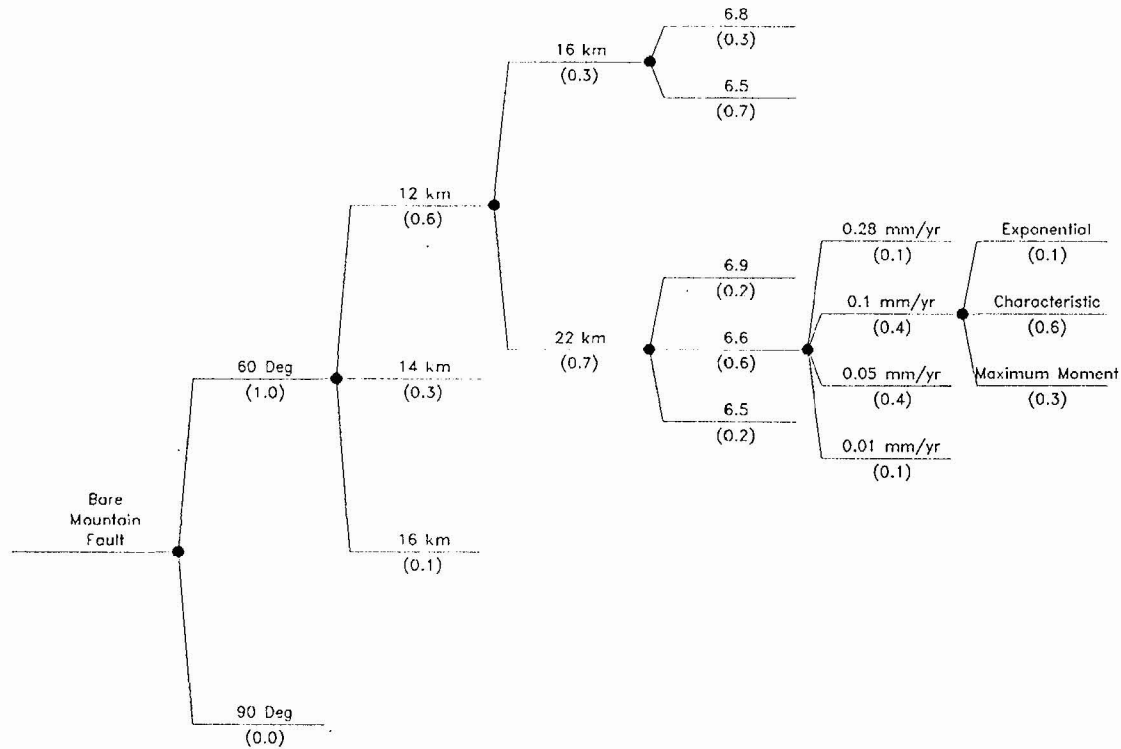


Figure DFS-7 Example of the logic tree used to characterize regional fault sources

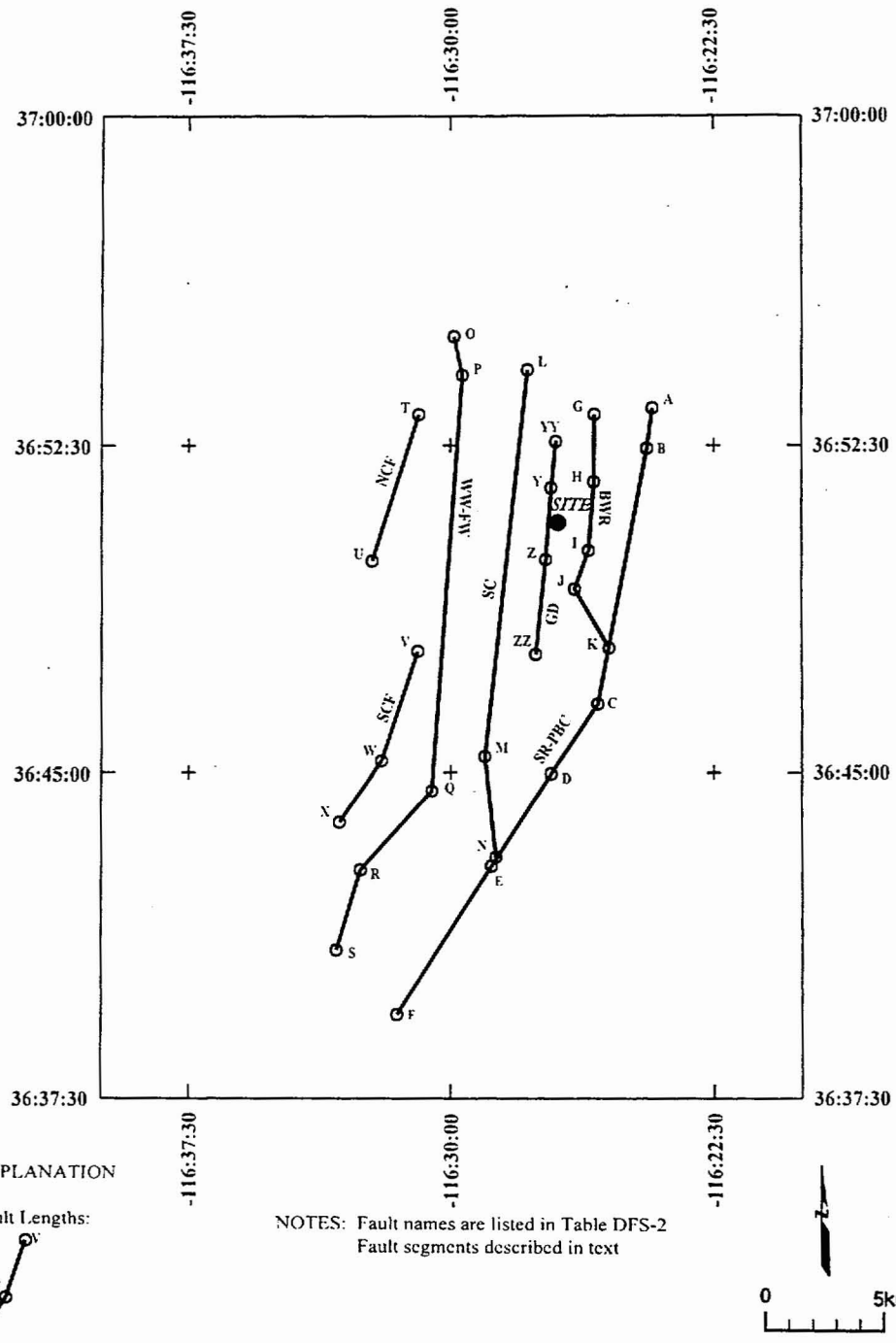
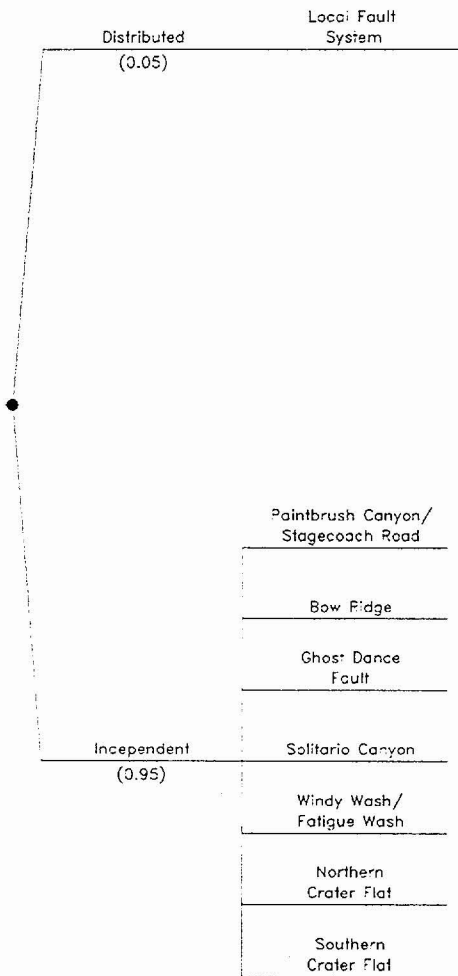


Figure DFS-8 Map showing local fault sources included in the seismic source model

<i>Fault Behavior</i>	<i>Sources</i>
-----------------------	----------------



same geometry as INDEPENDENT BEHAVIOR, but M-max is not constrained by total length of any one fault.

M-max on individual faults is constrained, in part, by the total length of the faults.

Figure DFS-9 Logic tree showing dependence of local fault model on distributive versus independent fault-behavior models

Seismic Source	Total Fault Length Scenarios	Maximum Rupture Length	Structural Model	Dip/Width	Slip Rate (mm/yr)	Maximum Earthquake Method	Earthquake Recurrence Model
----------------	------------------------------	------------------------	------------------	-----------	-------------------	---------------------------	-----------------------------

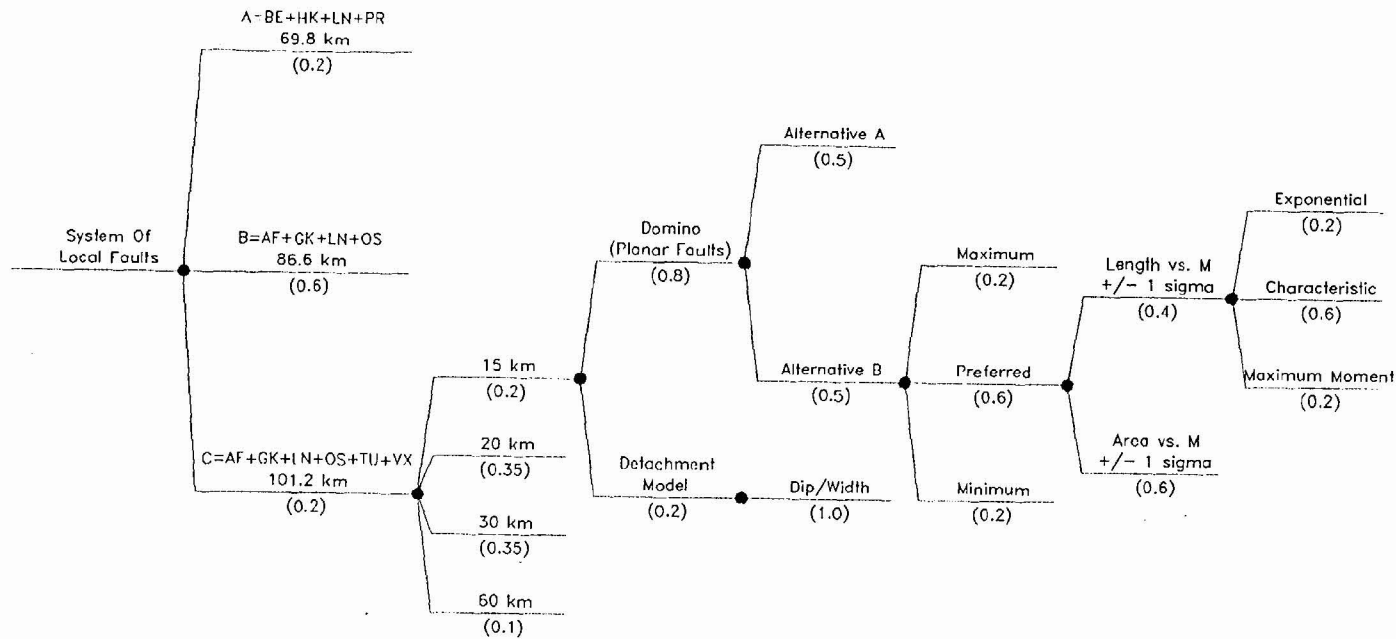


Figure DFS-10 Example logic tree used to characterize fault sources given distributed fault behavior

<i>Seismic Source</i>	<i>Total Fault Length</i> <i>(Table 4.3-3)</i>	<i>Maximum Rupture Length</i> <i>(Table 4.3-3)</i>	<i>Structural Model</i> <i>(Table 4.3-4)</i>	<i>Dip/Width</i> <i>(Table 4.3-4)</i>	<i>Slip Rate (mm/yr)</i> <i>(Table 4.3-5)</i>	<i>Maximum Earthquake Method</i>	<i>Earthquake Recurrence Model</i>
-----------------------	---	---	---	--	--	----------------------------------	------------------------------------

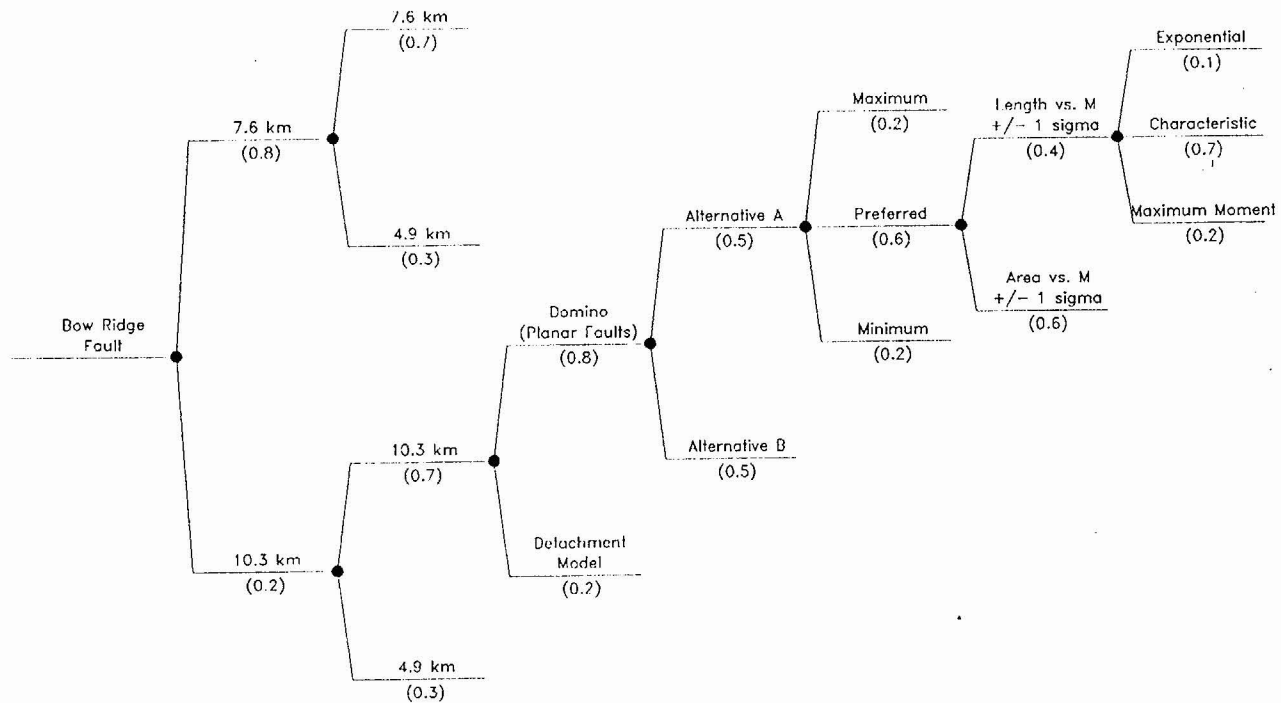


Figure DFS-11 Example logic tree used to characterize local fault sources given independent fault behavior

<i>Fault Behavior Model</i>	<i>Earthquake Recurrence Model</i>
-----------------------------	------------------------------------

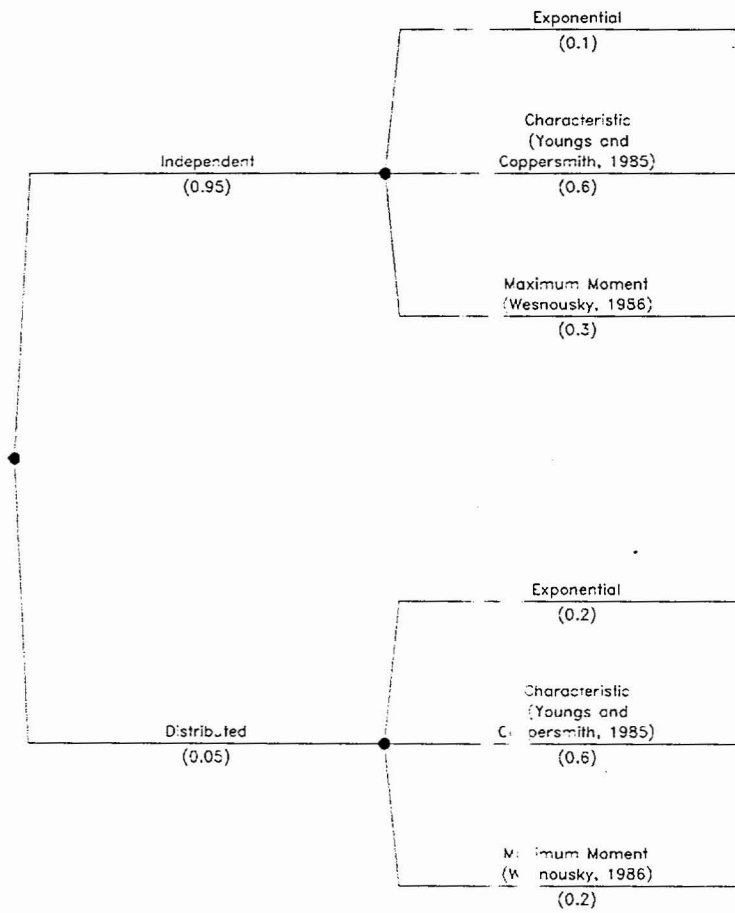
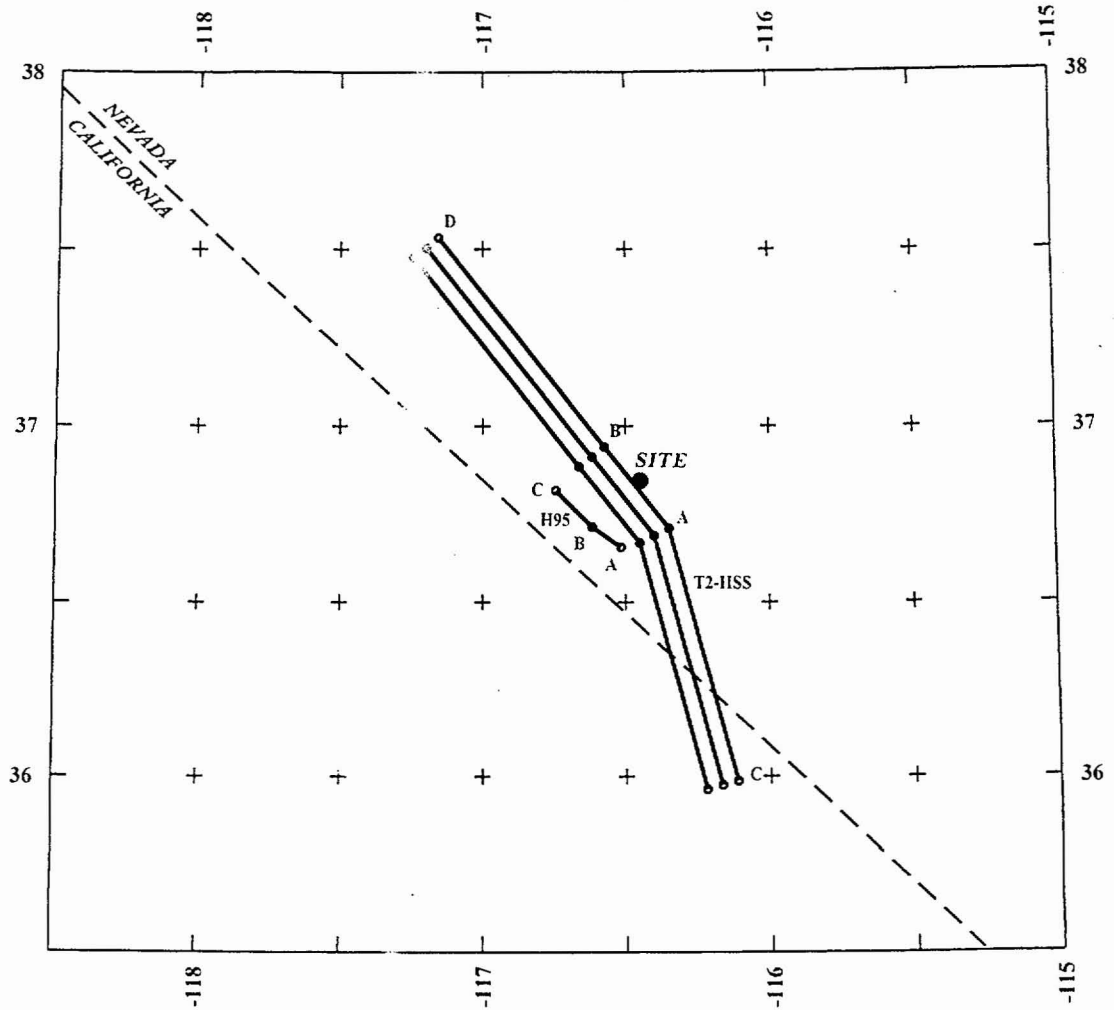
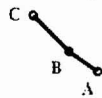


Figure DFS-12 Logic tree for conditional probability weights assigned to earthquake recurrence models



EXPLANATION

Fault Lengths:



NOTES: Fault names are listed in Table DFS-7
 Fault segments described in text

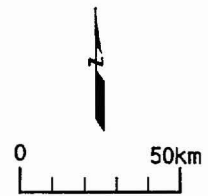
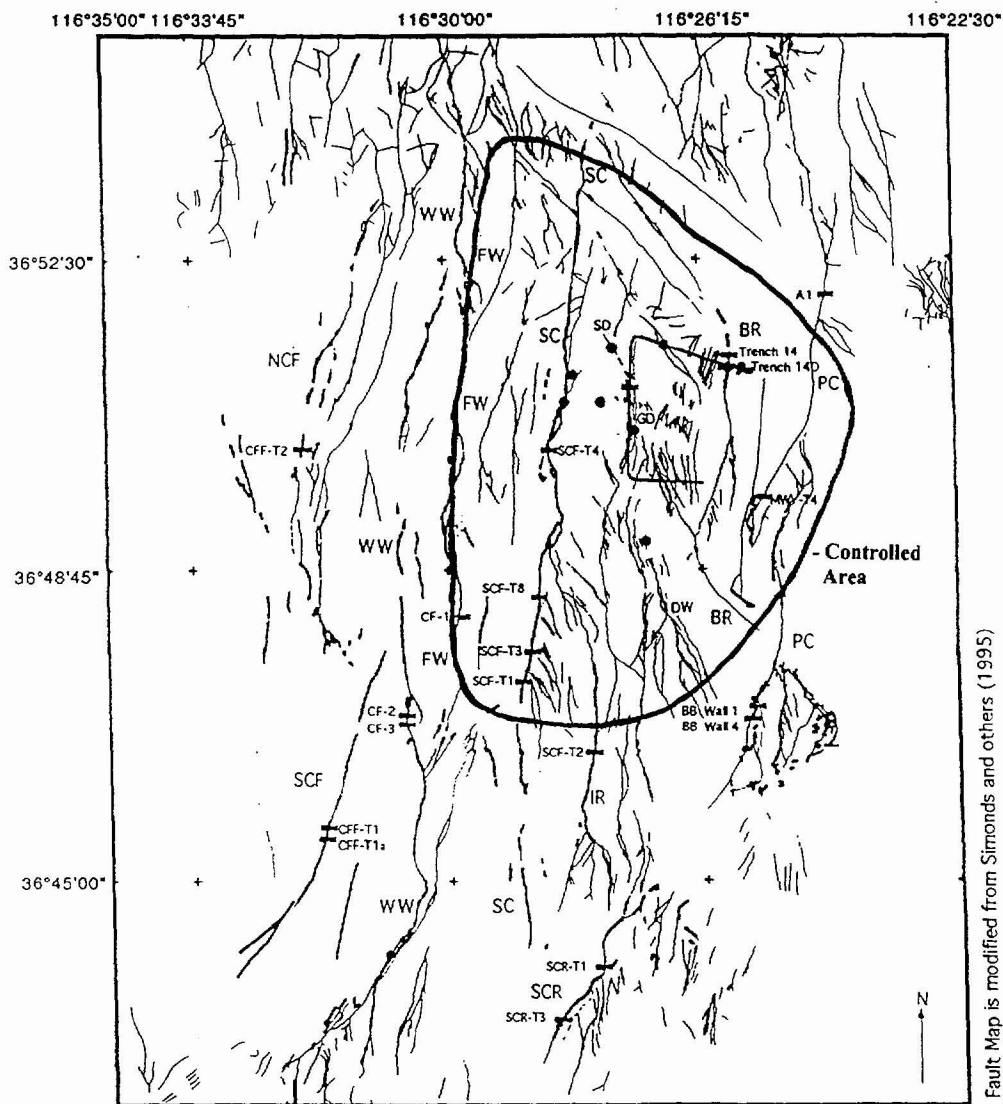


Figure DFS-13 Map showing hypothetical fault sources included in the seismic source model



Fault Map is modified from Simonds and others (1995)

EXPLANATION

- Fault Displacement Hazard Test Calculation Sites
- Approximate Controlled Area Boundary
- Approximate Potential Repository Area and Exploratory Studies Facility
- Paleoseismic Trench Locations
- Faults; Quaternary and suspected Quaternary age of last movement
- Faults; pre-Quaternary or undetermined age of last movement

0 kilometers 5

Fault		Abbreviations	
BR	Bow Ridge	PC	Paintbrush Canyon
DW	Dune Wash	SD	Sundance
FW	Fatigue Wash	SC	Soltario Canyon
GD	Ghost Dance	SCF	Southern Crater Flat
IR	Iron Ridge	SCR	Stagecoach Road
NCF	Northern Crater Flat	WW	Windy Wash

USGS-YMP Pezzopane Jan 97

Figure DFS-14 Map showing fault displacement hazard test calculation sites.

Test Calculation Site	Activity	Cumulative Displacement Tiva Canyon Tuff	Age: Tiva Canyon Tuff	SLIP RATE Estimation Technique	Quaternary Slip Rate	Assessment Method	Average Displacement per event (cm)	Average Recurrence Interval (Ka)
-----------------------	----------	--	-----------------------	--------------------------------	----------------------	-------------------	-------------------------------------	----------------------------------

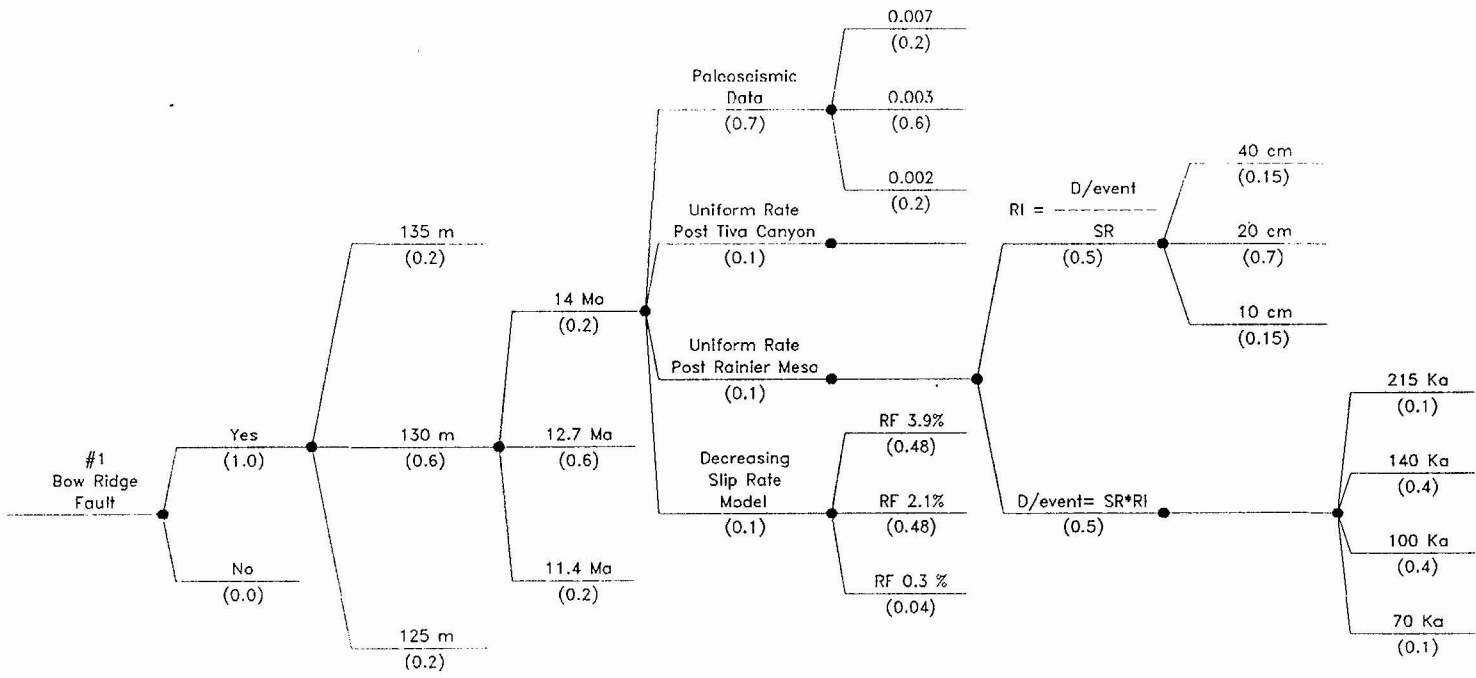
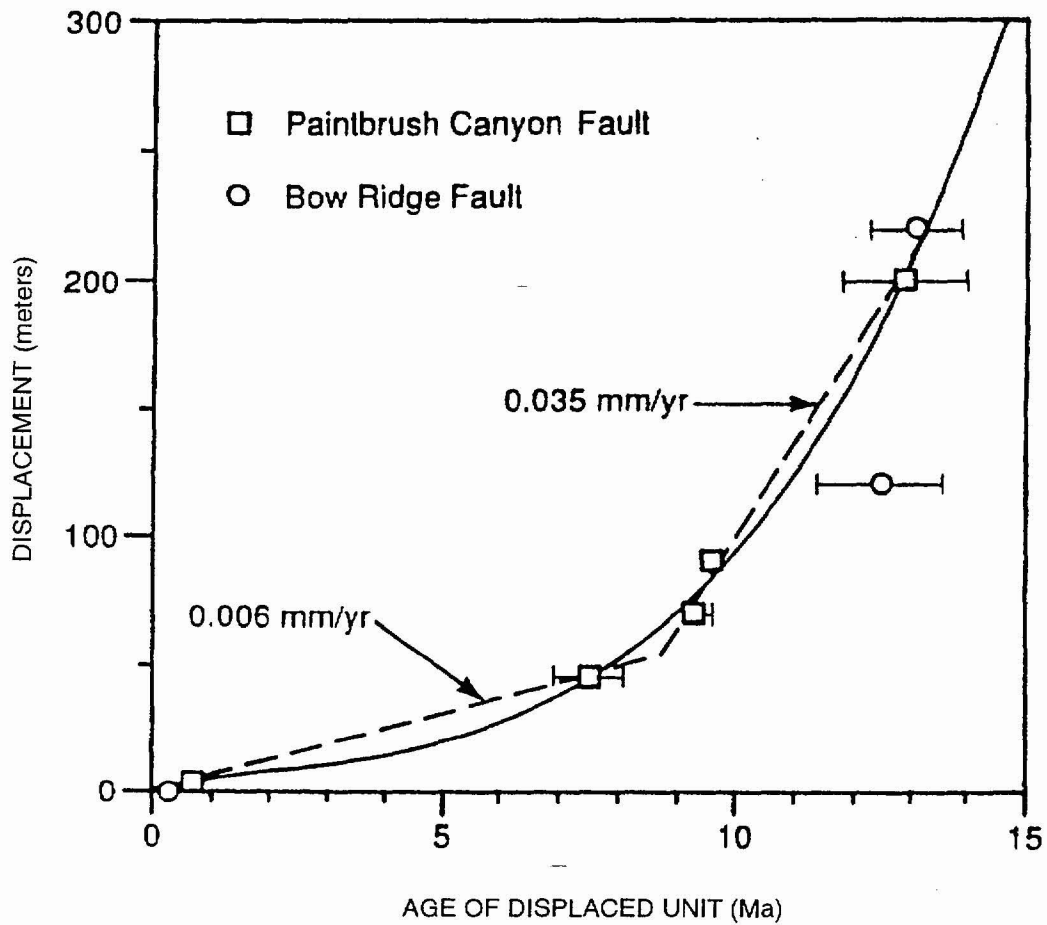


Figure DFS-15 Logic tree used to characterize the fault displacement hazard based on fault slip rates



Source: Gibson and others (1990)

Figure DFS-16 Graph showing displacement versus age of displaced unit for the Paintbrush Canyon and Bow Ridge faults (From: J.D. Gibson *et al.*, SNL, written communication, 1992)

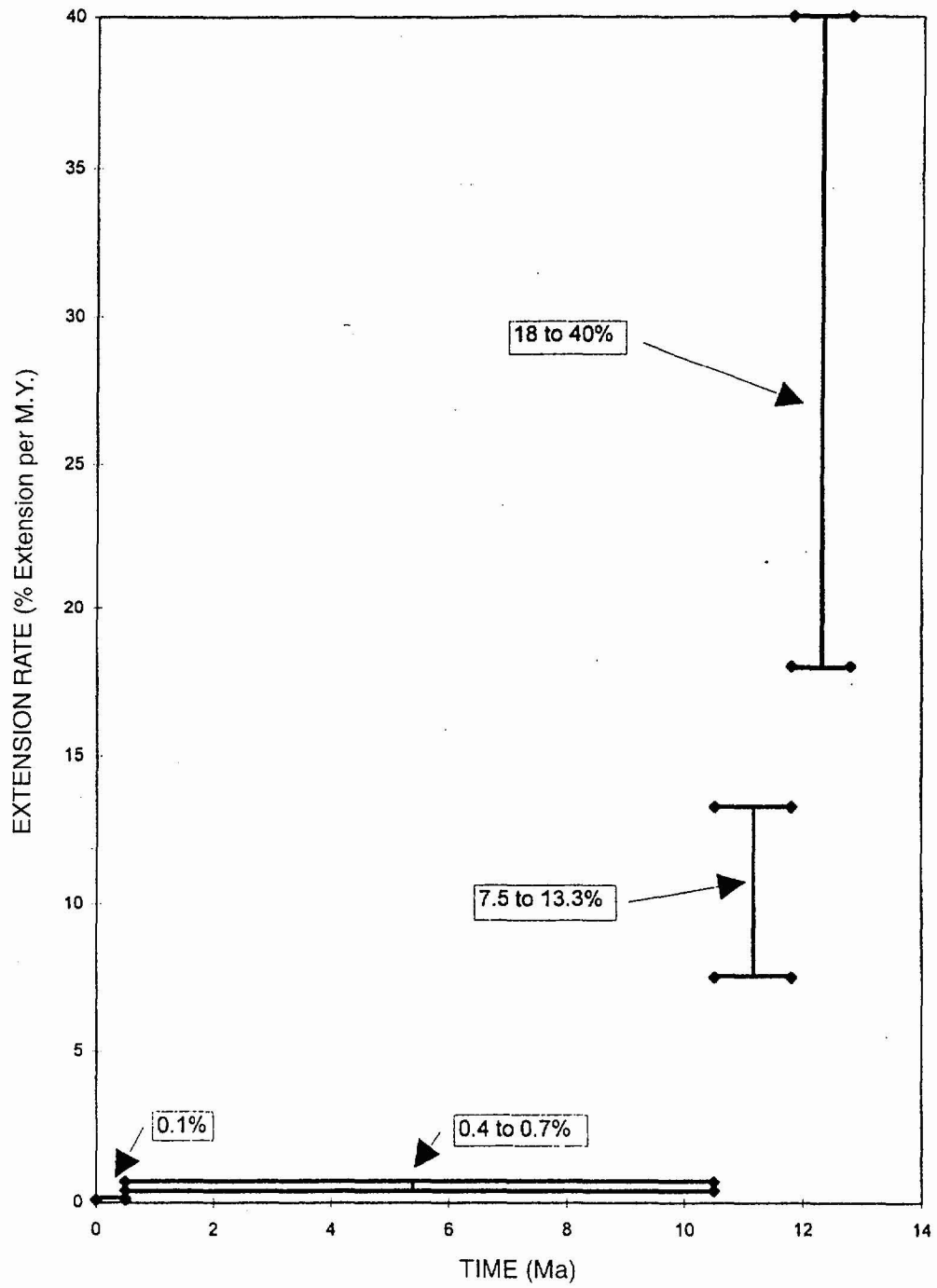


Figure DFS-17 Graph of estimated extension rates in Crater Fault basin from middle Miocene to the present (From C. J. Fridrich *et al.*, USGS, written communication, 1996)

<i>Available Paleoseismic Data</i>	<i>Quaternary Slip Rate Estimation Technique</i>	<i>Reduction Factor</i>
--	--	-----------------------------

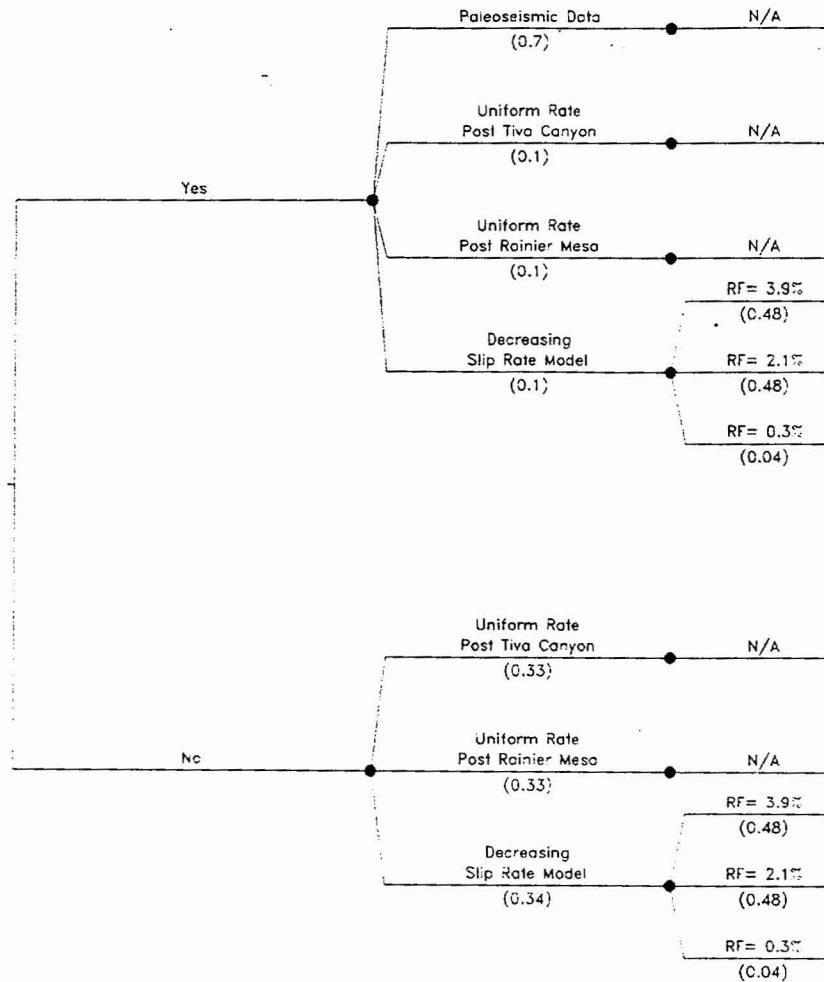


Figure DFS-18 Logic tree showing probability weights assigned to the different Quaternary-slip-rate-estimation techniques depending on the availability of site-specific paleoseismic information.

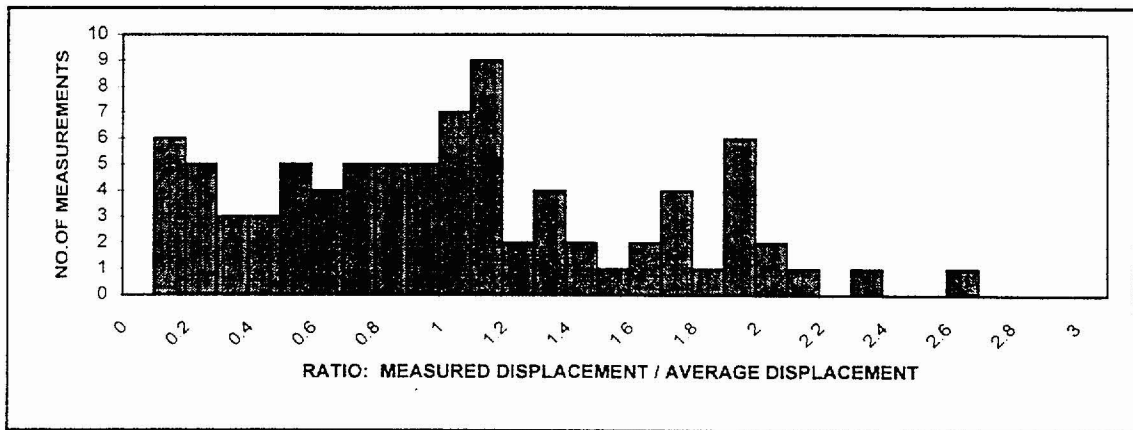
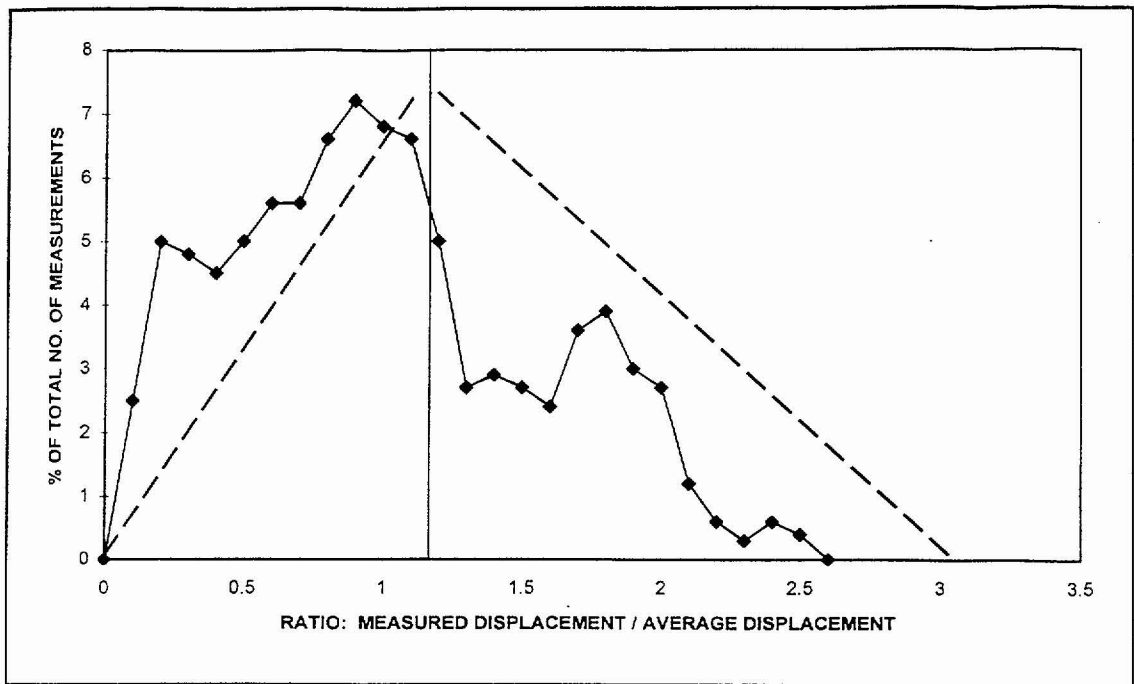


Figure DFS-19 Plots showing event-to-event variability in displacement relative to average displacement per event at a location along a fault based on data from paleoseismic investigations in the Yucca Mountain area.

Test Calculation Site	Potential for Activity Table DFS-14	Deformation History Model	Reduction Factor	Age of the Host Rock (Tiva Canyon Truff)	Probability of an "Event" (Pe) Table DFS-15	"Event" defined as Threshold of Detection of Fault Displacement (Section 8.3)
-----------------------	-------------------------------------	---------------------------	------------------	--	---	---

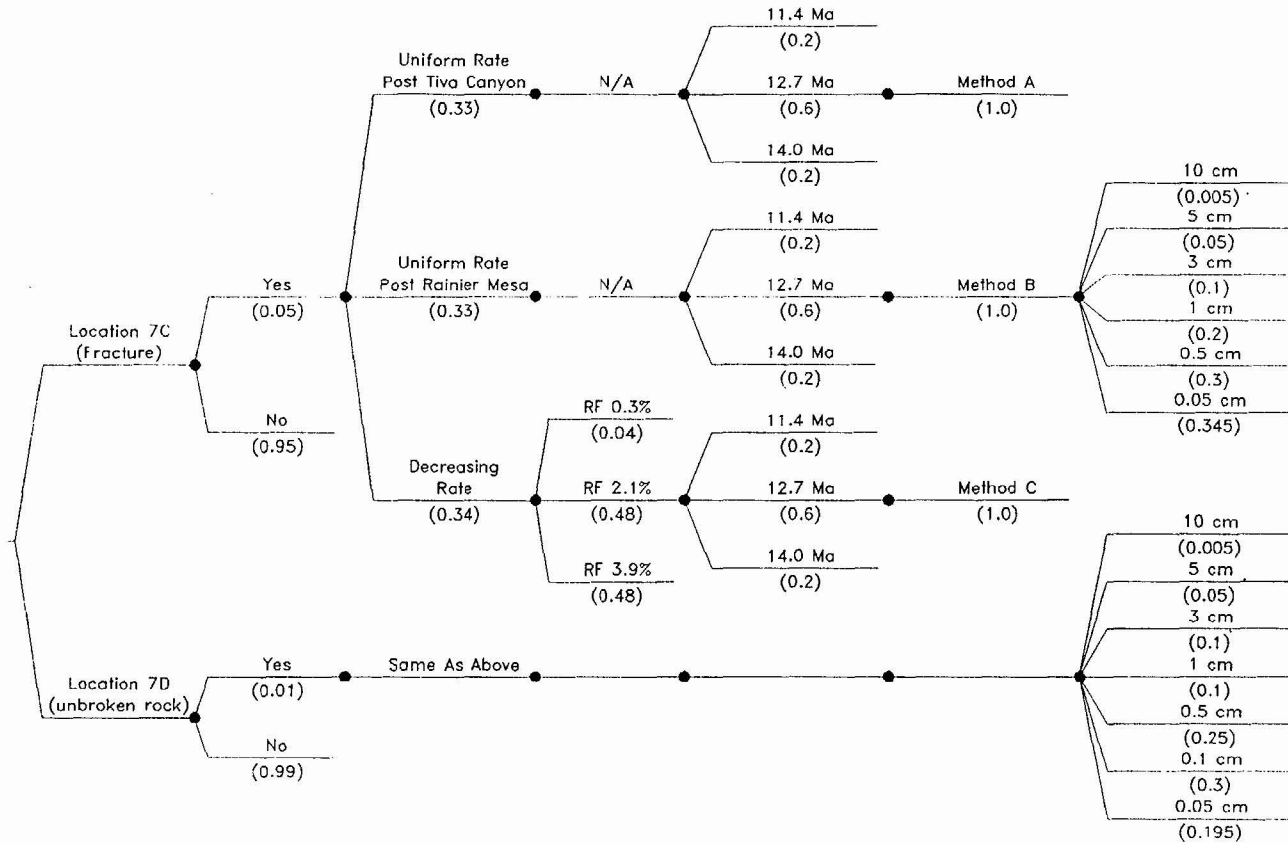


Figure DFS-20 Logic tree for assessing potential fault displacement hazard across a fracture or in unbroken rock.

ELICITATION SUMMARY

ALBERT M. ROGERS, JAMES C. YOUNT, AND LARRY W. ANDERSON

TABLE OF CONTENTS

Page: i

1.0	INTRODUCTION.....	RYA-1
2.0	SEISMIC SOURCES	RYA-2
2.1	THICKNESS OF THE SEISMOGENIC CRUST	RYA-3
2.2	AREAL OR BACKGROUND SOURCES	RYA-3
2.2.1	Recurrence	RYA-3
2.2.2	Maximum Magnitude	RYA-6
2.3	LOCAL FAULT SOURCES	RYA-6
2.3.1	Coalescing Fault Structure.....	RYA-7
2.3.2	Maximum Magnitude Approach.....	RYA-9
2.3.3	Recurrence Approach.....	RYA-11
2.4	POSSIBILITY OF A BURIED SEISMIC SOURCE	RYA-11
2.5	VOLCANIC SOURCE	RYA-13
2.6	REGIONAL FAULT SOURCES	RYA-13
2.6.1	Maximum Magnitude Approach.....	RYA-14
2.6.2	Recurrence Approach.....	RYA-14
3.0	FAULT DISPLACEMENT CHARACTERIZATION	RYA-15
3.1	INTRODUCTION	RYA-15
3.2	APPROACH.....	RYA-17
3.2.1	Probability Slip can Occur	RYA-18
3.2.2	Frequency of Displacement Events.....	RYA-18
3.2.3	Estimation of Slip Rate	RYA-19
3.2.4	Estimation of Average Slip Per Event	RYA-19
3.2.5	Distribution for Displacement Per Event.....	RYA-21
3.3	DATA FOR CHARACTERIZATION OF DISPLACEMENT HAZARD AT THE NINE TEST CALCULATION SITES	RYA-21
4.0	REFERENCES.....	RYA-29

TABLES

Table RYA-1	Completeness times
Table RYA-2	Interval recurrence parameters
Table RYA-3	Fault source parameters, Area A

Table RYA-4	Coalescing fault source model, Area A—Three Yucca Mountain fault systems
Table RYA-5	Coalescing fault source model, Area A—Two Yucca Mountain fault systems
Table RYA-6	Coalescing source model, Area A—One fault system
Table RYA-7	M_{\max} for hypothesized buried seismic source 30 km long (M_{\max} derived from $M = 4.04 + 0.98 \log [\text{rupture area}]$) (Wells and Coppersmith, 1994)
Table RYA-8	Significant regional fault source parameters, Areas B and C

FIGURES

Figure RYA-1a	Logic tree for background source zones
Figure RYA-1b	Logic tree for local fault sources
Figure RYA-2	Map showing boundaries of zones used in the seismic source model
Figure RYA-3	Map showing earthquakes from the version 5 catalog and the background source zones
Figure RYA-4	Map showing earthquakes from the version 7 catalog and the background source zones
Figure RYA-5	Stepp plot of annual frequency versus years before 9/1996 for individual magnitude bins and the version 5 catalog
Figure RYA-6	Stepp plot of annual frequency versus years before 9/1996 for individual magnitude bins and the version 7 catalog
Figure RYA-7	Histogram showing b-values obtained for the version 5 catalog given uniform sampling of completeness times
Figure RYA-8	Histogram showing b-values obtained for the version 5 catalog given normal sampling of completeness times
Figure RYA-9	Histogram showing b-values obtained for the version 7 catalog given uniform sampling of completeness times
Figure RYA-10	Histogram showing b-values obtained for the version 7 catalog given normal sampling of completeness times
Figure RYA-11	Interval rates for the version 5 catalog that produced the modal b-value 1.09 (Figure RYA-7) and the fit to these data using the Weichert maximum likelihood method

- Figure RYA-12 Interval rates for the version 7 catalog that produced the modal b-value 1.17 (Figure RYA-9) and the fit to the data using the Weichert maximum likelihood method
- Figure RYA-13 Earthquake recurrence parameters. The paired a- and b-values calculated by uniform sampling from the range of likely completeness times and associated annual rates in the version 5 catalog. This plot shows the correlation between a- and b-values.
- Figure RYA-14 Earthquake recurrence parameters. The paired a- and b-values calculated by uniform sampling from the range of likely completeness times and associated annual rates in the version 7 catalog. This plot shows the correlation between a- and b-values.
- Figure RYA-15 Estimated age and amount (in cm) of late Quaternary displacement for faults in the Yucca Mountain area based on data in USGS (written communication, 1996). Faults are arranged from west to east; trench numbers under each fault are arranged from north to south. Bars and arrows show full uncertainties in estimated age of faulting event at each trench. "w" represents fracturing event (displacement < 20 cm). Age on far right of chart shows our best estimate for age of grouped event. See text and tables for fault abbreviations.
- Figure RYA-16 Map showing local fault sources included in the seismic source model
- Figure RYA-17 Map showing regional faults included in the seismic source model
- Figure RYA-18 Logic tree used to characterize fault displacement at sites with Quaternary data
- Figure RYA-19 Logic tree used to characterize fault displacement at sites without Quaternary data
- Figure RYA-20 Plots developed by DFS showing event-to-event variability in displacement relative to average displacement per event at a location along a fault based on data from paleoseismic investigations in the Yucca Mountain area
- Figure RYA-21 Probability density function (PDF) and cumulative distribution function (CDF) for 80 measurements single-event displacement, normalized to MD^{\max} for the corresponding fault, from 19 trenches in the Yucca Mountain area as developed by the AAR team

ELICITATION SUMMARY
ALBERT M. ROGERS, JAMES C. YOUNT, LARRY W. ANDERSON

1.0

INTRODUCTION

Yucca Mountain is located in the southern Great Basin of Nevada. The physiography and tectonic setting of this area are the product of late Cenozoic crustal extension and silicic volcanism that occurred primarily between 17 and 9 million years ago. This deformation created a complex structural setting that presents significant interpretational difficulties. A number of tectonic models, developed to explain this structural diversity, were presented and discussed at the Yucca Mountain Workshops held between October 1996 and April 1997. For example, see Carr (1982, 1990); Carr *et al.* (1986); Scott (1990); and Hamilton (1988). D. W. O'Leary (USGS, written communication, 1996) provides an extensive review of models and references, as well as a preferred interpretation. These models each have unique merit in explaining certain aspects of the structural evolution and present-day seismotectonic setting of the Yucca Mountain area. Although tectonic models can be useful tools, none of the models presented provide a complete, unified explanation of all the seismic, geologic, and geophysical data for Yucca Mountain and the larger Walker Lane-western Great Basin-Death Valley regions. Therefore, our approach was first to examine what appear to be the primary potential seismogenic sources, and then to use geologic and geophysical constraints to define the source properties. We find that a coalescing fault model best fits the Yucca Mountain structural domain. A question raised at several workshops was whether the Yucca Mountain faults are capable of generating earthquakes. For our assessment, faults in the Bare Mountain-Yucca Mountain area are treated as potential seismic sources. We include the following seismic sources in our assessment of the earthquake hazard at Yucca Mountain: (1) background seismicity not associated with mapped faults; (2) Yucca Mountain faults, which we interpret to have varying degrees of lateral and vertical coalescence; (3) the Bare Mountain fault; (4) volcanic activity; and (5) large, regional, late Quaternary faults.

Our analysis is based on the following fundamental interpretations: (1) the Bare Mountain fault is a planar seismogenic fault that penetrates to mid-crustal depths; (2) the faults at Yucca Mountain are planar to listric and coalesce into one, two, or three master faults at

unknown depths above or at the Bare Mountain fault; the depth at which this coalescence occurs is considered an uncertain variable (see D. W. O'Leary, USGS, written communication, 1996, for a summary of the geologic and geophysical data that support these assumptions; theoretical modeling also provides support for steeply dipping and coalescing faults); and (3) other faults, not mapped at the surface, exist in the region that can produce earthquakes below the threshold magnitude for surface rupture.

Yucca Mountain faults are considered to behave independently and/or truncate downdip in a detachment fault or a zone of decoupling. Our evaluation of Yucca Mountain faults as coalescing at variable depths implicitly includes independent rupture and truncation, although we believe that the data exclude the possibility of a seismic detachment. Because no earthquakes have been observed on detachments faults worldwide (e.g., Jackson, 1987), we do not consider them to be seismically active structures; we remain unconvinced by arguments that the historical record is too short to include earthquakes on such faults worldwide (Wernicke, 1995).

Our analysis considers regional faults that are interpreted to be steeply dipping planar faults penetrating to mid-crustal depths. Because of their distance from the site and low contribution to the hazard, these faults are modeled more simply, with little variation in downdip width. In general, we model only the larger regional faults within 100 km of Yucca Mountain, as explained below; however, we do consider background seismicity, either as uniformly distributed faults or as a smoothed historical seismicity.

2.0

SEISMIC SOURCES

The logic tree that defines our interpretations of potential seismic sources for the Yucca Mountain area is given on Figures RYA-1a and b. Various aspects of these seismic sources are discussed below. We indicate the weights assigned to the branches of the tree on the figures or in the tables that follow.